Design and Optimization of Coiled Flow Inverters for Process Intensification in Sustainable CO_2 Capture and Organic Transformations

Thesis submitted in partial fulfillment

for the Award of Degree

Doctor of Philosophy

by

ANIKESH TRIPATHI

RAJIV GANDHI INSTITUTE OF PETROLEUM TECHNOLOGY

JAIS — 229304

22CE0010

2026

CERTIFICATE

It is certified that the work contained in the thesis titled **"*Design and Optimization of Coiled Flow Inverters for Process Intensification in Sustainable CO_2 Capture and Organic Transformations*" by "*Anikesh Tripathi*"** has been carried out under my supervision and this work has not been submitted elsewhere for a degree.

It is further certified that the student has fulfilled all the requirements of Comprehensive, Candidacy and SOTA.

Supervisor
(Dr. Koushik Guha Biswas)

DECLARATION BY THE CANDIDATE

I, ***"Anikesh Tripathi"***, certify that the work embodied in this thesis is my own bona fide work and carried out by me under the supervision of **"*Dr. Koushik Guha Biswas*"** from "August 2022" to "July 2026", at Rajiv Gandhi Institute of Petroleum Technology, Jais. The matter embodied in this thesis has not been submitted for the award of any other degree. I declare that I have faithfully acknowledged and given credits to the research workers wherever their works have been cited in my work in this thesis. I further declare that I have not willfully copied any other's work, paragraphs, text, data, results, etc., reported in journals, books, magazines, reports dissertations, theses, etc., or available at websites and have not included them in this thesis and have not cited as my own work.

Date:
Place:

Anikesh Tripathi
Roll No. 22CE0010

CERTIFICATE BY THE SUPERVISOR

It is certified that the above statement made by the student is correct to the best of our knowledge.

Dr. Koushik Guha Biswas
(Supervisor)

Signature & Seal of Head of Department

CERTIFICATE

Certified that the work contained in the thesis titled **"Design and Optimization of Coiled Flow Inverters for Process Intensification in Sustainable CO_2 Capture and Organic Transformations"** by **Mr. Anikesh Tripathi** has been carried out under my supervision. It is also certified that he fulfilled the mandatory requirement of TWO quality publications arose out of his thesis work.

It is further certified that the two publications (copies enclosed) of the aforesaid Mr. Anikesh Tripathi have been published in the Journals indexed by —

(a) SCI

(b) SCI Extended

(c) SCOPUS

(d) *Non-indexed Journals- (only in special cases) (*Please enclose DPGC resolution in this regard)

(Supervisor)	(Convener, DPGC)
Dr. Koushik Guha Biswas	**Dr. Supriya Pulipaka**

N.B.: Please strike out the category (a, b, c, d) that is not applicable.

COPYRIGHT TRANSFER CERTIFICATE

Title of the thesis: Design and Optimization of Coiled Flow Inverters for Process Intensification in Sustainable CO_2 Capture and Organic Transformations
Name of the student: Anikesh Tripathi

Copyright Transfer

The undersigned hereby assigns to the Rajiv Gandhi Institute of Petroleum Technology, Jais all rights under copyright that may exist in and for the above thesis submitted for the award of the" Doctor of Philosophy".

Date:

Place:

_____

Anikesh Tripathi

Roll No. 22CE0010

Note: However, the author may reproduce or authorize others to reproduce material extracted verbatim from the thesis or derivative of the thesis for author's personal use provided that the source and the Institute's copyright notice are indicated.

Dedicated to my family

Acknowledgements

I am very happy and proud to present this Ph. D. thesis. Before this I would like to express my sincere thanks to the Almighty God for giving me the strength, wisdom and fortuitous circumstances to successfully complete this important milestone of my academic journey through his blessings, guidance and grace. I am also thankful to the many people who have helped in this work, providing consistent support, encouragement, advice and kindness. I would like to express my sincere thanks to them for their invaluable help for the successful completion of this project.

I am very thankful to my supervisor Dr. Koushik Guha Biswas for his constant support, encouragement, academic motivation and help. While writing the thesis I have been very grateful for the advice and discussions that have been given to me. I will always cherish the enjoyable and enlightening discussions with my supervisor at each stage of my writing, which consistently lasted for several hours and have facilitated the completion of this thesis. Furthermore, I would like to extend my appreciation to Dr. Debashis Panda, for their invaluable support and constant encouragement throughout the entire process. His unique approach in nurturing independent thinking, exploring novel ideas and systematically solving research problem has been one of the most valuable lesson of my Ph.D. journey

I would like to express my sincere gratitude to Prof. K.D.P. Nigam, Department of Chemical Engineering, IIT, Delhi. His research publications have been great source of inspiration throughout my Ph.D. journey and have significantly motivated me in successfully completed the Ph.D.

I am grateful to the one more member of my RPEC committee member, Dr. Gunjan Agrahari, for his insightful comments and encouragement, as well as for the challenging question that inspired me to broaden my research from a variety of perspectives, in addition to my supervisor. My labmates and friends are Swapna Patel, Sachin Kumar, Pravesh Narain Singh, Arvind Kumar, Uttsav Mishra, Ayush Singh, Surja Kanta Pal, Suvodeep Panda and Karan Sarkar, thank you for the stimulating discussions, the days we spent together working in the labs, and the joy we shared over the last four years. I am very thankful to my senior Dr Pooja Jaiswal and my juniors Abhishek Kumar, Abhijeet Anand, Aditya Kashyap, Anubhuti and Nimisha Verma for their support and encouragement.

I am extremely thankful to my parents for their constant support and love, which have been a motivation for me to move forward with my academic and professional pursuits. The constant love, support and encouragement of my parents has always been a driving force to move forward. There's been such a depth of optimism and peace in my mom's warmth, always. My sister and brother always pushed me to do better. I am equally grateful for the compassion, forbearance and affection shown me by my in-laws. Last but not the least I would like to thank my beloved wife Dr. Piyushika Dixit and my kids Mr. Kanishk Tripathi and Mr. Kratikesh Tripathi. I am so thankful for his continuous love, compassion and support. They gave me their full support in every situation and made sure that this journey was filled with unforgettable experiences. Since they have given me love, patience, support and sacrifices all my family members have been very important in my life. "I could not have reached such heights without their blessings.

Anikesh Tripathi

Table of Contents

Acknowledgements ..... **i**

Table of Contents ..... **iii**

List of Figures ..... **ix**

List of Tables ..... **xv**

List of Abbreviations ..... **xvii**

Preface……. ..... **xxiii**

Chapter 1: Introduction and Literature Survey **1**

1.1 Introduction 1

1.2 Literature Survey 5

1.2.1 Reactor Geometrical Modifications as a tool of Process Intensification: Coil Flow Invertor 5

1.2.2 Process Intensification in Gas-Liquid reaction for carbon capture 8

1.2.3 Process Intensification of CO_2 Capture through Bio-Derived Lignin-Based Absorbents for a Circular Carbon Economy 15

1.2.4 Fluorescent chemical synthesis via flow chemistry as a process intensification strategy 20

1.3 Lacuna in past literature 22

1.4 Objective of the present study 22

1.5 Organization of the thesis 24

Chapter 2 Experimentation 25

2.1 Introduction 25

2.2 Test Fluids Used.....25

2.2.1 Aqueous Solution of Amines.....25

2.2.2 Alkanolamine- free CO_2 capture solvent.....26

2.2.3 Gallic acid and N, N-dimethylformamide (DMF) Solution 27

2.3 Reactor Systems 28

2.3.1 Helical Coil reactor.....28

2.3.2 Coiled Flow Invertor 29

2.3.3 Stacking of CFI.....29

2.4 Experimentation 30

2.4.1 CO_2 Absorption in Amines 30

2.4.2 Experimental Setup for CO_2 absorption in Alkanolamine- free Lignin based solvent 32

2.4.3 Experimental Setup for synthesis of Xanthene dye from Gallic acid and DMF 34

2.5 Experimental Procedures.....35

2.5.1 Estimation of percentage of CO_2 absorption 35

2.5.2 Estimation of heat transfer in synthesis of Xanthene Dye 39

2.6 Error Analysis 40

2.7 Synthesis of Low-density Lignin (LDL) 40

2.8 Summary 41

Chapter 3: Hydrodynamics-driven CO_2 Absorption in Coiled Flow Inverters using Alkanolamines[1] 43

3.1 Brief Introduction 43

3.2. Results and Discussions 44

3.2.1 Deciphering the role of geometrical medication of reactors 44

3.2.2 Reduction of CO_2 gas bubble size 46

3.2.3 Effect of N-Methyldiethanolamine (MDEA) blended Diethanolamine (DEA) in CO_2 absorption 48

3.2.4 Nano cellulose-aided CO_2 capture at low flow rate 50

3.4 Conclusion 53

Chapter 4: Alkanolamine-free 96% CO_2 Capture using Coiled Flow Inverters: A Sustainable Scope[1] 55

4.1 Brief Introduction 55

4.2 Results and Discussions 56

4.2.1 Characterization of amine-functionalized lignin 56

4.2.2 Efficacy of functionalized lignin on CO_2 Capture 61

4.2.3 Effect of bio-gas and temperature in CO_2 absorption 62

4.2.4 Effect of absorbent flow rate on hydrodynamics parameter 64

4.2.5 Resolving the Contributions of Components of Urea-functionalized Lignin (Ur-L) 65

4.2.6 Efficacy of Bio urea present in Human Urine for CO_2 Capture 67

4.2.7 Quantification of CO_2 absorption by CO_2 bubble size reduction method 68

4.2.8 Residual Performance of functionalized lignin absorbents 69

4.3 Conclusion 71

Chapter 5: Intensifying the Synthesis of Xanthene Dyes from Gallic Acid using Coiled Flow Inverter[1] 73

5.1 Brief Introduction 73

5.2 Results and Discussion 74

5.2.1 Effect of residence time on product formation 74

5.2.2 Effect of Temperature on Product Formation 80

5.2.3 Impact of Heat Flux on Gallic Acid Condensation 82

5.2.4 Product characterization 86

5.3 Conclusion 90

Chapter 6: Conclusion and Future Work 91

6.1 Conclusion 91

6.2 Future Work 92

References 95

Appendix A 115

A.1 Calculation of amount of heat received by oil bath and Heat flux 115

A.2 Calculation of Velocity of reactant in reactor..... 115

A.3 Calculation of Residence Time..... 115

A.4 Calculation of percentage of CO_2 absorption by Acid –Base Titration (Chemical Method)..... 115

A.4 Calculation of Reynolds Number (Re) of Gas-Liquid mixture 116

List of Publications.....117

List of Figures

Figure 2.1: Schematic of synthesis of Alkanolamine free CO_2 capture solution……27

Figure 2.2: Helical Coil Reactor..... 28

Figure 2.3: Images of Coil Flow Invertor (CFI) [A] Horizontal axis of inlet/outlet [B] Vertical axis of inlet/outlet..... 29

Figure 2.4: Real Image of stack of CFI..... 30

Figure 2.5: Experimental Setup [1] Syringe Pump [2] Gas inlet pipe [3] Syringe [4] Mass flow meter [5] CFI [6] Separator flask [7] Inverted Burette for employed for flow-directed CO_2 capture in Amines..... 31

Figure 2.6: Image of experimental setup **[1]** Syringe Pump, **[2]** Syringe, **[3]** liquid inlet pipe, **[4]** Gas Flow meter, **[5]** CFI Reactor, **[6]** gas inlet pipe, **[7]** collection flask, **[8]** inverted burette, **[9]** pressure gauge, **[10]** CO_2 cylinder..... 33

Figure 2.7: Experimental Setup of synthesis of Xanthene Dye from Gallic acid and DMF 34

Figure 2.8: Schematic of Inverted burette method **[a]** CO_2 loaded liquid and unabsorbed gas coming from reactor **[b]** Unabsorbed CO_2 and air coming from collection flask **[c]** Volume displaced by gases coming from collection flask **[d]** volume of CO_2 loaded liquid 37

Figure 2.9: Schematic of synthesis of Low-density lignin..... 41

Figure 3.1: CO_2 absorption efficiency in aqueous Diethanolamine (3%) solution for two different reactors. The flow rates for CO_2 gas and aqueous Diethanolamine solution have been represented as Q_G and Q_L respectively. For helical reactor; Q_G = 30 mL/min (red square), Q_G = 60 mL/min (grey square). Whereas, for CFI; Q_G = 30 mL/min (red circle), Q_G = 60 mL/min (grey circle). 45

Figure 3.2: Snapshot of size reduction CO_2 gas bubble in millimetre-sized CFI. Pink color is due to presence of phenolphthalein indicator in solvent. 48

Figure 3.3: [A] CO_2 absorption efficiency in aqueous solution of 1% MDEA and 3% DEA using CFI. For CO_2 gas flow rates —30 mL/min (black square), 40 mL/min (red square), 50 mL/min (green square), and 60 mL/min (blue square). The flow rates CO_2 gas and blended amine solution have been represented as Q_G and Q_L respectively. **[B]** Comparative analysis of CO_2 capture efficiency with conventional microchannel and millimeter-sized CFI used in this study. 50

Figure 3.4: [A] CO_2 absorption efficiency in aqueous solution of 0.01% Nano cellulose (NC) and 3% DEA using CFI in alkaline medium (20 mM NaOH). For CO_2 gas flow rates —30 mL/min (black square), 40 mL/min (red square), 50 mL/min (green square), and 60 mL/min (blue square). The flow rates for CO_2 gas and blended amine solution have been represented as Q_G and Q_L respectively. **[B]** Comparison of CO_2 absorption efficiency in three different solvents at constant gas flow rate, 30 mL/min. 0.01% NC in aqueous 3% DEA (red circle), 0.01% NC in aqueous solution (blue circle), aqueous 3% DEA (dark brown circle). 52

Figure 4.1: [A] UV-Vis spectra of functionalized lignin, Ur-L and Amn-L (Inset), Before CO_2 capture (dotted line) and after the CO_2 capture (solid line). Colour of as-synthesized aqueous solutions of Ur-L and Amn-L. **[B]** Viscosity of Ur-L (blue square) and Un-L (green circle) as a function of shear rate. Human Urine from age group of less than 20 years has been used. 57

Figure 4.2: FTIR spectra of - low density lignin (grey line), Ur-L (blue line) and Ur-L at CO_2 captured state (green line)..... 60

Figure 4.3: FESEM images of **[A]** Ur-L Sample before CO_2 Loading **[B]** Ur-L sample after CO_2 loading **[C]** Un-L (20) Sample before CO_2 Loading **[D]** Un-L (20) sample after CO_2 loading..... 60

Figure 4.4: Comparison of CHNS elemental composition of Ur-L (Urea-Lignin) absorbent before and after CO_2 loading..... 61

Figure 4.5: Comparison of CO_2 Absorption in different aqueous absorbents, functionalized lignin using ammonia, hydrazine and urea – Ammonia-Lignin (Amn-L) (black square), Hydrazine-Lignin (Hzn-L) (red square) and Ur-L (blue square). and ammonia (black colour) at gas flow rates **[A]** 20 mL/min **[B]** 30 mL/min 62

Figure 4.6: Comparison of percentage absorption in different conditions **[A]** Pure CO_2 vs Bio gas at gas flow rate 30 mL/min for Urea-lignin (Ur-L) absorbent **[B]** Effect of temperature at 70°C and 30°C for gas flow rate 30 mL/min with Urea-Lignin (Ur-L) (blue colour) and Urine-Lignin (Un-L) (green colour) absorbent..... 63

Figure 4.7: [A] Comparison of pressure difference inside CFI reactor during CO_2 absorbance in Urea-Lignin (Ur-L) (blue colour) and Urine-Lignin (20) (Un-L) (green colour) at gas flow rate of 30 mL/min **[B]** Comparison of Reynolds number for 30 mL/min gas flow rate and variation in absorbent flow rates of Un-L (20) (green colour) and Ur-L (blue colour) 65

Figure 4.8: [A] Quantifying the role of each component of Ur-L for CO_2 absorption at gas flow rate 20 mL/min– aqueous Ur solution (solid blue line), Ur+L solution (dotted green line) Ur-L solution (solid green line). **[B]** Comparison of CO_2 absorption for Ur-L at gas flow rate of 20 mL/min (hollow square), 30 mL/min (blue square) and 40 mL/min (purple square). 66

Figure 4.9: [A] Absorption of CO_2 in lignin with urine at gas flow rate of 30 mL/min. **[B]** Comparison of CO_2 absorption of Ur-L (blue square) with Un-L absorbents (green circle) at 30 mL/min gas flow rate. Human Urine from age group of less than 20 years has been used. 67

Figure 4.10: Images of CFI reactor during gas-liquid reaction for absorbents- **[A]** Amn-L, **[B]** Ur-L, **[C]** Un (20)-L. The length of gas-bubble at arm-1 of CFI reactor is considered near inlet, whereas the length of same at arm-3 is considered near inlet exit points for determination of reduction of bubble size **[D]** Reduction of CO_2 gas bubble length for four aqueous functionalized lignin adsorbents. 69

Figure 4.11: CO_2 capture efficiency of aqueous functionalized lignin absorbents in 2^{nd} cycle. 71

Figure 4.12: CO_2 capture efficiency of **[A]** Urine-Lignin (20) **[B]** (Ur-L) and Urea-Lignin (Ur-L) absorbents in 10^{th} cycle. 71

Figure 5.1: Absorption spectra of the product obtained at 170 ℃ at different flow rates– **[A]** 3 mL/h, **[B]** 4 mL/h, **[C]** 6 mL/h. Emission spectra of product at the same temperature at the respective flow rates– **[D]** 3 mL/h, **[E]** 4 mL/h, **[F]** 6 mL/h. CFI Stack (red line) and CFI (green line) 76

Figure 5.2: Contour plots of the emission spectra with the corresponding excitation wavelengths of product obtained at 170 ℃ by varying length of CFI and flow rate. CFI at different flow rates – **[A]** 3 mL/h, **[B]** 4 mL/h, **[C]** 6 mL/h. Stack CFI at different flow rates –[**D]** 3 mL/h, **[E]** 4 mL/h, **[F]** 6 mL/h. 78

Figure 5.3: Real time images of reactor during synthesis- **[A**] in ambient light (representative), **[B]** under UV-light irradiation. Inset: Zoom-in section of stack CFI..... 79

Figure 5.4: Impact of temperature on formation of fluorescent product for stack CFI. Colour of product solution obtained by varying temperature at flow rate– **[A]** 3mL/hr, **[B]** 5 mL/hr. Fluorescence spectra of product in solution at three different temperatures for flow rate- **[C]** flow 3mL/hr **[D]** 4mL/hr **[E]** 6mL/hr. 160°C (blue line), 180°C (red line), 190°C (green line), The excitation wavelength, λ_{exc} has been kept at 425 nm. 81

Figure 5.5: Dependence of operating conditions: flow rate and temperature on product formation for stack CFI. Contour plot of fluorescence intensity on reactant flow rate and temperature of the reaction. 82

Figure 5.6: Dependence of product yield (vis-à-vis fluorescence intensity) on temperature. Product yield (%) and fluorescence intensity have been measured independently. 85

Figure 5.7: [A] Emission spectra of product obtained at 170 ℃ using stack CFI at different flow rates. 3 mL/hr (green line), 4 mL/hr (dark yellow line), 5 mL/hr (red line), 6 mL/hr (blue line). **[B]** Time-resolved fluorescence decay of same product. **[C]** ATR FT-IR of same product (dark yellow) and Gallic acid (grey). 87

Figure 5.8: Plausible reaction mechanism for yielding Xanthene analogue by condensation of Gallic acid in DMF.....88

Figure 5.9: H^1-NMR (JEOL, 400MHz) spectra of the product in D_2O; δ 8.24 (s, –COOH), 7.72 (s, 1H, H–C9), 6.89 (s, 1H, H–C2, C7), 6.52 (s, –OH, C4), 6.33 (s, –OH, C5, C6), 2.03 (s, 6H, N–CH_3), δ 4.66 (solvent residual peak–because of exchangeable protons of –OH and –COOH groups, their peaks are highly diminished in the spectra). The singlet peaks at δ 2.5-2.9 are attributed to impurities, primarily due to residual DMF solvent. 89

Figure 5.10: C^{13}-NMR spectra (JEOL, 400MHz) spectra of the product in D_2O; C^{13}-NMR spectra (JEOL, 400MHz): δ 179.58 (C3, C1), δ 171.77 (C11), δ 144.35 (C6, C4, C10a), δ 137.05 (C5, C4a), δ123.81 (C8), δ 120.20 (C8a), δ 110. 57 (C7, C2), δ 108.61 (C9), and δ 31.08 (C13, C12). 89

List of Tables

Table 1.1: Development of gas-liquid reaction in mill channels, helical coils and coiled flow inverters 10

Table 1.2: Salient studies on CO_2 absorption using amine solvents 14

Table 1.3: Recent developments on CO_2 capture in amine functionalized liquids 18

Table 1.4: Arrangement of the different chapters in the dissertation 24

Table 5.1: Condensation experiments using CFI stack at 0.04 % (w/v) Gallic acid in DMF 75

Table 5.2: Quantification of heat flux for the reaction at varied flow rates 84

List of Abbreviations

1M HCL	One Molar Hydrochloride Acid
3D	Three Dimensional
AAS	Amino Acid Salts
ABTS	2,2-Azino-Bis (3-Ethylbenzothiazoline-6-Sulfonic Acid)
ACCFI	Asymmetrical Compact Coiled Flow Inverter
AEEA	2-((2-Aminoethyl) Amino) Ethanol
Amn	Ammonia
AMP	2-Amino-2-Methyl-1-Propanol
AN	Acrylonitrile
ANN	Artificial Neural Network
APTMS	(3-Aminopropyl) Trimethoxysilane
Au	Gold
BA	Butyl Acrylate
BPEI	Branched Polyethylenimine
C	Carbon
CCFIS	Compact Coiled Flow Inverters
CCUS	Carbon Capture Utilization and Storage
CDSE/ZNS	Cadmium Selenide / Zinc Sulphide
CFD	Computational Fluid Dynamics
CFI	Coil Flow Invertor
CNCS	Cellulose Nanocrystals
CNFS	Cellulose Nanofibers
CNW-CN	Graphitic Carbon Nitride-Supported Co-Ni Tungstate

Co(II)	Cobalt (Ii)
CO_2	Carbon Di Oxide Gas
COMSOL	Component Modeling Software
CSTR	Continuous Stirred Tank Reactor
DEA	Diethanolamine
DEEA	2-(Diethylamino)-Ethanol
DETA	Diethylenetriamine
DFT	Density Functional Theory
DI	Deionized
DMF	N, N-Dimethylformamide
EHA	2-Ethylhexyl Acrylate
FEP	Fluorinated Ethylene Propylene
FTIR	Fourier Transform Infrared
G-L	Gas-Liquid
G–L–L–S	Gas-Liquid-Liquid-Solid
H_2	Hydrogen Gas
HCR	Helical Coils Reactor
HPHT	High-Pressure High Temperature
HT	High Temperature
Hzn	Hydrazine Hydrate
ID	Internal Diameter
KOH	Potassium Hydroxide
LDL	Low Density Lignin
MCFI	Micro structured Coiled Flow Inverter

MDEA	Methyldiethanolamine
MEA	Monoethanolamine
MPDL	N-Methyl-4-Piperidinol
MTMR	Multitubular Millireactor
MW	Mega Watt
NC	Nano Celluloses
NMR	Nuclear Magnetic Resonance
O_2	Oxygen Gas
OD	Outer Diameter
PEHA	Pentaethylenehexamine
PEI	Polyethyleneimine
PEIS	Polyethylenimines
PI	Process Intensification
PPM	Parts Per Million
PT	Platinum
PZ	Piperazine
RTD	Residence Time Distribution
SCCFI	Symmetrical Compact Coiled Flow Inverter
SCCM	Standard Cubic Centimetres Per Minute
SDGS	Sustainable Development Goals
STP	Standard Temperature and Pressure
TCI	Tokyo Chemical Industry

T-MCR-SW	Spiral-Wired T-Type Microchannel Reactor
Un	Human Urine
Ur	Urea
Ur + L	Urea and Lignin solution without hydrothermally treatment
Ur – L	Urea and Lignin solution with hydrothermally treatment
USA	United State of America
UV	Ultraviolet
ZnO	Zinc Oxide

List of Symbols

SYMBOL	PARAMETERS	UNIT
Greek Letters		
σ	Standard Deviation	Same as original data set
ρ	Solution density	kg/m^3
τ	Residence Time	Sec
μ	Dynamic Viscosity	Pa-sec
Latin Letters		
A	Cross-sectional area of the Reactor	m^2
A_s	Surface Area of reactor	m^2
C_P	Specific Heat of solution of DMF and Gallic acid	$J/(kg℃)$
T_{Out}	Outlet temperature of solution from reactor	℃
T_{In}	Inlet temperature of solution from reactor	℃
$\dot{m}$	Mass Flow rate of solution of Gallic acid and DMF	Kg/hr
Q	Amount of heat	watt
V	Volume	mL
q'	Heat Flux	W/m^2
K_La	Overall volumetric mass transfer coefficient	1/sec
L	Total length of the test channel,	m

n	Number of data sets (number of times experiment conducted)	Dimensionless
Q_G	CO_2 gas flow rate	mL/min
Q_L	Liquid absorbent flow rate	mL/min
U	Velocity of solution inside reactor	m/sec
x_i	Original value obtained from experiments for each data set.	Same as original data set
$\bar{x}$	Average or the mean value.	Same as original data set

Preface

Industrial growth has significantly increased CO_2 emissions, creating an urgent need for efficient capture and utilization technologies. Conventional batch reactors are limited by slow processing, high energy use, poor heat and mass transfer rates, and lack of real-time monitoring. While continuous flow reactors offer some improvements, challenges such as flow visualization and controlling the hydrodynamics still remains. To overcome these limitations, this thesis proposes a novel glass-made Coiled Flow Inverter (CFI) reactor. Its transparent design allows real-time observation of product formation while its flow inversion at each 90° bend enhancing CO_2 capture and conversion efficiency due to its unique geometry. The work focuses on developing a continuous-flow CO_2 capture system using CFIs, along with exploring low-cost and eco-friendly absorbents such as lignin from agricultural waste and nitrogen-rich waste streams. Overall, the study aims to advance process intensification in CO_2 capture and promote sustainable materials, and also enable efficient organic transformations using flow chemistry.

Chapter 1- Introduction. This chapter presents an overview of the design and application of the Coiled Flow Inverter (CFI), along with its advantages over conventional batch and flow reactors. It includes a comprehensive survey of CO_2 capture in gas–liquid as well as liquid–liquid systems. Special emphasis is given to CO_2 capture using both amine-based and non-amine-based solutions, particularly sustainable materials such as biomass. Additionally, this chapter reviews recent advancements in organic reactions for the synthesis of fluorescent materials in liquid–liquid systems and also describes the methods used for spectroscopic interpretation and microscopic data analysis are systematically outlined.

Chapter 2- Materials and Methodology. This chapter outlines the materials and chemicals used for CO_2 absorption and the synthesis of fluorescent Xanthene dye in a Coiled Flow Inverter. It also provides a detailed description of the instruments and analytical techniques employed in the study. This chapter covers the synthesis procedures for CO_2 capture using both alkanolamines-based and amine-free systems. Also, chapter include bond formation along with C–H involving Gallic acid and N, N-dimethylformamide (DMF). In addition, it presents the experimental methodology for CO_2 capture and includes detailed mathematical calculations related to heat transfer processes.

Chapter 3- Hydrodynamics driven CO_2 Absorption in Coiled Flow Inverters using Amine Based Solvents. Driven by the United Nations' Sustainable Development Goals (SDGs), this study addresses the urgent need for efficient and sustainable carbon capture methods to reduce anthropogenic CO_2 emissions. Conventional batch processes using concentrated alkanolamines solutions are functional but hindered by high energy consumption and poor efficiency. To overcome these limitations, millimeter-sized coiled flow inverters (CFIs) have been used as point-source CO_2 capture tools capable of continuous operation. The study found that the solvent and CO_2 gas flow rates are key parameters that govern the slug flow regime and slug lengths within the CFI, with a high interfacial area and sufficient residence time identified as the primary drivers of enhanced CO_2 absorption. Notably, an approximate 98% CO_2 absorption efficiency was achieved using a 3% aqueous Diethanolamine (DEA) solution in the CFI system. Furthermore, the potential of Nano cellulose, an environmentally sustainable nanomaterial, is demonstrated for CO_2 capture at low flow rates, highlighting its promise as a green alternative for carbon-capture applications.

Chapter 4- Alkanolamine-free 96% CO_2 Capture using Coiled Flow Invertor: A Sustainable Scope. Conventional CO_2 capture systems use synthetic amines, which are energy-intensive, corrosive, and environmentally harmful. This creates a need for greener and more efficient alternatives. This study presents a flow-based approach for CO_2 absorption using waste-derived materials in a Coiled Flow Inverter (CFI) reactor. Human urine, rich in nitrogen compounds, is used as a natural amine substitute and combined with lignin obtained from rice straw, an abundant agricultural waste. The interaction between urine components and lignin improves CO_2 absorption, while the enhanced mixing and flow inversion in the CFI reactor increase mass transfer efficiency. Under optimized conditions, the lignin–urine system achieved up to 96% CO_2 removal, outperforming conventional systems. This approach demonstrates a low-cost, eco-friendly, and scalable solution for carbon capture, aligned with circular economy principles.

Chapter 5- Intensifying the Synthesis of Xanthene Dyes from Gallic Acid using Coiled Flow Inverter. Transparent coiled flow inverters (CFIs) offer clear advantages over opaque coil reactors but have rarely been used for condensation reactions. This study addresses that gap by demonstrating the continuous-flow condensation of Gallic acid in a 4 mm internal diameter CFI reactor. The length of the flow reactor is varied by connecting multiple CFIs in series, and real-time imaging of the reactor during flow synthesis provides valuable insights into reaction dynamics and the stages of desired product formation. The use of stacked CFIs ensures adequate residence time for carrying out reactions at high flow rates, while the condensation of Gallic acid in dimethylformamide (DMF) yields a green-emissive xanthene analogue, the production of which is optimized by regulating reactant flow rate and reaction temperature. The presence of a vapour–liquid phase boundary further enhances

interfacial area, contributing to improved product yield, and the optimized conditions for fluorescent product formation using the stacked CFI were identified as 190°C at a flow rate of 5 mL/h, with a residence time of approximately 14 hours and a heat flux of 4.46 W/m² required to maximize yield. Collectively, these findings demonstrate that CFI-based flow reactors are highly adaptable, easily tailored to specific reaction requirements, and economically viable, underscoring their broad potential for continuous flow organic synthesis.

Chapter 6- Summary and Future Scope. This chapter systematically conclude the design, hydrodynamics, and multifunctional applications of coiled flow inverter (CFI) reactors for sustainable CO_2 capture and continuous-flow organic synthesis. By enhancing mixing, mass transfer, and enabling real-time visualization, CFIs overcome key limitations of conventional reactors. The integration of waste-derived absorbents such as lignin and urine offer a low-cost, sustainable alternative to conventional amine systems, achieving high CO_2 removal efficiency. Additionally, the successful intensification of organic reactions highlights the broader applicability of CFIs in flow chemistry. Overall, this work establishes a scalable, eco-friendly approach that combines process intensification with waste valorization, contributing to sustainable carbon management and circular economy goals. A future direction of this work will be integration of carbon capture with CO_2 utilization through the catalytic conversion of CO_2-loaded absorbents into fuels and value-added chemicals.

Chapter 1: Introduction and Literature Survey

1.1 Introduction

Process intensification (PI) is a chemical engineering approach that aims to make a process smaller, safer, more energy efficient, and more sustainable while maintaining or improving product quality and production rates [1]. In simple terms, process intensification means achieving the same or better performance using less equipment, less energy, and less space [2]. One of the primary examples of process intensification is reducing the dimension of the reactor, such as millimeter-sized flow reactors and micrometer-sized flow reactors. As the reactor dimensions decrease, the surface area to volume ratio increases significantly, resulting in enhanced heat and mass transfer rates. This improvement allows better control of reaction conditions, reduced energy consumption, and higher process efficiency [3]. PI plays a crucial role in multiphase flow systems particularly in two-phase systems such as gas-liquid or liquid-liquid flow [4]. Reduction of diameter in two phase flow systems promotes the formation of flow patterns such as slug flow and dispersed flow which provides a large interfacial area and shorter diffusion paths. The most prominent being the slug flow in which two transport mechanisms, convection within individual slugs of each phase and interfacial diffusion between adjacent slugs of different phases occurs resulting in the enhancement of transport process. Consequently, mass transfer and reaction rates are substantially improved compared to other large-scale flow reactors and batch reactors.

The following are some examples in which process intensification techniques have been applied in varied areas:

- CO_2 absorption in a millimeter-scale flow reactor using an amine-based solvent in which formation of slug flow and Dean vortices continuously renew the gas-liquid interface. This phenomenon leads to enhancement of reaction performance, mass transfer and heat transfer as compared to a conventional absorption column.
- In a nitration or oxidation reaction, two immiscible liquid reagents while flowing simultaneously forms slug flow in a capillary. This removes the hotspots, improving selectivity, and avoiding runaway exotherms.
- The synthesis of fluorescence dyes in reduced dimensions (millimeter sized reactors) has more yield with higher process efficiency due to the large surface area to volume ratio of reactor geometry and higher mixing efficiency due to vortex flow.

Therefore, reduced-dimensional reactors and two-phase flow technologies have become powerful tools for process intensification, enabling compact equipment design, improved transport phenomena, enhanced product quality, and sustainable chemical processing. However, further process intensification in this system can be achieved by making appropriate geometrical modifications to the flow channels. In millimeter-sized reactors, the channel geometry strongly influences the fluid flow behavior and mixing characteristics. Various geometrical configurations such as bends, helical coils, and coil flow invertors (CFIs) have been studied by many researchers to enhance reactor performance beyond what can be achieved through miniaturization alone. Among these

designs, helical coils reactor (HCR) generate centrifugal forces due to channel curvature, leading to the formation of secondary flows known as 'Dean vortices [5]. Dean vortices are secondary counter-rotating flow structures generated in curved tubes due to centrifugal forces. These vortices improve radial mixing and enhance heat and mass transfer rates compared to straight channels. Further geometrical modifications involving periodic bends and changes in coil orientation can intensify these secondary flows. The periodic bends and changes in coil orientation continuously reform Dean vortices which enhances secondary flow and results in enhanced mixing. Among these various geometrical modifications, the coil flow inverter (CFI) is the most promising one for process intensification in millimeter-scale systems. A CFI consists of a helical coil with periodic 90° inversions in the coil plane [6]. These inversions repeatedly follow the direction of centrifugal forces acting on the fluid, causing the Dean vortices to break and reform continuously throughout the reactor length. As a result, fluid elements experience enhanced cross-sectional mixing, reduced axial dispersion and improved residence time distribution [7]. Glass-made millimeter-sized CFI offers several additional advantages. Glass is chemically inert, transparent, corrosion-resistant and capable of withstanding a wide range of operating conditions. The transparency of glass enables direct visualization of flow patterns, bubble dynamics, slug formation and phase interactions, making it particularly useful for fundamental hydrodynamics studies.

In gas-liquid systems, the periodic flow inversion in CFI promotes bubble breakup, increases gas-liquid interfacial area, and enhances mass transfer coefficients [8,9]. Consequently, glass-made CFI has emerged as a highly capable process intensification device for applications such as CO_2 capture, nanoparticle synthesis, mass and heat transfer

study and even synthesis of specialty chemicals. In current work, process intensification is achieved by performing the Gallic acid-DMF fluorescent dye synthesis in a millimeter scale CFI reactor. The enhanced mixing, better heat transfers and better hydrodynamics result in higher yield, lower reaction time and better process efficiency as compared to conventional batch synthesis. The current work also focusses on CO_2 capture using CFI. Conventionally, CO_2 capture has been carried out using large-scale absorption columns such as packed columns and bubble columns, where aqueous amine solution is commonly employed as a chemical absorbent. Monoethanolamine (MEA), Diethanolamine (DEA), methyldiethanolamine (MDEA) and their blends have been extensively used because of their high affinity towards CO_2 [10,11]. Although these conventional technologies are well established, they suffer from several limitations, including large equipment size, high energy consumption for solvent regeneration, limited gas-liquid interfacial area and mass transfer constraints. To overcome these limitations, process intensification strategies have been employed to enhance CO_2 absorption efficiency while reducing equipment size and optimizing the operating parameters. One such approach involves the use of a blended amine system, where two or more amines are combined to exploit their complementary advantages. In the present study, in addition to conventional CO_2 capture approaches, several process intensification strategies have been explored to enhance the absorption performance. The first approach involves the use of aqueous amine solutions of varying concentrations as well as blended amine systems for CO_2 absorptions in CFI. In addition, solvent modifications play a crucial role in intensifying the CO_2 capture process. The amine-functionalized alkali lignin (derived from rice straw) is one of these, and due to its low cost and wide availability, it offers significant potential as a sustainable solvent

component for carbon capture applications. The second approach applied in the current work is use of lignin-based solvents and combinations of various bio solvents like human urine for CO_2 capture in CFI as well as Nano celluloses derived from bio waste has been used as CO_2 capture absorbent. Furthermore, the utilization of biomass-derived materials aligns with green chemistry and the circular economy by converting a low-value industrial byproduct or agricultural waste into a value-added carbon-capture medium.

1.2 Literature Survey

The literature survey divided in three section as follows:

1.2.1 Reactor Geometrical Modifications as a tool of Process Intensification: Coil Flow Invertor

Any geometry-based PI strategy in tubular reactors starts from the observation that the curvature itself induces secondary motion. William Reginald Dean [5] was the first to investigate the flow in helically coiled circular tubes, and found that a pair of symmetric vortices is formed on the cross-sectional plane due to the centrifugal force, a phenomenon now characterized by the dimensionless Dean number [6,12,13]. In a helical pipe the flow is fully developed after about the first 2-3 turns for almost all laminar Reynolds numbers, and the fluid is then trapped in two counter-rotating vortices, so that the further turns only slowly improve mixing and the extra coil length is no longer of much use for mass or heat transfer[14].

This limitation motivated the device central to your reactor platform. Saxena and Nigam [15] studied the effect of introducing equally spaced 90° bends along a helically coiled tube, which produced a drastic narrowing of the residence time distribution and pushed the system

toward plug-flow behavior. They examined design parameters including the number of bends, bend angle, and bend spacing, and proposed an optimal configuration. The underlying mechanism is geometric: because the direction of centrifugal force is always perpendicular to the coil axis, a 90° bend in the coil axis rotates the plane of vortex formation a phenomenon termed flow inversion. This periodic reorientation forces a new vortex pair to develop at each bend, preventing the stagnation that limits plain helical coils and producing a significant increase in mixing, heat, and mass transfer. This inversion strategy is shown to be really effective in early characterization work. Saxena and co-workers [6,16] used a total of 57 bends to obtain the narrowest residence time distribution reported for any laminar-flow apparatus to date.

The design of CFI has evolved towards greater footprint efficiency. Two concepts of compact coiled flow inverters (CCFIs) have been introduced: one is a symmetrical design featuring numerous 90° bends, while the other is an asymmetrical design that maximizes the mixing volume. Both concepts occupy the same footprint as a standard CFI. The three geometries are then compared through experimental and numerical methods, employing the dimensionless dispersion number and a mixing efficiency metric that considers the pressure-drop penalty associated with induced radial mixing [17]. This research positions CFI design as a constrained optimization problem, focusing on maximizing mixing intensification per unit floor area rather than per unit reactor length. One of the earliest studies on CFI is deal with RTD characteristics in gas-liquid systems. Vashisth and Nigam [6] found that the dispersion number in a CFI is far lower than that of a conventional helical coil. The reduction of axial dispersion for two-phase flow is found to be 2.6 times higher in CFIs with multiple

bends, indicating better mixing and reactor performance. These results showed the promise of CFIs as intensified reactors for multiphase processes.

Other studies focused on the thermal performance of CFIs. Kumar et al. [18,19] reported that at low Reynolds numbers, the heat-transfer coefficients of the CFI heat exchangers are about 25% higher than those of the conventional helical coils due to the intensified radial mixing generated by flow inversion. A new set of hydrodynamic and heat-transfer correlations is developed, showing that CFIs can be used as compact heat-transfer devices. Further developments have been reported by Mandal et al.,[20,21] who compared the CFI heat exchangers with conventional shell-and-tube and plate heat exchangers. The CFI configuration showed better thermal performance and a smaller footprint, thereby confirming the applicability of the process intensification technology. The role of CFI in enhancing mixing and transport phenomena has also been investigated by using computational fluid dynamics (CFD) studies. Numerical analyses showed that periodic inversion of Dean vortices can enhance the chaotic advection and radial transport, leading to more effective mixing than a standard helically coiled tube. These studies verified that the repeated reorientation of secondary flow structures is the main mechanism for transport enhancement in CFIs [22,23].

Recently, CFIs have been used in reaction engineering applications. Studies of liquid-liquid reactive systems suggest that CFIs lead to better contact and mixing of reactants, resulting in improved reaction performance under laminar-flow conditions [7,21,24,25]. The improved mixing generated in CFIs makes them attractive alternatives to conventional tubular reactors for chemical synthesis and multiphase reactions. Also, enhancement of mass transfer in segmented gas-liquid flow has been observed. Numerical studies have shown that

the volumetric mass-transfer coefficients are greatly enhanced in coiled and CFI channels due to the simultaneous presence of Dean vortices and Taylor circulation inside the liquid slugs [6,14,16,26]. A 50% improvement in mass transfer over straight channels is observed, demonstrating the promise of CFI reactors for gas-liquid operations such as absorption, extraction, and carbon capture [26]. Further intensification of reactor performance has been sought by proposing several modified CFI geometries [27,28]. Compact Coiled Flow Inverters (CCFIs) are developed for improved mixing efficiency in the same footprint as traditional CFIs. The narrower RTD profiles and the better mixing performances detected by experimental and numerical studies suggest the enhanced capability of process intensification [15,25]. In general, the literature clearly shows that CFIs have significant advantages over straight and helical tubular reactors, improving heat transfer, mass transfer, mixing, residence time distribution, and reaction performance [6,7,13,15,29,30]. These features make CFIs highly attractive as process-intensification tools for applications such as heat exchange, liquid–liquid reactions, gas–liquid absorption, extraction, nanoparticle synthesis, biochemical processing, and carbon capture. The CFI is regarded as one of the most promising reactor configurations for modern intensified chemical processes due to the combination of improved hydrodynamics, compactness of the reactor, and enhanced transport phenomena [17,31,32].

1.2.2 Process Intensification in Gas-Liquid reaction for carbon capture

Gas-liquid absorption for carbon dioxide (CO_2) capture is one of the most mature technologies for greenhouse gas emission mitigation [10,31,33]. Conventionally, packed and tray columns with aqueous amine solutions such as monoethanolamine (MEA), diethanolamine (DEA), methyldiethanolamine (MDEA) have been widely used for post-

combustion carbon capture. However, these systems are characterized by large size of the equipment, high energy consumption and mass transfer limitations [11,34–36].

In the context of carbon capture, the main goal of process intensification is to maximize the interfacial area for gas-liquid mass transfer and to minimize the resistance to diffusion. To address this, different intensified technologies have been studied, such as rotating packed beds, spinning disc reactors, membrane contactors, microreactors and milli reactors [37–39]. The high shear rates, thin liquid films and enhanced mixing conditions generated by these devices lead to considerably higher volumetric mass-transfer coefficients than those of conventional absorbers [17,31,32,40,41]. In the various PI strategies, microreactors and millimeter-scale flow reactors have recently gained much attention owing to their high surface-area-to-volume ratio and accurate control of hydrodynamics. The small channel dimensions lead to shortened diffusion lengths and promote the formation of slug-flow, which increases the gas-liquid interfacial area and enhances the CO_2 absorption efficiency [36]. A detailed analysis and comparison of gas-liquid reaction in millichannels, helical coils and coiled flow inverters has been tabulated in Table 1.1.

Table 1.1: Development of gas-liquid reaction in mill channels, helical coils and coiled flow inverters

Author	System Used/Reactor	Development	Key findings
Kurt et al.[17]	Co(II)-catalysed air oxidation of sodium sulfite (G–L) (CFI)	First dedicated G-L mass transfer study in a microstructured CFI (MCFI, Fluorinated Ethylene Propylene tube, ID = 1 mm); benchmarked against straight capillary, helical coil and bend reactor.	MCFI achieved the highest G–L conversion; 90° bends inverted Dean vortices between planes, eliminating stagnant cross-sectional zones. Slug-flow pressure drop correlated with coil curvature and gas fraction. CFI outperformed all single-geometry benchmarks.
Jha et.al. [19]	Symmetric and asymmetric compact CFI (Symmetrical Compact Coiled Flow Inverter/ Asymmetrical Compact Coiled Flow Inverter) mixing RTD	Two novel compact CFI variants (symmetric SCCFI, asymmetric ACCFI) assessed against standard CFI through step-input RTD experiments and CFD under diffusion-free laminar flow.	Symmetric CCFI exhibited the highest mixing coefficient of all variants due to greater number of bends per footprint area. RTD narrowing confirmed superior plug-flow approach. CFD revealed stronger secondary flow inversion at bends in SCCFI.
Gaddem et al.[26]	G–L slug flow Computational Fluid Dynamics in helical coil and CFI	Novel CFD model using a virtual centrifugal body force in a straight-slug frame to simulate helical coil and CFI without meshing the full 3D geometry.	k_La in helical coil is 1.5X higher than in a straight channel; enhancement peaked at a modified Dean number of 1.2. The CFI further narrowed RTD beyond the helical coil alone.

Kockmann et al.[28]	Two-phase flow (L-L extraction + biocatalysis) batch-to-continuous transfer	Two-phase (organic aqueous) slug flow in CFI for (i) extraction into continuous phase and (ii) laccase-catalysed 2,2'-Azino-Bis (3-Ethylbenzothiazoline-6-Sulfonic Acid) oxidation; straight capillary used for initial screening before CFI scale-up.	Yields in CFI exceeded due to enhanced inter-phase mass transfer from Dean vortex mixing. Enhanced product partitioning into continuous organic phase observed versus batch.
Yang et al. [31]	G–L Taylor flow, local mass transfer at meandering (repeated bends) square channel bends	Visualization and CFD to resolve local mass transfer around Taylor bubbles in a meandering millimetric square channel, Dean flow asymmetry at bends compared with straight segments.	At bends, Dean flow broke the symmetry of liquid-slug recirculation vortices, enhancing convective mass transfer. Smaller bend radius and higher flow rate significantly increased vortex strength; mass transfer at bends exceeded straight-segment values.
Khan et.al.[32]	4-phase G–L–L–S selective hydrogenation of cinnamaldehyde (H_2 / Pt/C catalyst)	Continuous 4-phase (H_2, organic liquid, aqueous KOH, solid 5% Pt/C) helical coil reactor designed and optimized, role of gas solubility, kinetics, axial dispersion and mass transfer systematically analyzed.	Addition of aqueous KOH second liquid phase significantly increased selectivity toward cinnamyl alcohol. Helical coil provided adequate G–L–L–S contacting; flow hydrodynamics critical for maintaining selectivity at scale.
Tiwari et. al.[42]	Continuous flow photochemistry (ZnO-APTMS-Au photocatalyst,	CFI used as a static mixer inside a photoreactor chamber; fluorescence imaging introduced to map irradiance distribution on	Chaotic advection from Dean vortices and 90° bends combated light attenuation. Multiaxial lighting more effective than uniaxial for uniform irradiance;

	fluorescein degradation)	curved, non-planar CFI surfaces.	CFI delivered competitive photon efficiencies for continuous-flow photocatalysis.
Grühn et al.[43]	Biocatalytic oxidation of ABTS by laccase O_2 mass transfer (CFI)	G–L CFI used as a miniaturized bioreactor, enzyme concentration and O_2 content, k_La and specific interfacial area calculated from bubble count and size.	Continuous biocatalysis transferred successfully from CFI to stirred-tank using k_La as scale-up key parameter. Specific phase interface 449 bubbles × 20.1 mm² each; k_La two orders of magnitude lower than bubble columns due to limited O_2 supply (3 vol%), confirming oxygen-limited conditions.
Tomar et.al. [44]	Photocatalytic degradation of paracetamol (advanced oxidation, G–L)	CFI photoreactor with Graphitic Carbon Nitride-Supported Co-Ni Tungstate catalyst used for continuous pharmaceutical micropollutant degradation; recycle ratio, catalyst dose, and CFI configuration (4×4) systematically optimized.	99% photodegradation of paracetamol (10 ppm) in 36 min. CFI degradation rate is 2.7X faster than equivalent batch reactor. Chaotic advection from Dean vortices and bends enhanced photon–catalyst–reactant contact uniformly across reactor volume.
Ning et al. [45]	CO_2 absorption in glycerol–water, spiral-wire element millichannel (T-MCR-SW)	Straight millichannels with and without internal spiral-wire inserts compared for Gas–Liquid CO_2 mass transfer. K_La measured via chemical absorption, pressure drop also quantified.	Spiral-wire millichannel KLa substantially higher than smooth Spiral-Wired T-Type Microchannel Reactor; however, pressure drop nearly doubled — requiring a balance between mass transfer efficiency and energy cost. Provides design guidance

			for viscous-fluid millichannel G–L systems.
Mierka et.al. [46]	G–L slug flow DNS with 90° bend influence (Dean–Taylor flow)	Full direct numerical simulation of dispersion and mixing in G–L D Taylor slug flow through a helical capillary (ID = 1.6 mm) with a 90° bend; particle-tracking dispersion analysis performed.	Coil diameter influence on dispersion at the 90° bend is smaller than the influence of flow velocity (centrifugal force). High statistical variance of particle positions at bends challenges direct quantification. Mean mixing coefficient increased with gas velocity but is nearly independent of liquid velocity.

Apart from conventional amines, blended amines, ionic liquids, deep eutectic solvents and biomass derived absorbents have been studied to enhance the CO_2 loading capacity and to reduce the energy required for the regeneration [47–51]. The coupling of new generation solvents with intensified reactor configurations is considered a promising path towards sustainable and economic carbon capture processes. In addition, the hydrodynamics of gas-liquid has a very important role in absorption performance. Flow patterns such as slug flow, annular flow and bubbly flow directly affect interfacial area, liquid-film thickness and mass-transfer coefficients [52]. Some salient studies on CO_2 absorption using amine solvents is presented in Table 1.2.

Table 1.2: Salient studies on CO_2 absorption using amine solvents

Author	Reactor Used	Dimensions of rector		Solvent used	Capture Efficiency
Pan et al.,[11]	microporous tube-in-tube micro reactor	D=5-80 µm,	L= 17 mm	Aq. N-methyldiethanolamine, piperazine	97%
Durgadevi et.al.[36]	Glass, T-Shape straight milli channel	D= 2 mm,	L= 10 cm	Aq. NaOH	
Bangerth et al.[53]	Polyphenylsulfone, T- shape,	D=762 µm,	L= 1.37 cm	Aq. DEA	68%
Ganapathy et al.[54]	PTFE microchannel	D = 0.75 mm		Aq. DEA	90%
Ganapathy et al.,[55]	Polyphenylsulfone t-shape	D =0.762 mm,	L =0.5,0.3,0.1 m	Aq. DEA	95%
Zhu et al.,[56]	Square cross section Microchannel	L= 30 mm,	A_{CS} = 400 µm ×400 µm	Aq. Sodium glycinate	80%

The main post treatment methods are based on the chemisorption of the amine-based solvents like ammonia, monoethanolamides (MEA), diethanolamine (DEA) and N-methyldiethanolamine (MDEA). The traditional equipment of CO_2 absorption widely used in industry has the disadvantages of large volume and low efficiency. To enhance the absorption efficiency milli and micro reactors have been used [57–59]. However, microchannel-based process intensification has been widely studied to enhance the effectiveness of multiphase reactors [38,60–62]. Niu et al. experimentally studied the performance of microchannel contactors for the absorption of CO_2 with an aqueous solution

of piperazine (PZ) and N-methyldiethanolamine (MDEA) [63]. Several operational parameters have been studied: the activator, the temperature of the gas and liquid flow, the inlet CO_2 molar fraction, the superficial velocities of gas and liquid, and the operating pressure. Mikaelian et al. demonstrated the collapse of a series of gas bubbles in a non-volatile liquid. The authors observed the contraction of the slug and the physico-chemical features of the solution and the operational environment would influence its incomplete dissolution [40,41,64–66]. Amine-based solvents are unsustainable and easily oxidized in synthetic protocols of intensive energy economics such as High-Pressure High Temperature (HPHT) reactions that emit significant CO_2. Amine solvents are corrosive, volatile and toxic and regeneration via hydrogenation is energy intensive [50,67–71]. These problems are being addressed by using sustainable nanomaterials as co-solvents to improve the sustainability of CO_2 capture technology.

1.2.3 Process Intensification of CO_2 Capture through Bio-Derived Lignin-Based Absorbents for a Circular Carbon Economy

Process intensification (PI) has traditionally improved process performance by reactor design, transport phenomena and equipment miniaturization. Next-generation carbon capture systems are promising for bio-derived absorbents. In aqueous media, urea can stabilize bicarbonate through hydrogen-bonding, which can replace traditional amine-based solvents in CO_2 capture. However, the energy-intensive Haber–Bosch process for the synthesis of synthetic urea leads to indirect CO_2 emissions [72–75]. In contrast, the bio urea (10-20 g/L) present in human urine bypasses the energy intensive synthesis and is therefore inherently more carbon-efficient. Urine also has a high level of inorganic salts (10-20 g/L) which contribute to the bicarbonate stabilization capacity by ionic interactions [76–80].

However, the benefits are offset by the large volumes of water used to flush urine away, putting stress on sewer systems. Thus, the application of urine in CO_2 capture has a double advantage of carbon neutral storage and reduction of water consumption of waste management. However, in gas–liquid CO_2 absorption systems, the liquid viscosity is important; higher viscosity slows down the diffusion of CO_2 in the liquid and increases the overall capture efficiency [81–84]. Polymer-based viscosifiers are preferred over molecular additives such as ethylene glycol and glycerol due to their higher thickening efficiency at low concentrations, better thermal and chemical stability, and negligible volatility [85–87] . Alkali lignin is a natural polymer derived from lignocellulosic biomass and has a great potential, but is not fully exploited [88]. The aromatic backbone of lignin, the high density of hydroxyl groups and the strong hydrogen-bonding network, together with the solubility of lignin in aqueous media, can synergistically improve the CO_2 absorption in aqueous media [89,90]. Furthermore, alkali lignin can be conveniently amine-functionalized by bio urea and ammonia species in urine through a one-pot solvothermal process to improve the CO_2 solubility and mass transfer properties [91–94]. The combination of urine-lignin based absorbents is a promising approach to couple two abundant waste streams for a sustainable, circular and cost-effective route for CO_2 capture. The utilization of alkali lignin obtained from rice straw is especially important in countries producing rice. Due to the low bulk density that results in transportation and storage difficulties and the lack of feasible technologies for value-added utilization, rice straw is often subjected to extensive open-field burning which contributes significantly to severe air pollution and environmental degradation [95–98]. Nanocellulose, comprising cellulose nanocrystals (CNCs) from acid hydrolysis of cellulosic biomass and cellulose nanofibers (CNFs) by mechanical

defibrillation, has been recognized as a promising sustainable material for CO_2 capture. The properties of CNCs and CNFs are complementary, such as high aspect ratios (CNCs: 10–50, CNFs: 50–500), excellent mechanical strength comparable to Kevlar (Kevlar is high strength, lightweight synthetic fiber used as benchmark for exceptional mechanical strength), and abundant surface hydroxyl groups that can be chemically functionalized with amine, carboxyl, sulfonate, or other CO_2 -reactive groups [99]. The high specific surface area (150–300 m^2/g for well-dispersed CNCs) provides a large number of accessible active sites, which leads to the enhanced CO_2 adsorption and absorption performance [99–104]. The transformation of such agricultural waste into functional CO_2 -capture materials can not only reduce environmental pollution but also generate economic value, supporting the net-zero emission strategies [105–108]. Table 1.3 depicts some recent on CO_2 capture in amine functionalized liquids**.**

Table 1.3: Recent developments on CO_2 capture in amine functionalized liquids

Author	Absorbent	Key Findings
Rochelle, G. *et al.*[109]	Piperazine (40 wt%)	• A new solvent system with regeneration at 150 °C as an alternative to conventional 30 wt% Monoethanolamine (MEA) and 50% lower energy demand. • The absorbent offers higher oxidative stability, lower volatility, and reduced corrosion of stainless steel compared to MEA.
Apaiyakul, G. *et al.*[110]	2-amino-2-methyl-1-propanol (AMP) and N-methyl-4-piperidinol (MPDL)	• AMP–MPDL blended solvents (30–40 wt%) offers significantly enhanced CO_2 capture performance. • Compared with 30 wt% MEA, AMP–MPDL achieved 26–48% higher CO_2 absorption capacity, 3-4 times greater cyclic capacity, and 60-68% lower regeneration energy demand.
Hamzehie, M. E. *et al*[111]	Potassium glycinate and 2-amino-2-methyl-1-propanol (AMP)	• The blends offer higher CO_2 loading, faster absorption kinetics, and excellent oxidative stability, making them promising solvents for flue-gas carbon capture. • An ANN model accurately predicted CO_2 solubility, outperforming the extended Deshmukh–Mather thermodynamic model.
Xu, X. *et al.*[112]	Amino acid Salts (AAS) solution in acrylamide-based hydrogel particles	• Encapsulated amino acid salts into hydrogel particles offer increased CO_2 uptake by ~40% and enhanced absorption kinetics compared to aqueous AAS solutions. • Hydrogel sorbents enable low-temperature regeneration (60 °C–steam/vacuum).
Gurkan, B. E. *et al*[113]	Amine functionalized ionic liquids-trihexyl(tetradecyl)phosphonium methioninate [P66614][Met] and prolinate [P66614][Pro]	• Amine-functionalized ionic liquids offer near 1:1 CO_2 absorption stoichiometry, delivering up to twofold higher capture efficiency than conventional ionic liquids and aqueous amines.

		• DFT studies confirm reaction energetics, demonstrating their potential as high-capacity CO_2 absorbents.
Al Abdulghani, A. J. *et al.*[114]	Branched polyethylenimine (BPEI) functionalized with acrylonitrile (AN), 2-ethylhexyl acrylate (EHA), and butyl acrylate (BA) is impregnated onto fumed silica	• Functionalized BPEI–silica adsorbents achieved ultra-low CO_2 regeneration temperatures (as low as 25 °C) while maintaining stable performance over 20 adsorption–desorption cycles. • Machine-learning-guided Bayesian optimization identified optimal adsorbent compositions, balancing high CO_2 uptake with low regeneration energy requirements for industrial carbon capture.
Liu, F. *et al.*[115]	2-(diethylamino)-ethanol (DEEA) and 2-((2-aminoethyl)amino) ethanol (AEEA) blend	• A biphasic 60% DEEA/20% AEEA solvent achieves 60% higher CO_2 capacity and 44% lower regeneration energy than conventional MEA. • Phase separation concentrates CO_2-rich species in one phase, enabling selective regeneration and significantly reducing stripping energy requirements.
Wang, R. *et al.*[116]	Diethylenetriamine (DETA) + 1-propanol	• This biphasic solvent offers rapid CO_2 absorption, high loading (6.54 mol L^{-1}), and tunable phase separation through simple solvent composition control. • The solvent reduces regeneration energy to 2.12 GJ t^{-1} CO_2 (46.9% lower than MEA).
Choi, W. *et al.* [117]	Functionalized-polyethyleneimine (PEI)/silica	• Epoxybutane-functionalized PEI/silica adsorbents offer a high CO_2 working capacity of 2.2 mmol g^{-1} with >99% regeneration efficiency at 120 °C. • It lowers the heat of adsorption and suppressed urea formation and oxidative amine degradation.
Spinu, D. *et al.* [118]	Impregnated pentaethylenehexamine (PEHA) and branched polyethylenimines (PEIs) onto silica gel	• PEI12-40/silica sorbent offers vacuum-assisted CO_2 capture and regeneration at 100 °C and superior thermal stability.

		• High polymer loading (40 wt%) and higher-molecular-weight PEI (MW 1200) minimized polymer leaching and improved durability.
Nakrak, S. *et al.* [119]	2-amino-2-methyl-1-propanol (AMP) - piperazine (PZ) - monoethanolamine (MEA) blend	• AMP–PZ–MEA blend (1.5:1.5:3) enhances CO_2 removal by 14%, absorption capacity by 15.1%, and cyclic capacity by 66.7% compared with 5 M MEA. • Blend also reduces regeneration energy demand by 50%.

1.2.4 Fluorescent chemical synthesis via flow chemistry as a process intensification strategy

Fluorescent chemicals are used in bio imaging, chemical sensing, environmental monitoring, forensic analysis, photovoltaics, light-emitting devices, and biomedical diagnostics. Fluorescent compounds have been continuously synthesized using batch reactors [120–123]. The effectiveness of chemical synthesis depends on the kinetics of the reaction, temperature, catalyst concentration, and solvent choice. Batch processing is very convenient, but it often suffers problems of heat and mass transfer, non-uniform mixing, wide residence-time distribution, and scale-up [124–127]. These limitations can result in lower product yields, selectivity, and by-product formation in fast or highly exothermic reactions. The process intensification in this case can be attained through the design of the reactor geometry and the optimization of operative conditions [4,128–132]. These approaches improve mixing, heat and mass transfer and reaction kinetics leading to higher conversion of reactants, better product selectivity and higher product yield with lower reaction time and energy consumption [129,131]. In the context of intensification on operating conditions, flow rates, temperature, pressure are the key parameters. In continuous flow synthesis, oil bath heating is a common method of temperature control, as it is simple,

cost-effective and provides uniform heating over a wide temperature range. The thermal management of the reactor has been investigated by Liu et al. using COMSOL CFD simulations to study the effects of local heating and cooling at the reactor inlet and outlet [61,123,133–135]. Naughton et al. successfully synthesized high quality CdSe/ZnS and fluorescent nanocrystals using a continuous flow technique in a stainless steel microreactor heated by a Dynalene HT oil bath [136]. Pal et. al. demonstrated the synthesis of photoluminescent organic nanostructure by self-assembly of fluorophores by precursor as DMF and pyrogallol via Archimedean reactor made of stainless steel [137]. Narendra G. Patil et.al. demonstrated continuous-flow synthesis of 1,3-diphenyl-2-propynyl piperidine from piperidine, benzaldehyde and phenylacetylene using a multitubular millireactor/heat exchanger (MTMR) assembly. This process give a high product yield with a productivity of 1 kg/day. In the MTMR system, the reactants have been supplied through the mill tubular reactor channels while the coolant flowed in the shell side, allowing efficient heat transfer and temperature control [138]. Moreover, the continuous operation in a single-mode microwave cavity demonstrated that the microwave absorption has been significantly enhanced by coating a thin Cu film (350 ± 40 nm) on the inner walls of the reactor tubes, and the overall heating efficiency is improved [138]. Studies show that process intensification by temperature control improves reaction kinetics, product quality and synthesis efficiency [129,131,132].

1.3 Lacuna in past literature

Based on the literature review above the following lacunae have been identified:

- Very few studies have been reported for glass-made coil flow inverter (CFI) reactors, which allow in situ visualization of gas-liquid hydrodynamics, slug flow behavior and product formation at various locations within the reactor.

- Limited studies have been done on CO_2 capture by amine-functionalized lignin absorbents, and amine-functionalized Nano cellulose in glass-made CFI reactors.
- The effect of enhanced mixing in CFI reactors on the process intensification of single-phase reactions has not been systematically studied, especially in the case of the synthesis of fluorescent chemicals and fluorophores.
- The potential performance of human urine as a low-cost and sustainable absorbent for CO_2 has not been fully investigated. In addition, its incorporation into CCUS systems as a circular economy approach is a new frontier.

1.4 Objective of the present study

The objective of the present study, considering the widespread use of gas-liquid flow in milli channels and the research gaps identified in previous studies are as follows:

- To study the effect of reactor geometry (helical coil reactor and coil flow inverter), aqueous amine concentration, amine blending and Nano cellulose (NC) addition on the efficiency of CO_2 absorption in a gas–liquid flow systems.

- To study the potential of amine-functionalized lignin as a CO_2 absorbent in a coil flow inverter (CFI) reactor and to improve the process by optimizing the operating parameters to obtain the highest CO_2 absorption efficiency.
- To evaluate the feasibility of using human urine as a sustainable CO_2 absorbent and its integration into Carbon Capture, Utilization, and Storage (CCUS) for the production of value-added chemicals, thus promoting waste valorization and a circular economy.
- To investigate the effect of geometrical modifications by increasing the length of the reactor via stacking of coil flow inverter (CFI) reactors, and its effect on the product yield of xanthene fluorescent dye. And also, the operating conditions are designed for the maximum yield of the product.
- To develop a glass-made coil flow inverter (CFI) reactor for in situ visualization of gas-liquid slug flow, and to enable direct measurement of slug characteristics affecting the reaction and mass transfer rates.

1.5 Organization of the thesis

The work is divided into seven chapters. As shown in Table 1.4. The findings of the study have been elaborated in chapter three to five.

Table 1.4: Arrangement of the different chapters in the dissertation

Chapter Number	Study proposed
Chapter 1	This chapter deals with the general introduction of the topic with its application and the focus of the present study with a detailed literature survey with lacuna.
Chapter 2	The experimental facilities has been presented and the experimental procedure has been described in this chapter.
Chapter 3	Improvement of CO_2 absorption in a millimetre-sized coiled flow inverter. The effect of reactor geometry and the flow rates of gas-liquid on the slug flow and the efficiency of CO_2 absorption has been presented.
Chapter 4	Solvent Intensification for CO_2 Capture Using Alkanolamines-Free Bio-derived absorbents have been investigated in this chapter. Furthermore, effect of bio-derived lignin, amine-functionalized lignin, and human urine-based absorbents have been studied. In order to develop a sustainable approach for carbon capture, the effect of absorbent composition and operating conditions on gas-liquid mass transfer and CO_2 absorption has been systematically evaluated.
Chapter 5	Continuous flow synthesis of a xanthene dye from Gallic acid in a glass based coiled flow inverter have been studied in this chapter. Further the continuous-flow synthesis of fluorescent xanthene analogue in a glass-made Coiled Flow Inverter has been optimized by the geometry of the reactor. The effect of operating parameters to intensify the reaction kinetics and maximize the fluorescence yield have also been investigated in this chapter.
Chapter 6	Conclusion and future work.

Chapter 2 Experimentation

2.1 Introduction

Extensive experimental studies have been conducted for in-depth understanding of the hydrodynamics, mass transfer properties, and reaction kinetics of gas-liquid and single-phase flows in millimeter-sized continuous flow reactors. In-depth studies have been performed on low-density lignin synthesis, Nano cellulose loading's impact on CO_2 absorption, human urine as a sustainable CO_2-absorbing liquid, and continuous synthesis of a fluorescent dye using the CFI platform. The reactor system chosen includes a helical coil reactor and a coiled flow inverter, which have inner diameters of 4 mm and 6 mm, respectively, and a total tube length of 2.5 m. These designs are chosen to systematically study the effect of geometry and internal diameter on flow behavior and reaction performance under otherwise equivalent operating conditions. This chapter provides a full description of the experimental setup, reactor settings, instrumentation, and operating experimental protocols.

2.2 Test Fluids Used

2.2.1 Aqueous Solution of Amines

The test fluids used in work for the CO_2 absorption using amine solutions in helical coil reactor and Coil flow invertor comprised of aqueous amine solutions, including Diethanolamine (DEA) and methyldiethanolamine (MDEA), prepared with deionized (DI) water at concentrations ranging from 3 to 7 vol.%. In addition, blended amine solutions containing both MDEA (1 vol.%) and DEA (3 to 7 vol.%) in water have been also investigated. In order to visualize the flow behavior (slug flow dynamics) within the

millichannel, a high-resolution imaging system via digital camera is used. The amount of CO_2 absorbed by the absorbent solution has been evaluated using acid-base titration method, with phenolphthalein serving as the endpoint indicator. Titration data is used to determine absorbed CO_2 using normal stoichiometric formulas. Using a technique developed in our lab, nano cellulose (NC) has been prepared [139].

2.2.2 Alkanolamine- free CO_2 capture solvent

The absorbents used for CO_2 capture is low density lignin solution, whereas lignin is combined with hydrazine, ammonia, urea, and human urine at a molar ratio of 1:15 to create lignin-based absorbents for sustainable route. Urea (liquid-grade), hydrazine hydrate, and ammonia solution have been obtained from Molychem, Rankem, and Fine Chemical Co. Ltd., respectively. Ethanol (analytical grade) is also obtained from Fine Chemical Co. Before being used in CO_2 absorption studies, the resultant mixtures underwent an 8-hour hydrothermal treatment at 160 °C. Additionally, low density lignin is combined with hydrazine, ammonia, and urea at a molar ratio of 1:15 to create lignin-based absorbents, and human urine are combined with lignin at the same volumetric proportion. Human urine has been directly used fresh urine has been collected directly into a container preloaded with lignin. The resulting urine–lignin solution is used within 12 h of collection for solvothermal experiments. The alkali lignin is extracted from rice straw using the soda-pulping process with 3% NaOH.

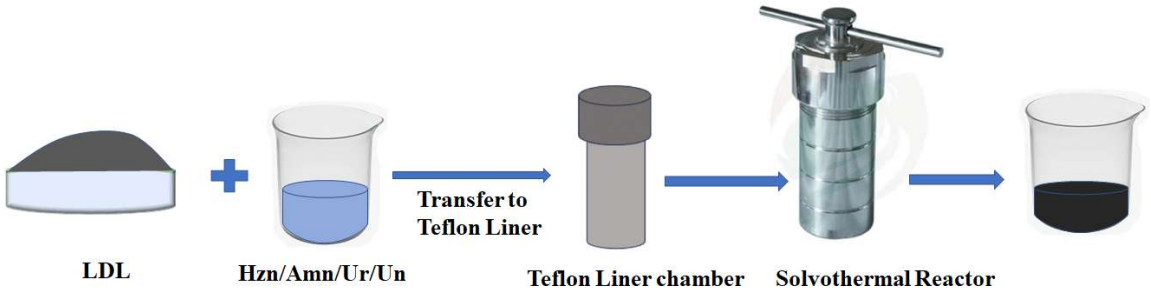


Figure 2.1: Schematic of synthesis of Alkanolamine free CO_2 capture solution

In Figure 2.1, Hzn denotes hydrazine hydrate, Amn denotes ammonia, Ur denotes urea, Un denotes human urine. The recovered lignin is separated by dispersing it in a binary solvent mixture of ethanol and water (9:1 v/v) in a 1:5 (w/v) ratio and stirring continuously at room temperature for 12 hours to ensure uniform distribution. The resultant suspension is centrifuged at 2000 rpm for 10 minutes before discarding the precipitated fraction and collecting the supernatant. To eliminate any remaining solvents, the collected solution is dried overnight on a hot plate at 90 ℃. The dried substance is referred to as low-density lignin (LDL) powder, and it is used as an absorbent material in future CO_2 capture tests. The scheme for synthesis of alkanolamines free CO_2 capture solvent has been depicted in figure 2.1.

2.2.3 Gallic acid and N, N-dimethylformamide (DMF) Solution

The test fluid has been used in the synthesis of fluorescent dyes, specifically xanthene dyes, are Gallic acid and N, N-dimethylformamide (DMF). Typically, 2.4 g of Gallic acid is dissolved in 60 mL of dry DMF while continuously stirring to produce a translucent yellowish solution. The resulting Gallic acid solution, with a concentration

of 0.04 g/mL, is employed as the precursor solution for the manufacture of xanthene-based fluorescent colors. The homogenous solution ensured that Gallic acid is completely dissolved and served as an appropriate reaction medium for color production. Methyldiethanolamine (MDEA, purity ≥ 98%) and Diethanolamine (DEA, purity ≥ 98%) are purchased from Tokyo Chemical Industry Co. Ltd. (TCI), Japan, and Merck Life Science Private Limited, Mumbai, India, respectively, and have been used exactly as received without additional purification.

All compounds used in the study are analytical grade. Deionized water (resistivity = 18.2 MΩ·cm at 25 °C) is prepared using a Millipore Direct-Q5 UV Water Purification System and used throughout all experiments.

2.3 Reactor Systems

2.3.1 Helical Coil reactor

The helical coil reactor (HCR) is made of borosilicate glass as depicted in Figure 2.2, of internal diameter 4 mm and outer diameter as 6 mm and the length of tubing of helical reactor is 2.5 m. Total helical turn and pitch in the reactor is 19 and 5 mm respectively. The reactor has T-shaped inlet for gas and liquid flow in either side.



Figure 2.2: Helical Coil Reactor

2.3.2 Coiled Flow Invertor

The coiled flow inverter (CFI) is fabricated from borosilicate glass with a tube inner diameter (ID) of 4 mm and an outer diameter (OD) of 6 mm, and a total reactor tube length of 2.5 m and 2.63 m. Two CFI configurations are employed in this study, as shown in Figure 2.3

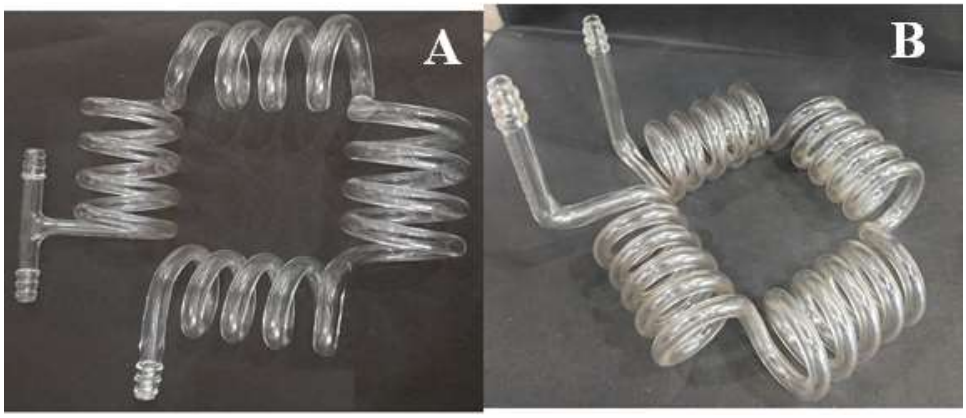


Figure 2.3: Images of Coil Flow Invertor (CFI) [A] Horizontal axis of inlet/outlet [B] Vertical axis of inlet/outlet

The CFI shown in Figure 2.3 [A] has a coil pitch of 5 mm and 4 turns per arm, whereas the CFI shown in Figure 2.3 [B] has 5 turns per arm. The arrangement shown in Figure 2.2 [B] also includes a vertical inlet and an exit arm, which allowed for indirect heating of the solvent inside the reactor using a silicone oil bath, guaranteeing that no silicone oil has been contaminated during operation.

2.3.3 Stacking of CFI

To enhance the residence time, two coiled flow inverters are connected in series, as shown in Figure 2.4. This stacked CFI design is used for the continuous synthesis of fluorescent xanthene dye from Gallic acid and DMF precursors.

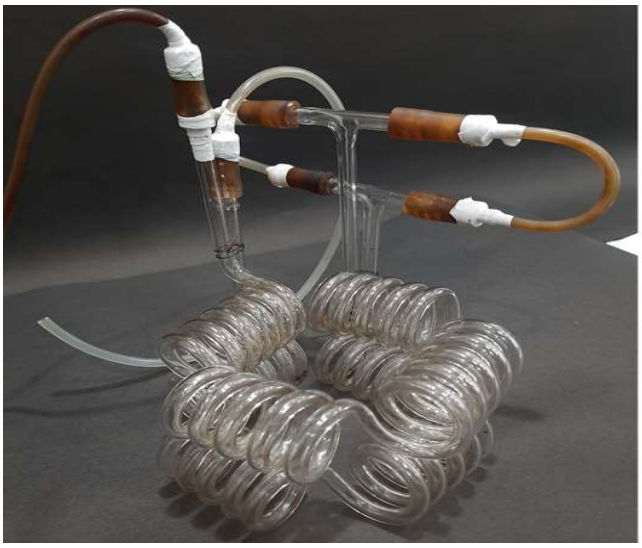


Figure 2.4: Real Image of stack of CFI

2.4 Experimentation

2.4.1 CO_2 Absorption in Amines

The experimental setup employed for flow-directed CO_2 capture is schematically shown in figure 2.5. The set-up includes four major components: (i) liquid phase delivery system, (ii) gas delivery and flow control system, (iii) millichannel reactor (CFI), and (iv) gas-liquid separation and analysis unit at the outlet.

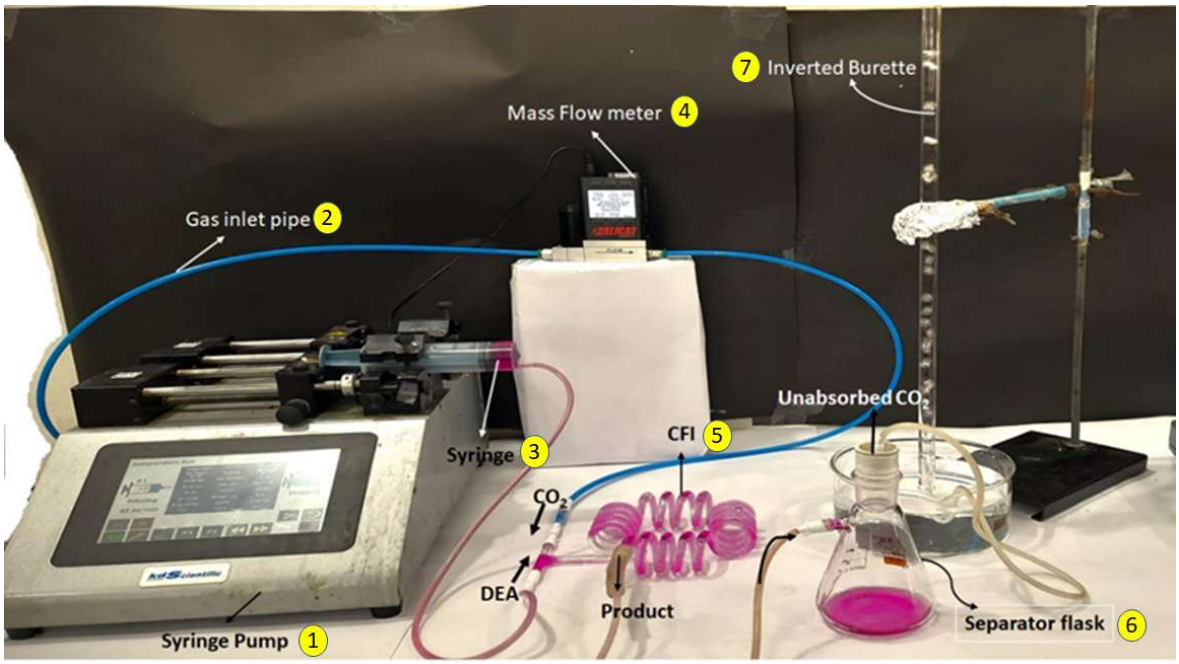


Figure 2.5: Experimental Setup [1] Syringe Pump [2] Gas inlet pipe [3] Syringe [4] Mass flow meter [5] CFI [6] Separator flask [7] Inverted Burette for employed for flow-directed CO_2 capture in Amines

Before every experiment, fresh aqueous solutions of the amine solvent (DEA, MDEA, or other absorbents) at the appropriate concentration are made and transferred to a 60 mL plastic syringe as a liquid phase. An automatic dual-syringe pump (Gemini 88, KD Scientific, USA) delivers the liquid to the reactor at a carefully regulated volumetric flow rates of 12, 20, 30, 42 and 56 mL/min, ensuring a steady, pulse-free liquid flow for the length of each experiment. Steady-state conditions are maintained in the reactor by using a dual-syringe arrangement, which permitted continuous flow even during syringe refilling. A high-purity CO_2 cylinder (purity: 99.9%, purchased from the local market) provided the CO_2 gas. A calibrated mass flow controller (Alicat Scientific, USA; range: 0–100 SCCM) has been used to control and monitor the gas flow rates of 30, 40, 50 and 60 mL/min after the cylinder

outlet pressure is initially lowered and stabilized using a two-stage pressure regulator. This configuration guaranteed accurate and consistent control of the gas-to-liquid flow rate ratio (G/L ratio) under all experimental conditions. The T-junction connector (T-inlet) connected the CO_2 gas and liquid solvent at the reactor inlet, resulting in a segmented gas-liquid slug flow pattern at the millichannel entry. The two-phase slug flow passed through a helical coil reactor (HCR) and coiled flow inverter (CFI) with same geometrical dimensions for analyzing effectiveness of reactor in CO_2 absorbance in liquid absorbing medium. At the reactor outlet, the unabsorbed gas and liquid have been collected and liquid is tested for CO_2 loading with standard titration.

2.4.2 Experimental Setup for CO_2 absorption in Alkanolamine- free Lignin based solvent

A schematic layout of the entire experimental apparatus is shown in figure 2.6. The overall effective tube length, measured from the syringe pump output to the product collection flask, is kept at around 5.5 meters. This total length includes both the CFI reactor section (2.5 m) and the inlet/outlet connecting tubing, ensuring adequate contact time between the CO_2 gas phase and the liquid absorbent under all operating conditions investigated. The amine-functionalized lignin solution, prepared at the correct concentration (1:15) at mol: mol basis and solvothermally treated is constantly supplied into the CFI reactor via one inlet of a T-shaped junction connector using an automatic syringe pump (Gemini 88, KD Scientific, USA). The liquid flow rate has been systematically altered across four set-points; 12, 20, 30, and 42 mL/min to explore the effect of liquid residence time and gas-to-liquid flow rate ratio on CO_2 absorption efficiency. The pressure drop in the reactor during gas-liquid

flow is measured using a pressure transducer (Model STD720-E1AC4AS-1-C-AHD-11C-B-11A0-F1-0000, Honeywell, Washington, USA). The density and viscosity of Ur-L and Un-L absorbent is measured by pycnometer and rheometer (modal no- Anton Paar MCR 302e) respectively.

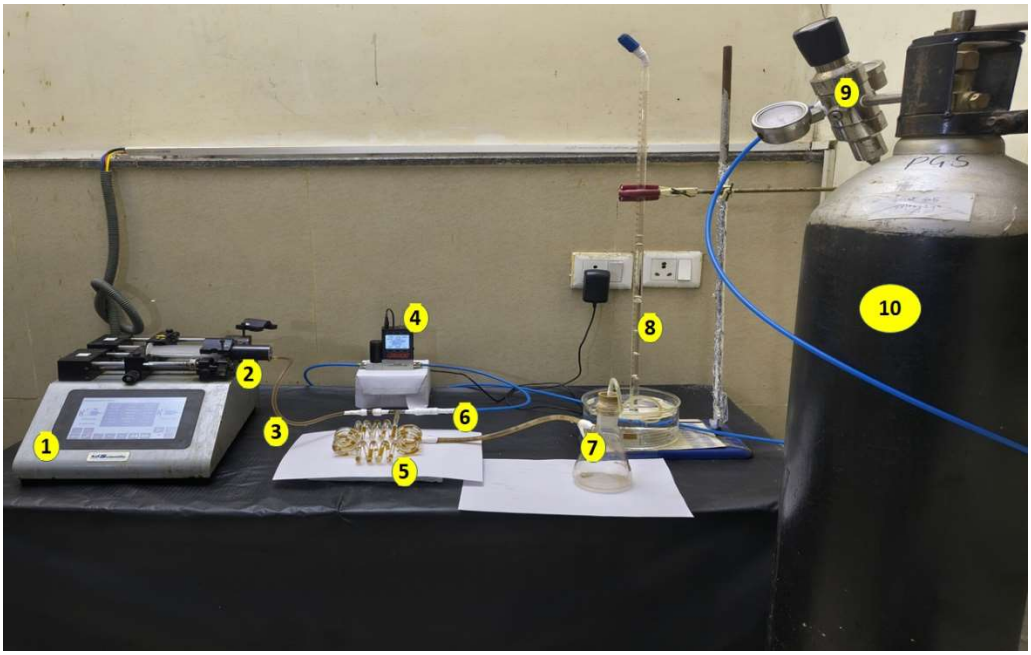


Figure 2.6: Image of experimental setup **[1]** Syringe Pump, **[2]** Syringe, **[3]** liquid inlet pipe, **[4]** Gas Flow meter, **[5]** CFI Reactor, **[6]** gas inlet pipe, **[7]** collection flask, **[8]** inverted burette, **[9]** pressure gauge, **[10]** CO_2 cylinder.

Simultaneously, CO_2 gas (purity: 99.9%) is introduced through the opposite inlet of the T-junction at a constant volumetric flow rates of 30, 60 mL/min, precisely regulated using a calibrated mass flow controller (Alicat Scientific, USA; range: 0-100 SCCM), ensuring a stable and reproducible gas-phase input across all experiments. The T-junction is the gas-liquid contactor inlet, resulting in a segmented slug flow pattern with alternating CO_2 gas plugs and liquid slugs at the CFI reactor channel entry. The amount of unabsorbed CO_2 exiting the reactor at the outlet is

quantified using a water-displacement inverted burette method. The volume of gas collected over a time interval is utilized to compute the unreacted CO_2 flow rate.

2.4.3 Experimental Setup for synthesis of Xanthene dye from Gallic acid and DMF

The experimental setup for the synthesis investigations is depicted in Figure 2.7. This configuration consisted of submerged stack of coiled flow inverters (CFIs) in a silicone oil bath that is heated with a hot plate to sustain the required reaction temperature. The experimentation has been performed at different temperatures of 150 °C, 160 °C, 170 °C, 180 °C, 190 °C, and 200 °C.

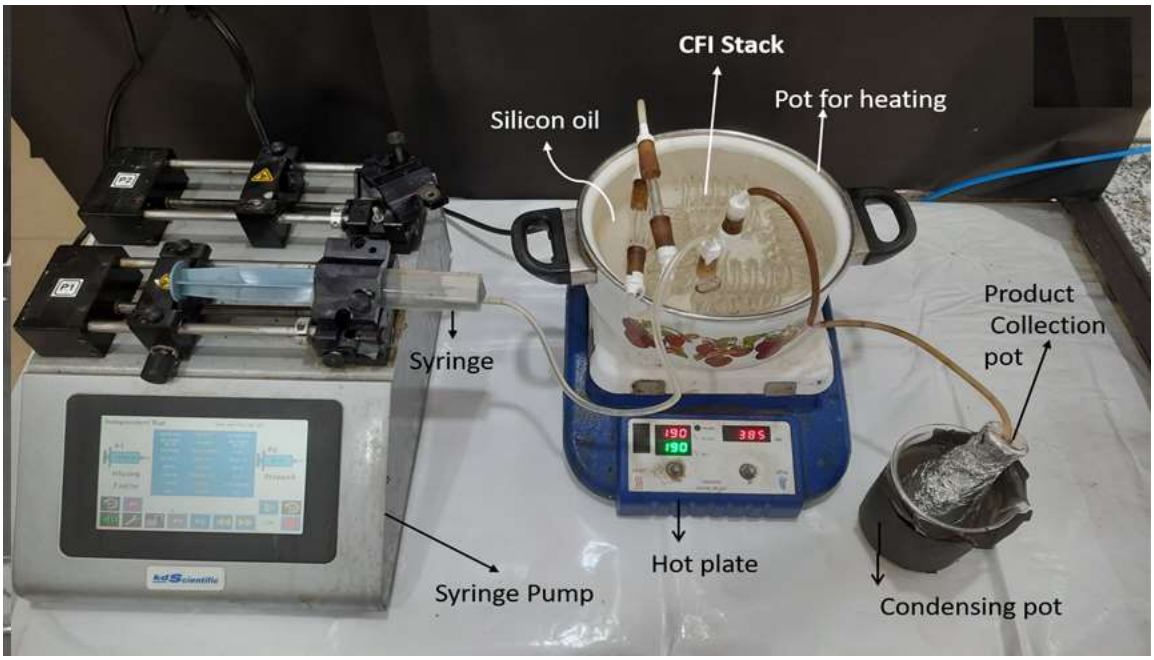


Figure 2.7: Experimental Setup of synthesis of Xanthene Dye from Gallic acid and DMF

Using a syringe pump (Gemini 88, KD Scientific, USA), the solution of Gallic acid and DMF is put into a 60 mL plastic syringe and transported to the CFI reactor at liquid flow rates of 3, 4, 5, 6, 7, and 8 mL/hour. One CFI has a volume of 35 mL, and

the solution travels 290 cm and 45 ml in total from the syringe to the collector via CFI. A single CFI and a stack of CFIs under the same input configuration and reaction temperatures have been compared in order to examine the impact of residence time. In order to condense the volatile vapors, the reaction product is collected in a flask submerged in cold water. To visualize the formation of fluorescent reaction product during the reaction process, a UV torch is used to illuminate the reactor and image of reaction mixture inside the reactor are captured.

2.5 Experimental Procedures

2.5.1 Estimation of percentage of CO_2 absorption

A chemical method [140] and an analytical method are used to estimate the amount of CO_2 absorbed by the liquid absorbent. These methods enable the quantification of CO_2 uptake and facilitate evaluation of absorption performance of different absorbent solutions under various operating conditions

In a chemical method, an acid-base titration method has been used to measure the amount of CO_2 absorbed in the liquid absorbent. Following the absorption experiment, a known volume of the CO_2-loaded absorbent solution is removed and titrated with a standardized hydrochloric acid (1M HCl) solution using phenolphthalein as the indicator. The disappearance of the pink color, which signified the neutralization of alkaline species created as a result of CO_2 absorption, marked the endpoint. Using stoichiometric relationships, the volume of HCl consumed during titration is used to compute the amount of absorbed CO_2. The appropriate volume of CO_2 at standard temperature and pressure (STP) is then calculated from

the absorbed CO_2 concentration [140–142]. Direct acid–base titration is used to calculate the amount of CO_2 absorbed in the Nano cellulose solution.

A standardized 1 M NaOH solution is used for titration after a known volume of the CO_2-loaded solution is combined with a few drops of phenolphthalein indicator. The titration has been carried out until the acidic species produced by dissolved CO_2 are completely neutralized, as indicated by the emergence of a faint, persistent pink tint. The amount of absorbed CO_2 is determined using stoichiometric relationships and the volume of NaOH consumed at the endpoint [143–145].

In an analytical Method as depicted in figure 2.8, the inverted burette method is used to measure the volume of unabsorbed gas exiting the absorption system. Using this method, a water-filled burette is positioned inside a water reservoir in inverted position. After leaving the collection flask, the gas stream is directed into the inverted burette, where it displaced an equal volume of water. The total volume of unabsorbed gas has been recorded as the displaced water volume.

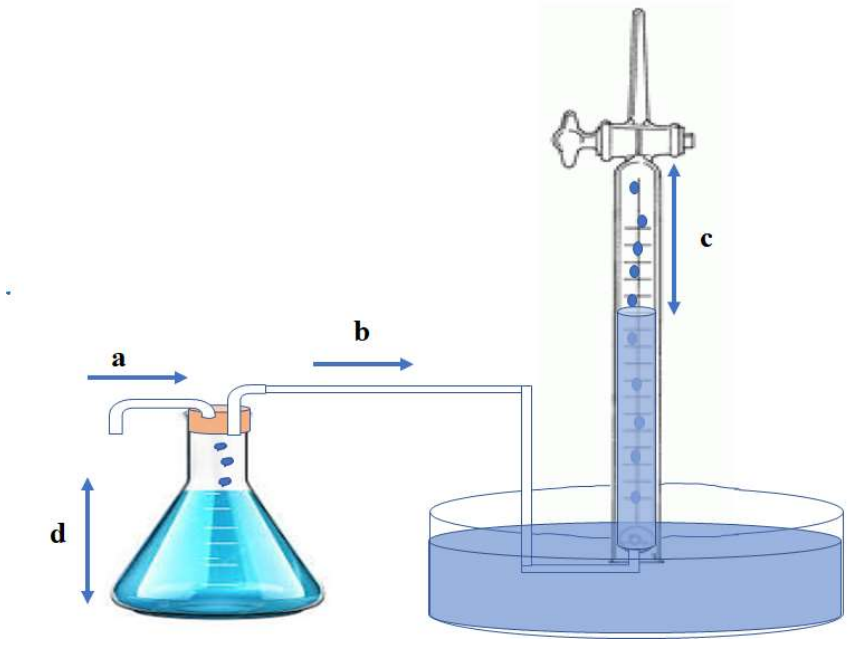


Figure 2.8: Schematic of Inverted burette method **[a]** CO_2 loaded liquid and unabsorbed gas coming from reactor **[b]** Unabsorbed CO_2 and air coming from collection flask **[c]** Volume displaced by gases coming from collection flask **[d]** volume of CO_2 loaded liquid

The collected gas consisted of air and unabsorbed CO_2 inside the inverted burette. The original air volume in the collection flask, which is moved during the experiment along with the unabsorbed CO_2, is the reason for the air's existence. As a result, the measured volume (displaced volume of water) from the inverted burette is the total volume of air and CO_2. By deducting the volume of CO_2-loaded absorbent solution collected in the flask from the total gas volume determined by the inverted burette, the volume of unabsorbed CO_2 is calculated. Lastly, the difference between the CO_2 volume at the input and the unabsorbed CO_2 volume at the outflow is used to compute the amount of absorbed CO_2.

The absorbed CO_2 volume and the percentage of CO_2 absorption has been calculated using the methodology described below and schematically represented in Figure 2.8.

$a = V_{liuid\ product\ and\ unabsorbed\ gas}$

$b = V_{unabsorbed\ gas\ and\ air}$

$c = V_{Collected\ unabsorbed\ gas}\ (CO_2 + Air)$

$d = V_{Collecetd\ liquid}$

$V_{Air} = c - d$

$V_{unabsorbed\ CO_2} = c - V_{Air}$

$V_{Supplied\ CO_2} = Flow\ rate\ of\ CO_2 \times time\ taken\ for\ sample\ collection$

All experiments used a consistent sample collection time to compare CO_2 absorption ability across varied operational conditions.

$$\%\text{Absorption} = 1 - \frac{V_{\text{unasorbed CO}_2}}{V_{\text{Spplied CO}_2}} \times 100 \quad \text{.....(2.1)}$$

To ensure the reliability and repeatability of the experimental data, each experiment is repeated five times under the same conditions. The CO_2 absorption data from the inverted burette method is confirmed by an independent acid-base titration methodology. Both methods produced similar results, with a variance

of less than ±5%. This level of agreement validates the accuracy of experimental measurements and the methodology for estimating CO_2 absorption.

2.5.2 Estimation of heat transfer in synthesis of Xanthene Dye

The rate of heat transfers during the synthesis of xanthene dye from Gallic acid and DMF is calculated by performing an energy balance across the CFI reactor. The heat transfer rate is estimated as the product of the reacting solution's mass flow rate, specific heat capacity, and the temperature differences between the reactor's exit and inlet streams. The heating environment is provided by a silicone oil bath into which the CFI reactor is submerged. The silicone oil bath provided a homogeneous and controlled temperature environment, allowing for efficient heat transmission to the flowing reaction mixture throughout the synthesis process. The heat transfer rate is calculated with the following expression:

$$Q = m \cdot C_p(T_{out} - T_{in}) \quad W \text{.....(2.2)}$$

Where Q is the heat transfer rate (W), m is the mass flow rate of the reaction mixture (kg/sec), C_p is the specific heat capacity of the fluid (J/Kg K), T_{out} and T_{in} are the outlet and inlet temperatures of the solution, respectively.

The heat flux is calculated as the ratio of the heat transferred to the reaction mixture to the heat transfer surface area of the reactor. The heat transfer rate (Q) is determined using the energy balance across the reactor, and the related heat flux is produced by dividing Q by the CFI reactor's effective surface area available for heat transmission. The heat flux has been computed with the following relationship:

$$Heat\ Flux\ (q)\ (W/m^2) = \frac{Heat\ received\ (W)}{Surface\ Area\ of\ reactor\ (m^2)} \text{.....(2.3)}$$

2.6 Error Analysis

All experiments have been conducted at least four to five times under identical operating conditions to ensure the repeatability and reliability of the experimental data. Four data points are chosen at random and used to estimate the standard deviation in order to quantify the experimental uncertainty. The following relation is used to compute the standard deviation:

$$\sigma = \sqrt{\frac{\sum_{i=1}^{n}(x_i - \overline{x})^2}{n-1}} \quad \text{.....(2.4)}$$

In Eq. (2.4), "x_i" is the original value derived from experiments for each data set, "n" is the number of data sets (number of times experiments are conducted), and $\bar{x}$ is the average or mean value. The standard deviation has been computed for each experimental result. As a result, all of the figures that show the results in the following chapters now include error bars.

2.7 Synthesis of Low-density Lignin (LDL)

The lignin produced from rice straw is used as the starting material for the synthesis of low-density lignin. Initially, 20 g of lignin is combined with 40 mL of ethanol and 10 mL of deionized (DI) water. The resulting suspension is continually agitated for at least 12 hours to ensure perfect dispersion and homogeneity.

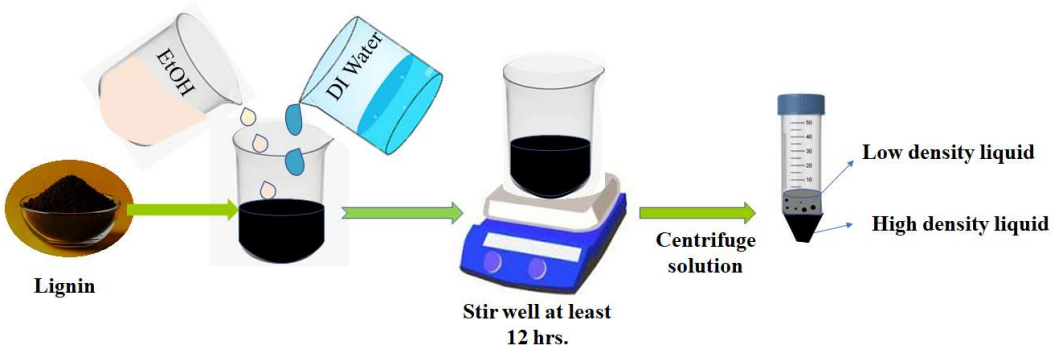


Figure 2.9: Schematic of synthesis of Low-density lignin

The mixture is then centrifuged at 1500 rpm for 10 minutes. After centrifugation, the denser fraction settled to the bottom, while the top, lighter liquid phase is carefully separated. The recovered supernatant is dried in an oven at 50 °C overnight to remove the solvent. The dried product obtained after evaporation is collected and labeled as low-density lignin (LDL), which is then used in further experimental research.

2.8 Summary

The experimental methods used in this investigation are described in this chapter. It provides a concise overview of the preparation and synthesis of the test fluids used for CO_2 capture and synthesis of fluorescence die. The methodology for fabricating reactors, synthesizing LDL, estimating CO_2 absorption efficiency, and evaluating heat transfer parameters are presented in details. The Coiled Flow Inverter (CFI) and Helical Coil Reactor (HCR) used in this work are designed in our lab and fabricated at the Indian Institute of Technology (IIT), Kanpur Glass Blowing Section.

Chapter 3: Hydrodynamics-driven CO_2 Absorption in Coiled Flow Inverters using Alkanolamines[1]

3.1 Brief Introduction

Recent advances in process intensification have highlighted gas–liquid flow systems as promising platforms for CO_2 capture because of their enhanced mass transfer and high process efficiency. Their compact, modular, and scalable design, coupled with low operational complexity, makes them attractive for continuous CO_2 capture using aqueous amine-based absorbents. Concentrated alkanolamine solutions are being used as CO_2 capture mediums for conventional batch processes amid several disadvantages, such as energy intensiveness and poor efficiency. In this chapter, the efficacy of millimeter-sized coiled flow inverters (CFI) have been explored as a point-source CO_2 capture tool for highly efficient, continuous operations using alkanolamines solutions. In this study, an aqueous 3 vol.% diethanolamine (DEA) and blended of amine solution consisting of 1 vol.% methyldiethanolamine (MDEA) + 3 vol.% DEA are used as absorbent for CO_2 capture. The solvent and CO_2 gas flow rates are found to dictate the slug flow regime and, more specifically, slug lengths which affects the CO_2 absorption rates. A higher solvent flow rate promotes formation of shorter gas slugs which increase the gas-liquid interfacial area and improve internal recirculation so that liquid renewal at interface and increasing absorption of gas. Further the high interfacial area and residence time remain the driving factors for enhanced CO_2 capture using CFI. About 98% CO_2 absorption efficiency has been achieved for 3 vol.% aqueous diethanolamine solution in CFI.

[1]*The work discussed in this chapter have been published in Chemical Engineering and Processing - Process Intensification Volume 205, November 2024, 110022*

In this chapter, efficacy of nano cellulose, a sustainable nanomaterial for CO_2 capture at low flow rates is explored.

3.2. Results and Discussions

3.2.1 Deciphering the role of geometrical medication of reactors

Two prototype reactors (i) helical and (ii) single CFI are used in the study have already been illustrated in Figure 2.2 and 2.3 [A] in chapter 2. The reason for using these two reactors is to deconvolve the role of four 90-degree bends in augmenting CO_2 absorption efficiency. Aqueous diethanolamine (3 vol.%) solution has been taken for CO_2 capture medium depicted in Figure 3.1, demonstrates that the reactor type influences the percentage of carbon dioxide absorption in the DEA solution. At a constant flow rate of CO_2 gas, the efficiency of CO_2 absorption gradually increases. The CO_2 gas flow rates of 30 and 60 mL/min are selected based on preliminary experiments and the stable operation range of the CFI setup. These flow rates are used to study the influence of gas flow rate under stable gas-liquid flow conditions. The present study aims at an experimental investigation of Q_G rather than at a mathematical optimization of Q_G over the whole range of possibilities. As expected, the CO_2 absorption efficiency in CFI is significantly higher than that in a helical reactor. However, the CO_2 absorption efficiency at higher gas flow rates does not alter significantly for a specific reactor. Surprisingly, at low gas flow rates and high solvent flow rates, CFIs have been more effective as compared to helical reactors. It is interesting to note that 97% CO_2 absorption efficiency has been quantified for coiled flow inverter at 30 mL/min CO_2 gas flowrate, whereas that in helical reactor 61% absorption efficiency has been noticed at the same flow rate. The observation of high CO_2 absorption efficiency may be attributed to unique geometrical features (presence of four 90° bends) of CFI that redirect the flow and

mixing in the liquid phase, thus increasing the driving force for mass transfer at the gas-liquid interface. Further, Slug flow regime has higher transport characteristics as compared to other gas-liquid and liquid-liquid flow patterns such as bubbly/dispersed flow and annular flow [146–148].

Slug flow has also been considered a tool of process intensification owing to its unique characteristics of the dual transport mechanism of diffusion and convection [149,150]. Moreover, it has been observed that CFI augments the slug flow range in our case, thus enhancing the percentage absorption of CO_2.

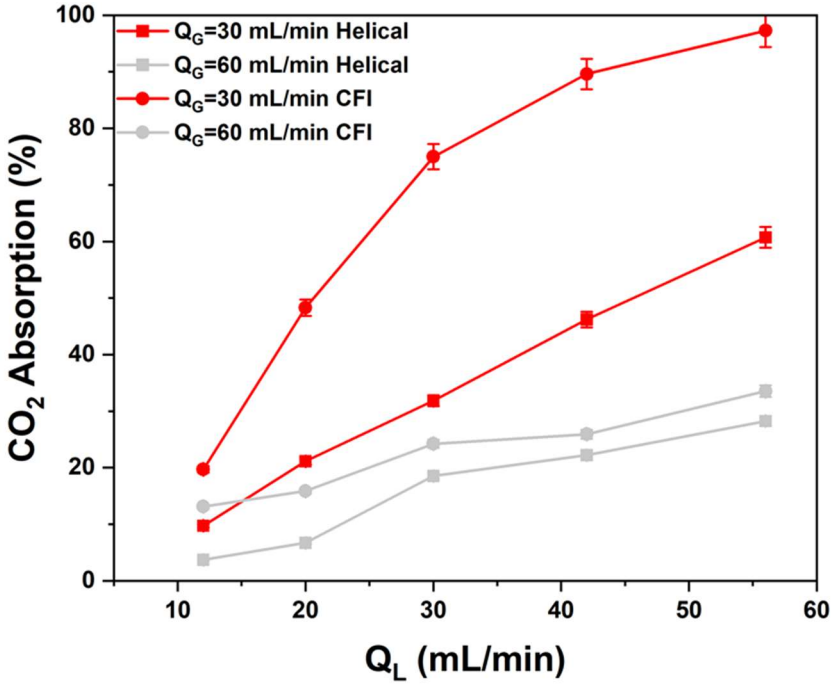
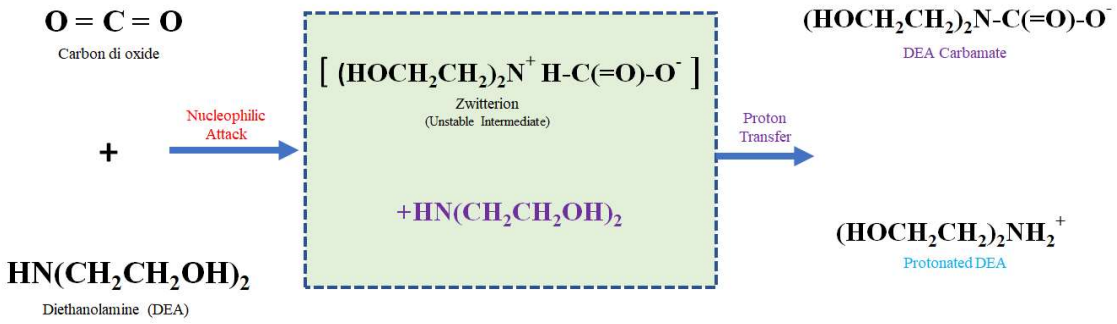


Figure 3.1: CO_2 absorption efficiency in aqueous Diethanolamine (3%) solution for two different reactors. The flow rates for CO_2 gas and aqueous Diethanolamine solution have been represented as Q_G and Q_L respectively. For helical reactor; Q_G = 30 mL/min (red square), Q_G = 60 mL/min (grey square). Whereas, for CFI; Q_G = 30 mL/min (red circle), Q_G = 60 mL/min (grey circle).

3.2.2 Reduction of CO_2 gas bubble size

Glass-made reactors are advantageous for studying gas-liquid reactions over their non-transparent counterparts because the progress of reactions can easily be monitored with spatiotemporal resolution by optical imaging methods. The chemisorption reaction of alkanolamines with CO_2 is expected to yield carbamate, and thus, with the progress of the reaction, the size and concentration of CO_2 bubbles in a millimeter should get reduced gradually.



$$\text{DEA } (l) + CO_2\,(g) \longrightarrow \text{Carbamate } (l) + \text{unabsorbed } CO_2\,(g)$$

$$\text{DEA } (l) + \text{MDEA } (l) + CO_2\,(g) \longrightarrow \text{Carbamate } (l) + \text{unabsorbed } CO_2\,(g)$$

The above reaction mechanism/schematic explains as follows: -

The chemical absorption of CO_2 into Diethanolamine (DEA), which is a secondary amine (R_2NH where R = $-CH_2CH_2OH$, follows the widely accepted Zwitterion Mechanism [53].

1. Formation of Zwitterion (Rate-determining step): The lone pair of electrons on the electrophilic nitrogen atom of the DEA molecule attacks the carbon atom of CO_2, leading to the formation of a transient, unstable zwitterion intermediate:

$$HN(CH_2CH_2OH)_2 + CO_2 \rightleftharpoons (HOCH_2CH_2)_2N^+H\text{-}COO^-$$

2. Deprotonation (Carbamate Stabilization): Since the zwitterion is highly unstable, a second molecule of DEA acts as a base to extract the proton H^+ from the nitrogen

center. This results in the final stabilization into a soluble amine carbamate and a protonated amine ion:

$$(HOCH_2CH_2)_2\,N^+\,H\text{-}COO^- + HN(CH_2CH_2OH)_2 \longleftrightarrow (HOCH_2CH_2)_2\,N\text{-}COO^- + (HOCH_2CH_2)_2NH^+$$

A significant reduction in the size of CO_2 gas has been noticed as shown in Figure 3.2. It can be seen that the length of the CO_2 slug near the inlet is 2.16 mm, whereas it gets unprecedently reduced to 0.593 mm. This progressive shrinkage of slug occurs due to CO_2 continuously diffuse across the gas-liquid interface into the absorbent, where it is rapidly consumed. The gas volume decreases as slug progressively becomes shorter. The reduction in slug length also increase the interfacial area

(m^2/m^3) and enhance internal recirculation within the liquid absorbent, thereby improving mass transfer and accelerating CO_2 absorption.

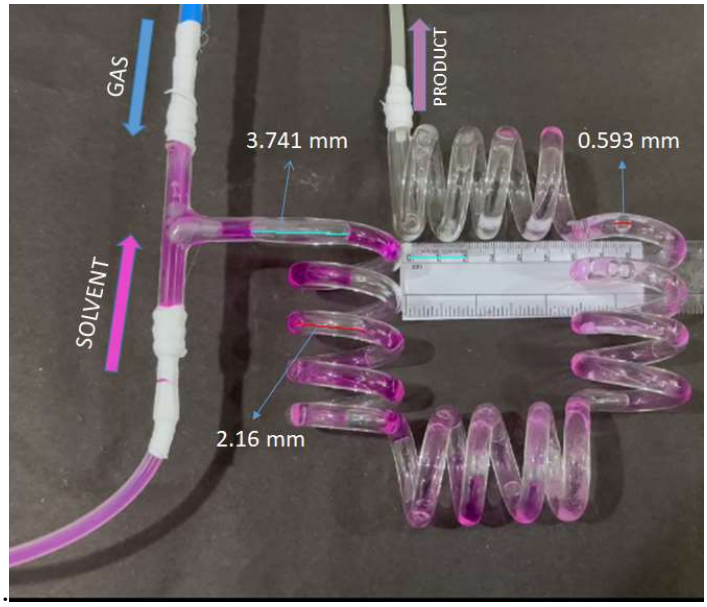
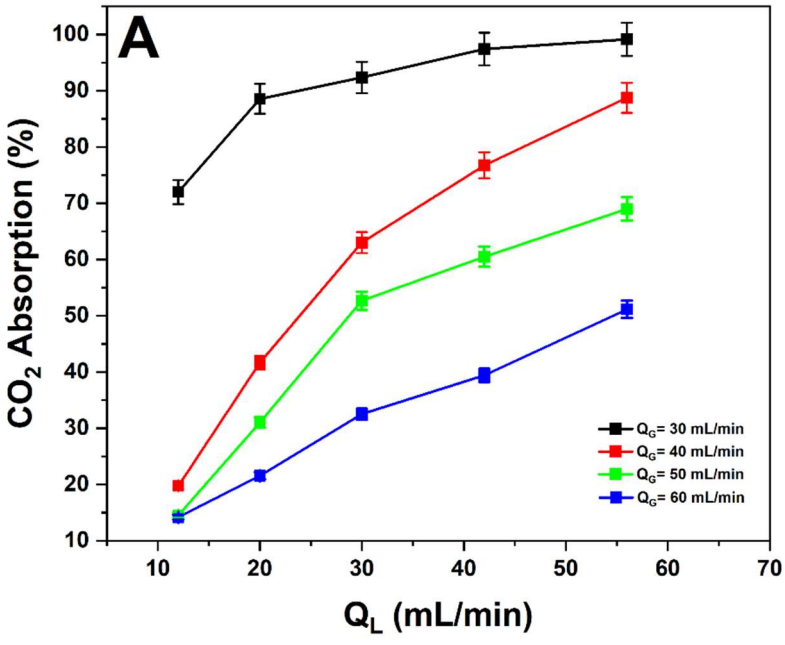


Figure 3.2: Snapshot of size reduction CO_2 gas bubble in millimetre-sized CFI. Pink colour is due to presence of phenolphthalein indicator in solvent.

3.2.3 Effect of N-Methyldiethanolamine (MDEA) blended Diethanolamine (DEA) in CO_2 absorption

Among the alkanolamines, N-methyldiethanolamine is often used in CO_2 capture along with diethanolamine for gas-sweetening purposes. Hence, we have considered the blending of 1 vol.% MDEA in an aqueous DEA (3 vol.%) solution for augmenting CO_2 absorption efficiency at high gas flow rates. The CO_2 absorption efficiency increases with the increase in liquid flow rates for a constant gas flow rate, and a reverse trend is observed upon variation of gas flow rates at a constant solvent flow rate (Figure 3.3 A). It is evident that the use of 1 vol.% MDEA has contributed to about a 20 % increase in CO_2 absorption at a gas flow rate of 60 mL/min. A maximum

98 % absorption of carbon dioxide at 30 mL/min gas flow rate and 56 mL/min solvent flow rate have been observed which is depicted in Figure 3.3 [A]. However, at the same solvent flow rate, absorption efficiency drops to 51% at a 60 mL/ min gas flow rate. From these results, it can be concluded that when tends to 0.5, the absorption efficiency of CO_2 reaches its maximum value. The higher gas flow rate has contributed to a decrease in residence time, thereby reducing mass transfer significantly [9,151,152]. Moreover, it contributes to the significant increase in slug length, causing a reduction in interfacial. CO_2 capture efficiency with conventional microchannel and millimeter-sized CFI used in this study has been compared and presented in Figure 3.3 [B]. Therefore, it highlights the seminal role of flow rates in CO_2 capture using CFI as a process intensification tool.



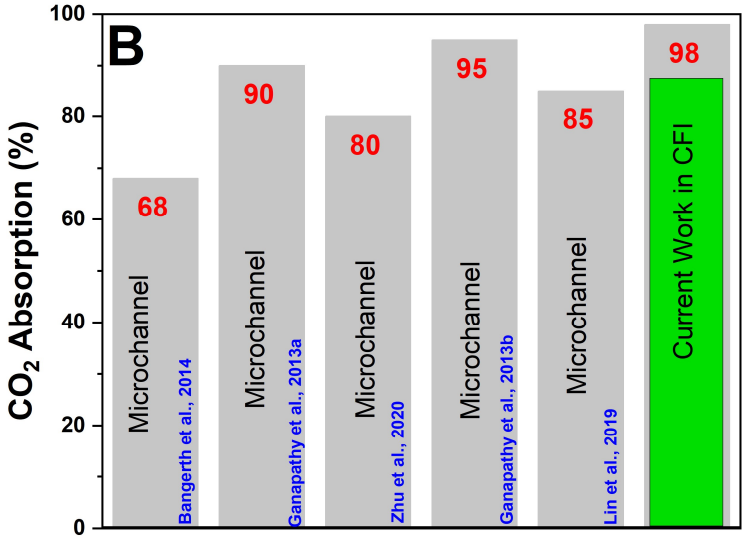


Figure 3.3: **[A]** CO_2 absorption efficiency in aqueous solution of 1% MDEA and 3% DEA using CFI. For CO_2 gas flow rates —30 mL/min (black square), 40 mL/min (red square), 50 mL/min (green square), and 60 mL/min (blue square). The flow rates CO_2 gas and blended amine solution have been represented as Q_G and Q_L respectively. **[B]** Comparative analysis of CO_2 capture efficiency with conventional microchannel and millimeter-sized CFI used in this study.

3.2.4 Nano cellulose-aided CO_2 capture at low flow rate

The use of sustainable nanomaterials for CO_2 capture has been stressed in recent times. Among the sustainable nanomaterials, nano cellulose derived from lignocellulosic biomass remains the preferred choice owing to its surface functional (hydroxyl) groups and intrinsic viscosity. In this work, we have used 0.01 % (w/v) nano cellulose in an aqueous DEA (3%) solution. A generic trend has been observed here also that CO_2 absorption efficiency is kept on increasing with a decrease in ratio of flow rates, specifically from 2.5 to 1 which is depicted in Figure 3.4 [A]. About 93% CO_2 absorption efficiency has been achieved for nano cellulose systems at (Q_G/Q_L) = 0.5. With an increase in gas flow rates, the CO_2 absorption efficiency follows the same decreasing trend. It is therefore quite evident that DEA plays a

decisive role in CO_2 capture over Nano cellulose for this solvent system. Therefore, to unearth the contribution of Nano cellulose in CO_2 absorption studies, a series of control experiments have been performed depicted in Figure 3.4 [B]. We have identified that there is a need for aqueous alkaline mediums for Nano cellulose studies. The pH neutral aqueous solution of nano cellulose turns acidic upon reacting with CO_2 slugs, as indicated by the gradual fading followed by the disappearance of the pink color of phenolphthalein. Hence, we have made the nano cellulose solution a bit alkaline for imaging and quantification purposes by adding a flex of NaOH. The CO_2 absorption efficiency for this solvent system remains very low, 10–15 %. Interestingly, upon addition of 3 % DEA to this alkaline Nano cellulose solution, the CO_2 absorption efficiency gets expectedly increased and reaches a maximum of 72 % at a 0.5 flow rate ratio (Q_G/Q_L). This is 25 % less than what we observed with only 3 % DEA for the same flow rate ratio. The reason for such a drop can be attributed to the protonation of the amine functional group of DEA, preferably at the Nano cellulose interface. Interestingly, at a lower solvent flow rate, specifically Q_G/Q_L = 2.5, CO_2 absorption efficiency is comparatively higher, about 15 %. Interaction of CO_2 with nano cellulose decorated with surface hydroxyl groups is perhaps relatively a bit slower process in comparison to that with homogeneous DEA. Hence, it can be stated that the efficacy of Nano cellulose is prominent at low solvent flow rates owing to increased residence time.

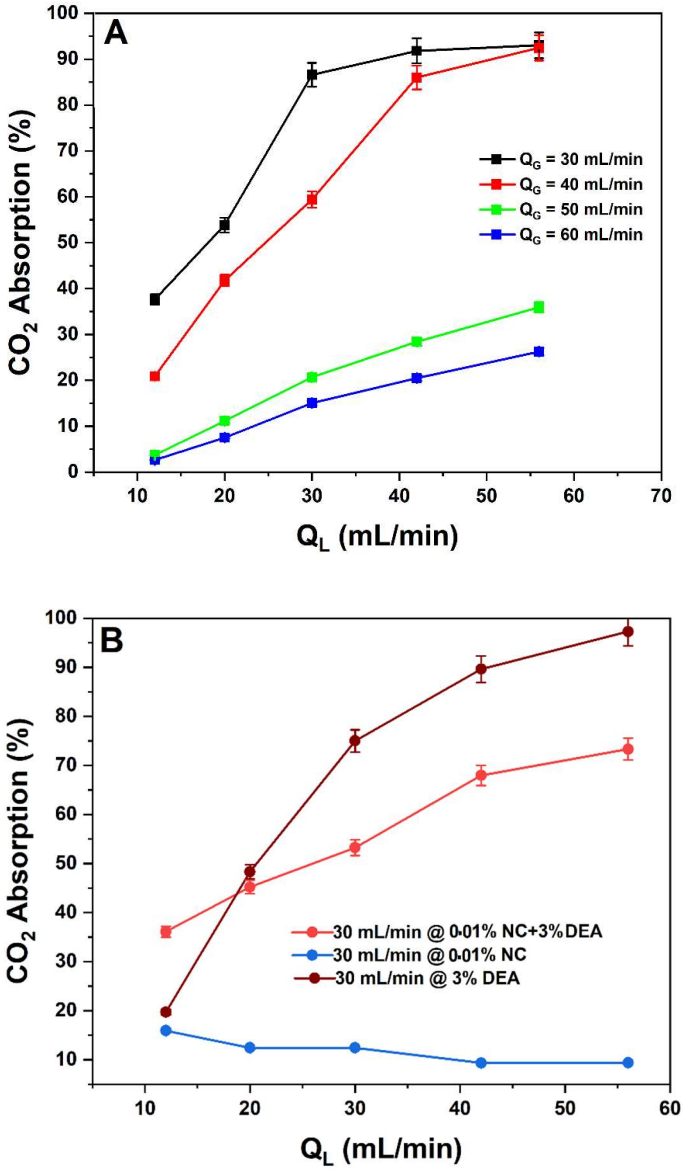


Figure 3.4: [A] CO_2 absorption efficiency in aqueous solution of 0.01% Nano cellulose (NC) and 3% DEA using CFI in alkaline medium (20 mM NaOH). For CO_2 gas flow rates —30 mL/min (black square), 40 mL/min (red square), 50 mL/min (green square), and 60 mL/min (blue square). The flow rates for CO_2 gas and blended amine solution have been represented as Q_G and Q_L respectively. **[B]** Comparison of CO_2 absorption efficiency in three different solvents at constant gas flow rate, 30 mL/min. 0.01% NC in aqueous 3% DEA (red circle), 0.01% NC in aqueous solution (blue circle), aqueous 3% DEA (dark brown circle).

3.4 Conclusion

A millimeter-sized coiled flow inverter has been used for the very first time as a process intensification tool for augmenting CO_2 capture. Its effectiveness has been compared with that of a conventional helical channel of the same length and diameter. Very low concentrations of Diethanolamine (3%) and its blend with 1 % methyl Diethanolamine are selected as a CO_2 capturing medium. The flow rates of solvent and gas have been varied to modulate the slug length in CFI. The CO_2 absorption efficiency increases with the increase in liquid flow rates for a constant gas flow rate, and a reverse trend is observed upon variation of gas flow rates at a constant solvent flow rate. About 98% CO_2 absorption efficiency has been recorded by using an aqueous 3% Diethanolamine solution at a 30 mL/min gas flow rate and a 56 mL/min solvent flow rate in CFI. A blend of 1 vol.% MDEA in a 3 vol.% Diethanolamine solution significantly enhances CO_2 capture at low solvent flow rates. A sustainable scope of CO_2 capture has been illustrated using nano cellulose. This study demonstrates a sustainable solution for CO_2 capture with nanocellulose, and highlights the potential of the use of nanocellulose as a renewable material for the development of sustainable CO_2 capture systems and CCUS technologies

Chapter 4: Alkanolamine-free 96% CO_2 Capture using Coiled Flow Inverters: A Sustainable Scope[1]

4.1 Brief Introduction

Increased CO_2 levels in Earth's atmosphere have rendered carbon capture a foremost priority for achieving net-zero targets. Carbon capture coupled with closing the nitrogen loop offers a complementary and underexplored avenue. Herein, we report a continuous CO_2 capture process employing a Coiled Flow Inverter (CFI) reactor with aminated alkali lignin solution as absorbents. CFI is a model process intensification tool used here for its improved gas–liquid interfacial renewal and mass-transfer rates. Ammonia, hydrazine, and urea are selected as amine precursors for amination of alkali lignin (amine-to-lignin molar ratio = 15:1) using solvothermal method. Spectroscopic characterization confirms successful amination and CO_2 binding. Systematic optimization of gas and liquid flow rates have established optimal conditions of 20 mL/ min (CO_2) and 40 mL/ min (absorbents), achieving 95% CO_2 capture efficiency for the urea–lignin absorbent, which decreased to 85% at 30 mL/min CO_2 flow. Remarkably, a urine-lignin absorbent synthesized using human urine achieves 96% CO_2 capture efficiency even at the CO_2 flow rate of 30 mL/min. Slug-length quantification corroborates capture efficiency trends. Both absorbents retained ≥83% residual CO_2 absorption in second absorption cycle. This work integrates flow-chemistry-driven process intensification with dual waste valorization (lignin and urine) for advancing Sustainable Development Goal (SDGs) 6, 13, and 15.

[1]*The works discussed in this chapter is under revision in Energy and Fuels, ACS (2026).*

4.2 Results and Discussions

4.2.1 Characterization of amine-functionalized lignin

Spectroscopic signatures of lignin which is rich in phenolic and phenylpropanoid moieties can be effectively exploited to monitor changes in− (i) the chromophoric absorption arising from the phenylpropanoid conjugated system, and (ii) the characteristic stretching frequencies corresponding to aromatic skeletal vibrations and C–O bonds of phenolic and etherified units. UV–vis spectra of Amn-L (Ammonia-Lignin) and Ur-L (Urea-Lignin) at free and CO_2 absorbed states are shown in Figure 4.1 [A]. It is broad with characteristic shoulder peaks (250–500 nm) suggesting the blackish color of solution, peak at 278 nm attributable to the $\pi \rightarrow \pi^*$ transitions of the aromatic rings of guaiacyl and syringyl units [153,154]. Upon absorption of CO_2 the peak at 278 nm becomes more intense and sharper, indicating enhanced electronic interactions on chromophoric units of lignin. An illustration of the relationship between shear rate and the viscosity of functionalized lignin solutions, Ur-L and Un-L (Urine-Lignin), can be found in Figure 4.1 [B].

The viscosity of Un-L is significantly higher than that of Ur-L when shear rates are low representing an internal network that is more highly structured within the system that is derived from urine. Because of this, it is possible that there is a stronger intermolecular interaction which increased hydrogen bonding and ionic interactions that occur between the functional groups of lignin that are present in Un-L. When it comes to continuous-flow CO_2 absorption in the coiled flow inverter (CFI) reactor,

this behavior is advantageous because it does not impose excessive pumping penalties.

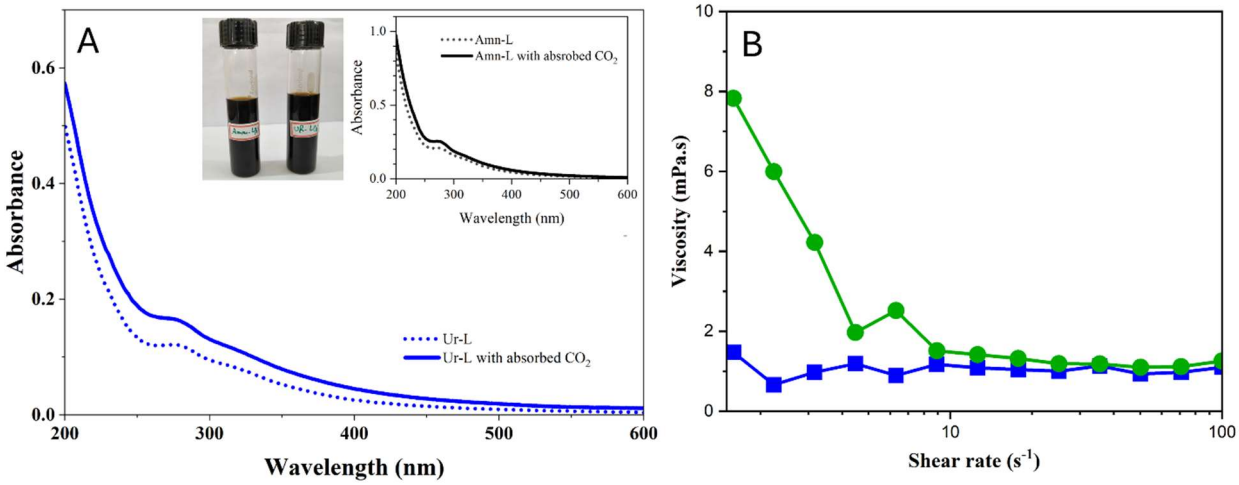


Figure 4.1: [A] UV-Vis spectra of functionalized lignin, Ur-L and Amn-L (Inset), Before CO_2 capture (dotted line) and after the CO_2 capture (solid line). Colour of as-synthesized aqueous solutions of Ur-L and Amn-L. **[B]** Viscosity of Ur-L (blue square) and Un-L (green circle) as a function of shear rate. Human Urine from age group of less than 20 years has been used.

The Fourier transform infrared (FTIR) spectrum of low-density lignin reveals a broad band around 3400 cm^{-1}. This band corresponds to O-H stretching vibrations, which are characteristic of phenolic and aliphatic hydroxyl groups is shown in Figure 4.2. The aliphatic C-H stretching is responsible for the bands that are located close to 2900 cm^{-1}. Strong absorptions are associated with C-O stretching vibrations of ether and alcohol functionalities associated with lignin structure and they are observed in the region between 1300 and 1000 cm^{-1}. It has been observed that there are no significant spectral changes in the region 1700-1500 cm^{-1} after functionalization with urea (Ur-L). The 1700-1600 cm^{-1} spectrum, on the other hand, has shown a discernible shift, which indicates the incorporation of a C-N bond into the structure

of the lignin particle. In the region 1700-1600 cm^{-1}, the peak that is characteristic of the carbonyl (C=O) stretch has emerged as a result of the absorption of carbon dioxide. There is a clear indication that functionalized lignin and carbon dioxide interact with one another. Furthermore, in the region of 1200-1000 cm^{-1}, there are observed to be slight variations in the vibrational frequencies of C-O/C-O-C components. When taken as a whole, these findings provide evidence that the structural network that is produced by the amine functionalization of lignin is exceptionally well-suited for the capture of carbon dioxide.

The FESEM images of the urea-lignin (Ur-L) absorbent before and after CO_2 loading are presented in Figure 4.3[A] and Figure 4.3[B], respectively. Before CO_2 loading, the Ur-L absorbent exhibits a relatively smooth surface with well-defined cubic urea crystals uniformly dispersed over the lignin matrix. The particles are discrete with limited agglomeration, indicating good accessibility of active sites for CO_2 absorption. After CO_2 loading, the surface morphology changes significantly, becoming rougher, denser, and highly agglomerated. The disappearance of discrete crystals and formation of compact aggregates suggest strong interactions between CO_2 and the functional groups of urea and lignin, confirming successful CO_2 loading. Similarly, the FESEM images of the urine-lignin (Un–L (20)) before and after CO_2 loading are shown in Figure 4.3[C] and Figure 4.3[D], respectively. Before CO_2 loading, the absorbent exhibits irregularly shaped crystalline particles with an open and porous morphology, indicating a high accessible surface area. After CO_2 loading, the surface becomes considerably denser and more compact with extensive particle agglomeration and reduced pore spaces. These morphological changes indicate the

formation of CO_2-induced reaction products and strong interactions between CO_2 and the functional groups of the absorbent. Overall, the FESEM results provide clear morphological evidence of successful CO_2 capture by both Ur–L and Un–L (20) absorbents. The CHNS elemental analysis of the urea–lignin (Ur–L) absorbent before and after CO_2 loading is presented in Figure 4.4. Prior to CO_2 loading, the C/H and C/N ratios are 5.32 and 5.05**,** respectively. Following CO_2 capture, these ratios increased to 6.10 **(**C/H) and 5.92 (C/N). The increase in both C/H and C/N ratios is primarily attributed to an increase in the carbon content of the absorbent after CO_2 loading, whereas the hydrogen and nitrogen contents remained nearly unchanged. Specifically, the carbon content increased from approximately 20.30 % to 22.01 %**,** while only marginal variations were observed in the H, N, and S contents. This trend provides strong evidence for the successful uptake of CO_2 by the Ur-L absorbent, resulting in carbon enrichment without causing any significant alteration in the overall elemental composition. The relatively stable nitrogen content further suggests that the urea-derived nitrogen-containing functional groups remain chemically stable during the absorption process, indicating that CO_2 capture predominantly occurs through interaction with the existing functional groups rather than through degradation or loss of the absorbent constituents.

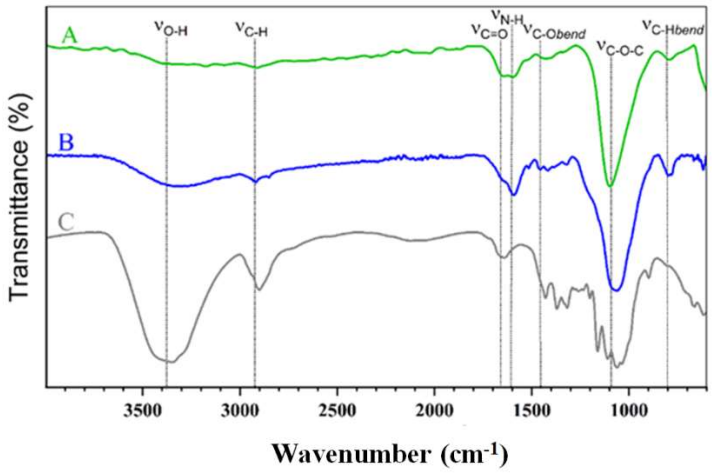


Figure 4.2: FTIR spectra of - low density lignin (grey line), Ur-L (blue line) and Ur-L at CO_2 captured state (green line)

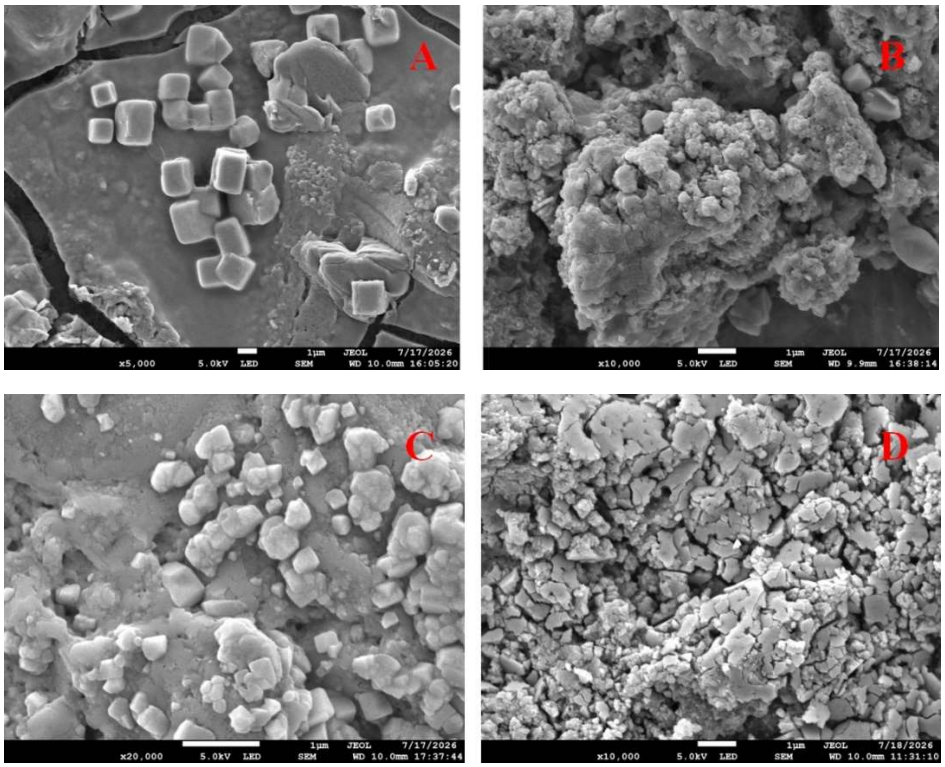


Figure 4.3: FESEM images of **[A]** Ur-L Sample before CO_2 Loading **[B]** Ur-L sample after CO_2 loading **[C]** Un-L (20) Sample before CO_2 Loading **[D]** Un-L (20) sample after CO_2 loading

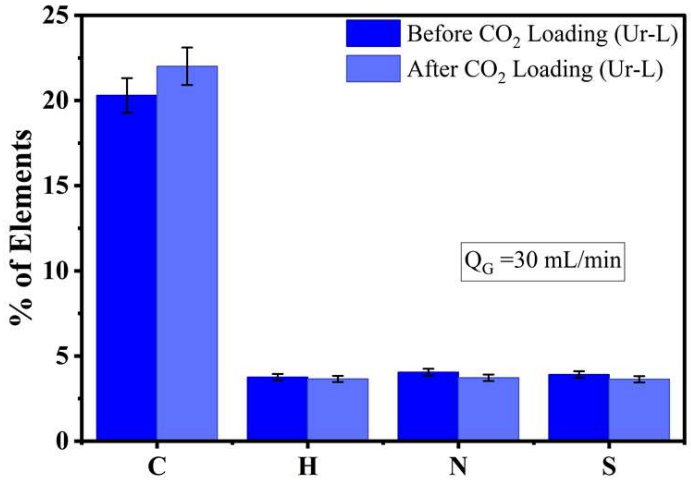


Figure 4.4: Comparison of CHNS elemental composition of Ur-L (Urea-Lignin) absorbent before and after CO_2 loading

4.2.2 Efficacy of functionalized lignin on CO_2 Capture

Gas–liquid reaction between CO_2 and aqueous solution of functionalized lignin is carried out in a CFI reactor. The flow rate of the liquid CO_2 absorbent is varied from 12 to 42 mL/ min, while the CO_2 flow rate is maintained at fixed values of 20, and 30 mL/min. The effect of varying liquid flow rates on the CO_2 absorption performance is systematically investigated. Figure 4.5 demonstrates the role of functionalized lignin on efficiency of carbon dioxide absorption. At a constant flow rate of CO_2 gas, the efficiency of CO_2 absorption gradually increases with increasing flow rate of liquid absorbent and tends to plateau, suggesting reaction equilibrium. Ur-L exhibits superior CO_2 absorption efficiency compared to Hydrazine-Lignin (Hzn-L), while the performance of Ammonia-Lignin (Amn-L) remains comparable to that of Ur-L. Lower gas flow (Q_G = 20 mL/min) consistently gives higher absorption due to longer residence time, while increasing Q_L reduces gas–liquid contact limitations and leads to convergence at higher Q_L. Expectedly, the CO_2

absorption efficiency has decreased significantly with increasing gas flow rates and decreasing liquid flow rates. Notably, the maximum CO_2 absorption efficiency of Ur-L reaches 95% at a gas flow rate of 20 mL/min, whereas it decreases to 85% at 30 mL/min. Liquid absorbent, Ur-L emerges as the most efficient and stable absorbent among Amn-L and Hzn-L for continuous-flow CO_2 capture.

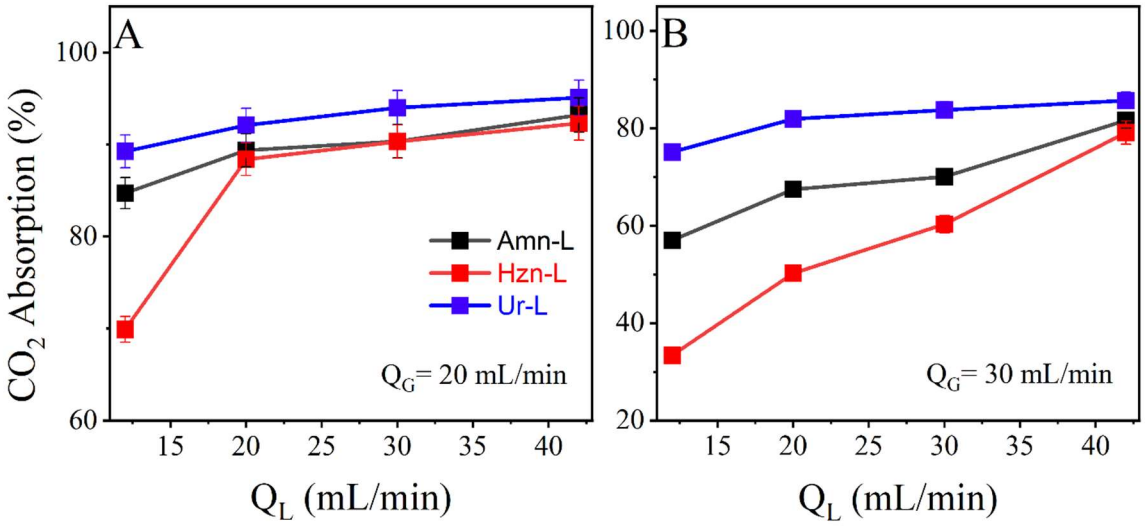


Figure 4.5: Comparison of CO_2 Absorption in different aqueous absorbents, functionalized lignin using ammonia, hydrazine and urea – Ammonia-Lignin (Amn-L) (black square), Hydrazine-Lignin (Hzn-L) (red square) and Ur-L (blue square). and ammonia (black colour) at gas flow rates **[A]** 20 mL/min **[B]** 30 mL/min

4.2.3 Effect of biogas and temperature in CO_2 absorption

The effect of biogas (60% CH_4, 39% CO_2, and 1% N_2) on CO_2 absorption using the urea–lignin (Ur–L) absorbent is presented in Figure 4.6 [A] and compared with pure CO_2 at a constant gas flow rate of 30 mL min^{-1}. For pure CO_2, the absorption efficiency increased from 75% to 86% as the liquid flow rate increased from 12 to 42 mL/min. In comparison,

biogas exhibited lower absorption efficiencies, increasing from 13% to 64% under the same operating conditions. This reduction is attributed to the lower CO_2 partial pressure in biogas, which decreases the gas-liquid mass transfer driving force. Figure 4.6 [B] shows the effect of temperature on CO_2 absorption by Ur-L and Un-L (20). At 30°C, Un-L (20) achieved a maximum absorption efficiency of 95%, while Ur–L reached 84% at a liquid flow rate of 42 mL/min. However, increasing the temperature to 70°C reduced the absorption efficiencies to 45% for Un-L (20) and 31% for Ur-L. The decline at higher temperatures is attributed to the reduced solubility of CO_2, the exothermic nature of the absorption process, and weaker interactions between CO_2 and the active functional groups. Overall, Un-L (20) consistently exhibited superior CO_2 capture performance compared to Ur-L under all operating conditions.

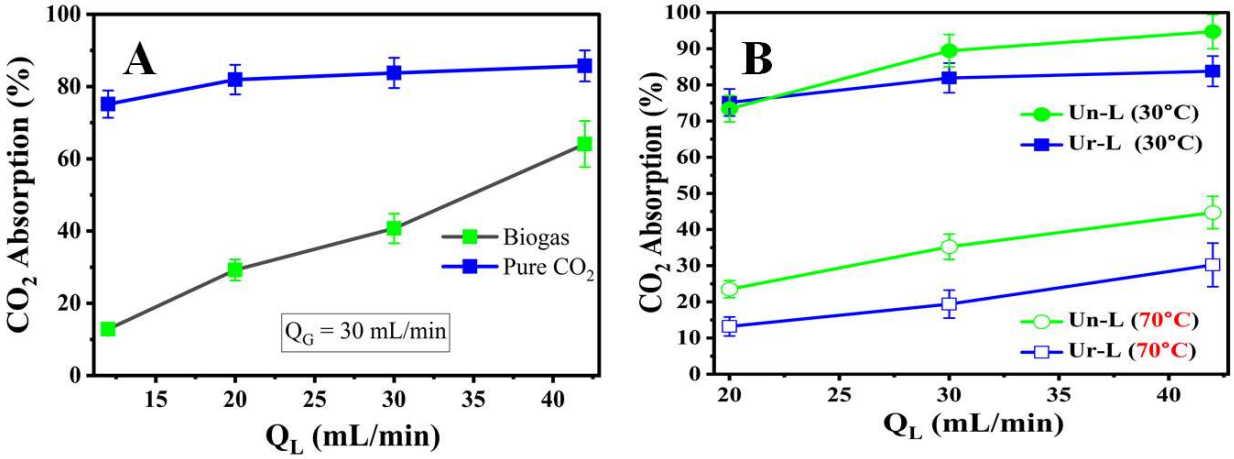


Figure 4.6: Comparison of percentage absorption in different conditions **[A]** Pure CO_2 vs Bio gas at gas flow rate 30 mL/min for Urea-lignin (Ur-L) absorbent **[B]** Effect of temperature at 70°C and 30°C for gas flow rate 30 mL/min with Urea-Lignin (Ur-L) (blue colour) and Urine-Lignin (Un-L) (green colour) absorbent

4.2.4 Effect of absorbent flow rate on hydrodynamics parameter

The variation of pressure drops (ΔP) and Reynolds number (Re) with liquid flow rate for the Ur-L and Un-L (20) absorbents at a constant gas flow rate of 30 mL/min is presented in Figure 4.7. As shown in Figure 4.7 [A], the pressure drop increases with increasing liquid flow rate for both absorbents due to the higher fluid velocity and greater frictional resistance within the CFI reactor. Un-L (20) exhibits a consistently higher pressure drop than Ur-L, with the difference becoming more pronounced at higher flow rates, indicating its comparatively higher flow resistance, likely resulting from its greater viscosity. Figure 4.7 [B] shows that the Reynolds number increases almost linearly with liquid flow rate for both absorbents, reflecting the increase in fluid momentum. However, Ur-L exhibits higher Reynolds numbers than Un-L (20) under identical operating conditions because of its lower viscosity. Despite the increase in Reynolds number, all values remain below 1000, confirming that the flow remains in the laminar regime throughout the study. Overall, increasing the liquid flow rate enhances fluid motion and mixing but also increases the hydraulic resistance inside the reactor. The results demonstrate that although Un-L (20) requires a higher pumping pressure, it maintains stable laminar flow conditions suitable for efficient CO_2 absorption.

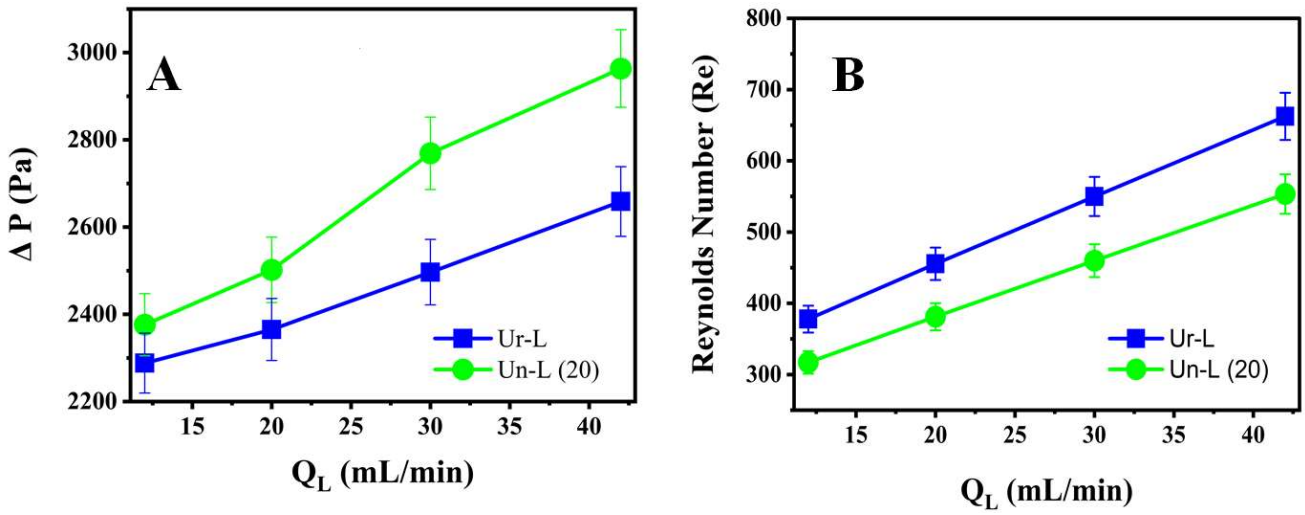


Figure 4.7: [A] Comparison of pressure difference inside CFI reactor during CO_2 absorbance in Urea-Lignin (Ur-L) (blue colour) and Urine-Lignin (20) (Un-L) (green colour) at gas flow rate of 30 mL/min **[B]** Comparison of Reynolds number for 30 mL/min gas flow rate and variation in absorbent flow rates of Un-L (20) (green colour) and Ur-L (blue colour)

4.2.5 Resolving the Contributions of Components of Urea-functionalized Lignin (Ur-L)

Here, we address the contributions of different components of urea-functionalized lignin (Ur-L) toward CO_2 absorption. To elucidate this, two additional liquid absorbents are prepared: (i) an aqueous urea solution without lignin, Ur (0.5 g urea dissolved in 130 mL water), and (ii) an aqueous mixture of urea and lignin (Ur+L) (2.0 g lignin and 0.5 g urea dissolved in 130 mL water). The CO_2 absorption efficiencies of these absorbents are compared with that of hydrothermally synthesized urea-functionalized lignin (Ur-L) prepared using the same composition (2.0 g lignin and 0.5 g urea dissolved in 130 mL water). The effect of liquid flow rate (Q_L) on CO_2 absorption for aqueous solution of Ur, Ur+L and Ur-L is presented in Figure 4.8 [A]. For urea solution only, CO_2 absorption increases moderately from

66% to 79% as liquid flow rate (Q_L) rises from 12 to 42 mL/min at a constant gas flow rate of 20 mL/ min, indicating improved gas–liquid contact at higher flow rates. In contrast, Urea+Lignin solution exhibits much lower CO_2 absorption (22–52%), despite increasing with Q_L. It therefore underscores the necessity of solvothermal processing for functionalization of urea in lignin. The CO_2 absorption efficiency of Ur-L is found to be strongly influenced by the gas flow rate depicted in Figure 4.8 [B]. The absorption efficiency reaches a maximum value of 95 % at a gas flow rate of 20 mL/min. However, the CO_2 absorption decreases to 85% after reaching its maximum value with the increase of the gas flow rate. At a gas flow rate of 20 mL/ min, the absorption efficiency reaches a maximum value of 95%, whereas at higher gas flow rates, the CO_2 absorption decreases to 85%.

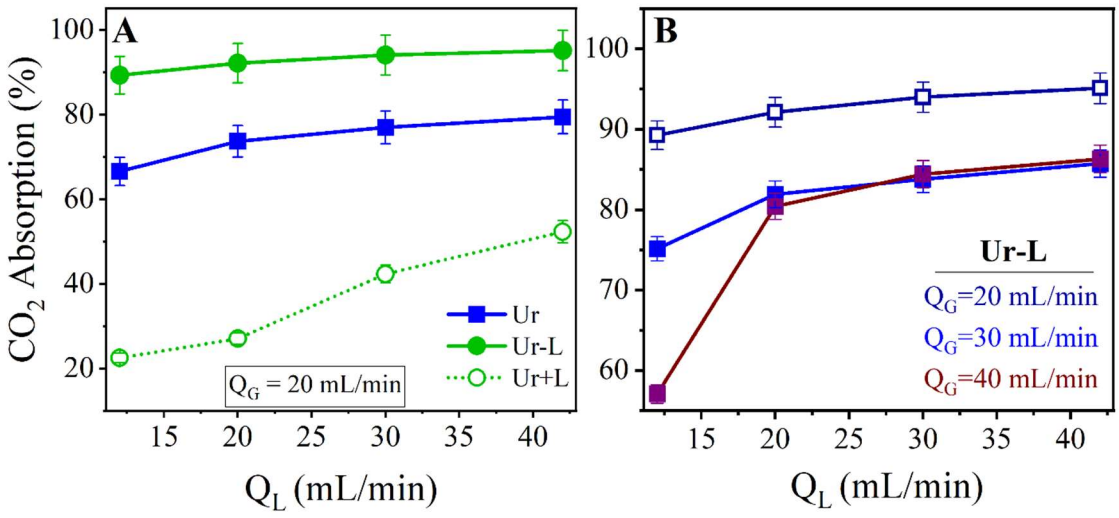


Figure 4.8: [A] Quantifying the role of each component of Ur-L for CO_2 absorption at gas flow rate 20 mL/min– aqueous Ur solution (solid blue line), Ur+L solution (dotted green line) Ur-L solution (solid green line). **[B]** Comparison of CO_2 absorption for Ur-L at gas flow rate of 20 mL/min (hollow square), 30 mL/min (blue square) and 40 mL/min (purple square).

4.2.6 Efficacy of Bio urea present in Human Urine for CO_2 Capture

CO_2 absorption for the Un-L absorbents at a fixed gas flow rate of 30 mL/min is shown in Figure 4.9 [A]. CO_2 absorption increases gradually with increasing liquid flow rate, Q_L for all Un-L adsorbents, indicating improved gas-liquid contact at higher flow rates. Un-L (20 yr) adsorbent exhibits the highest absorption efficiency across the range, reaching 96% at 42 mL/min liquid flow rate, followed by Un-L (30 yr) and Un-L (50 yr). Comparatively lower absorption for Un-L (50 yr) could be attributed to variation of bio urea content in human urine. At higher liquid flow rates, the Un-L adsorbent (20) is more effective than the Ur-L adsorbent as shown in Figure 4.9 [B]. It could reach above 95% CO_2 absorption. The improved performance as explained above is due to the presence of salts and higher viscosity of Un-L (20) as compared to Ur-L.

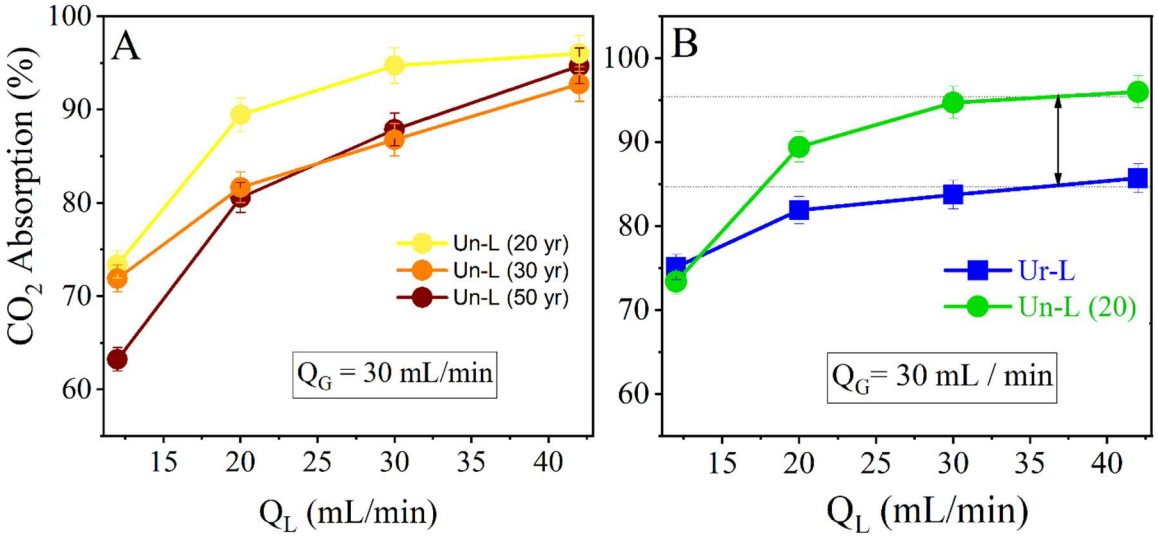


Figure 4.9: [A] Absorption of CO_2 in lignin with urine at gas flow rate of 30 mL/min. **[B]** Comparison of CO_2 absorption of Ur-L (blue square) with Un-L absorbents (green circle) at 30 mL/min gas flow rate. Human Urine from age group of less than 20 years has been used.

4.2.7 Quantification of CO_2 absorption by CO_2 bubble size reduction method

Imaging-based methods offer direct quantification of the progress of gas–liquid reactions and are therefore often employed for such reactions carried out in transparent CFI reactors [155,156]. The applicability of such methods for CO_2 absorption using aqueous functionalized lignin solution becomes highly feasible owing to excellent contrast between the gas and liquid phases. Figure 4.10 presents the bubble size reduction for different lignin-based absorbent systems, where bubble lengths have been determined using ImageJ software. Amn-L and Hzn-L absorbents show relatively low reductions of bubble length (42% and 34%). In contrast, Un (20) -L absorbent achieves the highest bubble size reduction (86.4%) whereas Ur-L achieves a reduction of about 77.3%. This bubble length reduction trend is in good agreement with our results on CO_2 capture efficiency as presented in Figure 4.10 & 4.4.

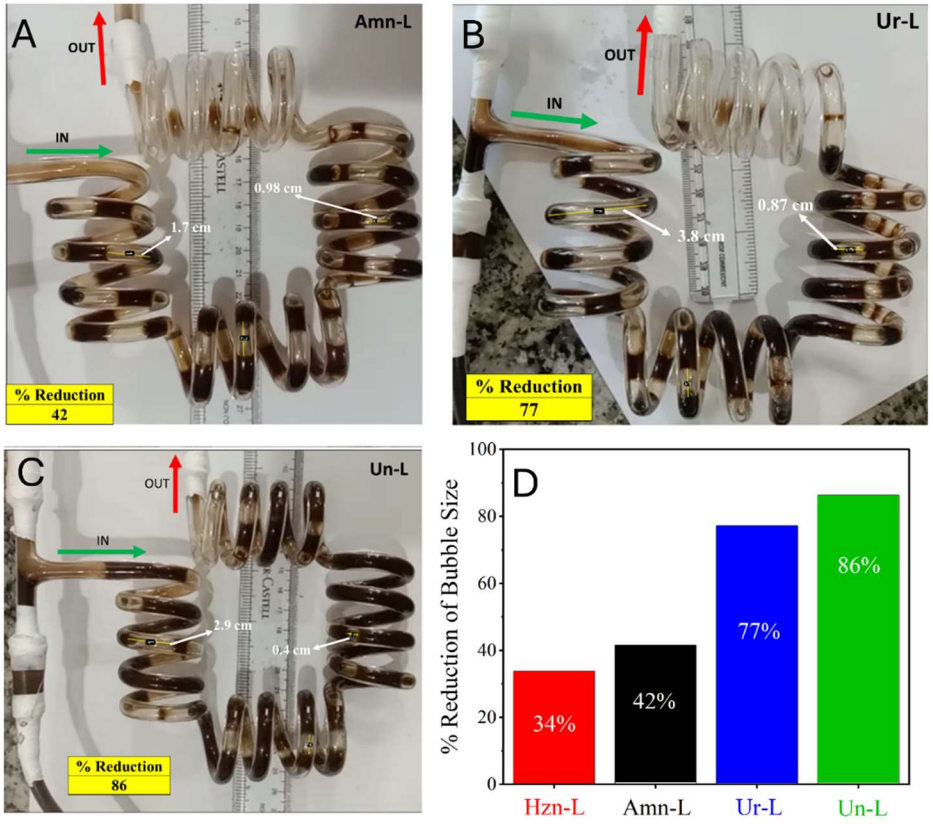


Figure 4.10: Images of CFI reactor during gas-liquid reaction for absorbents- **[A]** Amn-L, **[B]** Ur-L, **[C]** Un (20)-L. The length of gas-bubble at arm-1 of CFI reactor is considered near inlet, whereas the length of same at arm-3 is considered near inlet exit points for determination of reduction of bubble size **[D]** Reduction of CO_2 gas bubble length for four aqueous functionalized lignin adsorbents.

4.2.8 Residual Performance of functionalized lignin absorbents

The absorbent solutions have been reused in a second absorption cycle to evaluate its full potential in CO_2 absorption. Figure 4.11 compares CO_2 absorption performance of fresh and reused lignin-based absorbents. As expected, fresh absorbents show higher absorption than reused ones, indicating limited availability of amine sites. Amn-L and Hzn-L exhibit significant performance drops of about 20-28% upon reuse, whereas Ur-L and Un-L retain relatively high absorption efficiencies of about

80%. Notably, Un-L exhibits the performance in second cycle by maintaining 83% CO_2 absorption. These results demonstrate that Ur-L and Un-L absorbents possess superior performance, making them more suitable for sustainable CO_2 capture applications. Since both Ur-L and Un-L absorbent exhibit high CO_2 absorption efficiency and their reusability is evaluated by conducting repeated cycles under same identical condition without regeneration of absorbent and this is shown in Figure 4.12. The experiments are carried out for up to 10 consecutive cycles. A gradual decrease in CO_2 absorption is observed per cycle. For Ur-L absorbent, the CO_2 absorption decreases from 87% to 29% and similarly Un-L absorbent shows reduction from 96% to 25%. The gradual decline in CO_2 absorption efficiency is attributed progressive loss of active absorption sites during repeated cycle. Both absorbents show a substantial drop in CO_2 capture efficiency across ten consecutive cycles, attributed to either partial deactivation of active amine sites, incomplete thermal regeneration or accumulation of non-volatile species, but they still retain a baseline functional capacity. This implies that the system is promising for cyclic recycling operations, but further optimizations of the regeneration protocols are required to reduce the performance decay over extended use.

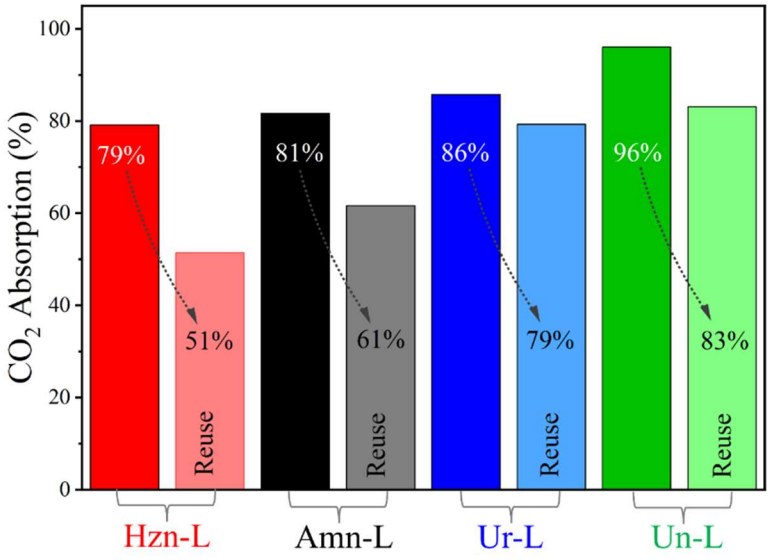


Figure 4.11: CO_2 capture efficiency of aqueous functionalized lignin absorbents in 2nd cycle.

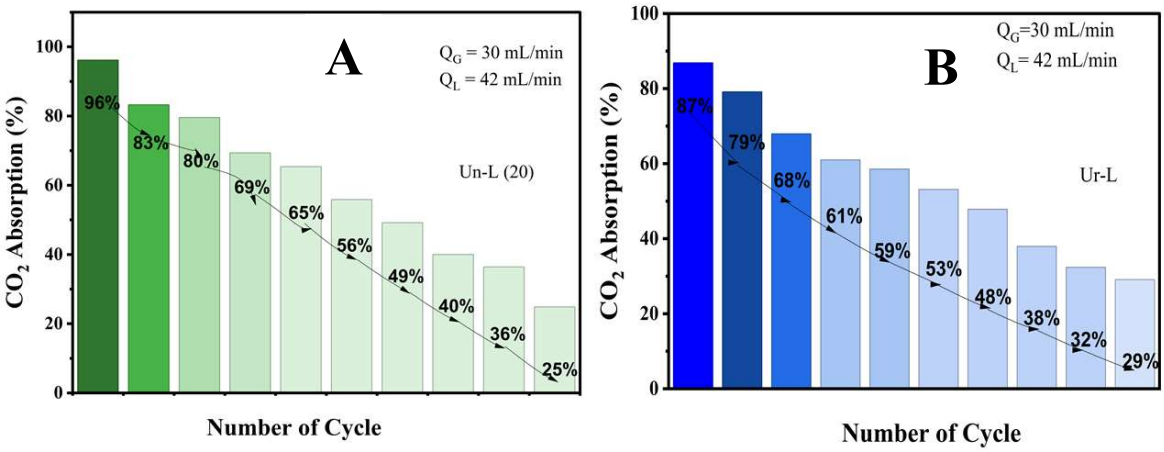


Figure 4.12: CO_2 capture efficiency of **[A]** Urine-Lignin (20) **[B]** (Ur-L) and Urea-Lignin (Ur-L) absorbents in 10th cycle.

4.3 Conclusion

In summary, aminated lignin absorbents have been synthesized using ammonia, hydrazine, and urea as amine precursors and evaluated for continuous CO_2 capture

in a coiled flow inverter (CFI) reactor. CFI enables efficient gas–liquid mixing, thereby enhancing mass transfer and absorption performance. The CO_2 capture efficiencies of the absorbents are systematically investigated by varying the CO_2 flow rate (20–40 mL/min) and absorbent flow rate (12–42 mL/min). Among the three systems studied, the urea-functionalized lignin exhibits the highest performance, achieving up to 95% CO_2 absorption under optimized continuous-flow conditions. Furthermore, a urine-derived lignin absorbent, synthesized using human urine as a sustainable source of urea, demonstrates an even higher maximum CO_2 capture efficiency of 96% at a CO_2 flow rate of 30 mL/min, compared with 85% for the conventionally prepared urea–lignin absorbent under identical conditions. Image-based hydrodynamic analysis reveals that both lignin–urea and lignin–urine absorbents promote greater bubble size reduction and more favorable flow characteristics. Slug-length analysis further establishes a direct correlation between reduced slug length and improved CO_2 absorption efficiency. Importantly, both urine–lignin and urea–lignin absorbents retained high CO_2 capture performance during a second absorption cycle. The integration of waste-derived lignin and human urine offers a carbon-neutral absorbent-driven strategy for efficient CO_2 capture.

Chapter 5: Intensifying the Synthesis of Xanthene Dyes from Gallic Acid using Coiled Flow Inverter[1]

5.1 Brief Introduction

Transparent Coiled flow inverters (CFI) which are superior to opaque coil reactors are hardly explored in performing condensation reactions of organic molecules. Herein in this chapter the continuous flow condensation reaction of Gallic acid using CFI with a 4 mm internal diameter have been reported. The length of the flow reactor is varied by connecting CFIs in series. Real-time images of reactor captured during flow synthesis resolve the intricacies of reaction dynamics and stages of desired product formation. Stack CFI provides a desired residence time for carrying out reaction at high flow rate. Condensation of Gallic acid in dimethyl formamide yields a green emissive xanthene analogue. The production of organic emitter is optimized by regulating reactant flow rate, and temperature of the reaction. The presence of vapour-liquid phase boundary enhances the interfacial area that further contributes to increasing the product yield. The optimized condition for fluorescent product using stack CFI is 190 °C ($\pm$ 5) temperature at 5 mL /h ($\pm$ 0.5) flow rate. A residence time of about 14 hours ($\pm$ 1) and a heat flux of 4.46 W/m^2 ($\pm$ 0.5) are desired for maximizing product yield using stack CFI. These suggest that CFI-based flow reactor can easily be tailor-made and economical as well.

[1]*The work discussed in this chapter have been published in Chem Plus Chem 90, no. 11 (2025): e202500313*

5.2 Results and Discussion

5.2.1 Effect of residence time on product formation

The purpose of opting transparent CFI over helical coil reactor is because of monitoring the progress of reaction and enhanced mixing and heat transfer by the change in the flow direction by 90°[157]. Moreover, CFI is transparent, economical, and compact. The length of CFI has been kept at 2.63 m for a single CFI, whereas it is increased to 5.26 m by connecting CFIs in series (stack CFI). In general, reactions carried out under continuous flow synthesis are optimized by primarily regulating two independent parameters- (i) residence time by either regulating the flow rate or reactor's length, and (ii) temperature of the reaction. In this work first residence time have been regulated to decipher its impact on condensation of Gallic acid in DMF. It can be noted here that vapour pressure of DMF in the temperature range of 180-190 °C is above 2 bar. The dependence of pressure on condensation reaction can be highlighted by using CFI. Flow experiments performed on Gallic acid condensation in DMF have been tabulated in Table 5.1. The temperature of oil-bath at 170°C have been fixed, just above the boiling point of DMF (153°C). Steady-state absorption and fluorescence of product have been monitored by varying flow rates and lengths of CFI depicted as in Figure 5.1.

Table 5.1: Condensation experiments using CFI stack at 0.04 % (w/v) Gallic acid in DMF

Sl. No.	**Flow Rate** (mL/h)	**Residence Time** (Hrs)	**Temperature** (°C)					**Fluorescence Intensity** λ_{ems}: 525 nm at λ_{exc}: 425 nm				
1	4	16.51	160	170	180	190	200	247	282	454	405	650
2.	5	13.21	160	170	180	190	200	397	609	288	1024	744
3.	6	11.01	160	170	180	190	200	343	412	310	658	127
4.	7	8.25	160	170	180	190	200	164	216	189	495	23

Absorption spectra of products coming out from the flow reactor is relatively broad with a strong absorption near 400 nm and a shoulder peak at 550 nm. The product obtained from stack CFI exhibits relatively strong absorption than that obtained using CFI only as illustrated in Figure 5.1 [A]-[C]. The absorption of products has been kept very low to avoid inner-filter effect. As expected, upon excitation at 425 nm (λ_{exc} = 425 nm) product obtained from stack CFI displays a higher emissivity than that collected from CFI only depicted in Figure 5.1 [D]-[F]. By analyzing fluorescence peak maxima at 525 nm of products, it can be mentioned here that the stack CFI is perhaps providing sufficient residence time for condensation reaction even at varied flow rate 3 mL/hr–6 mL/hr.

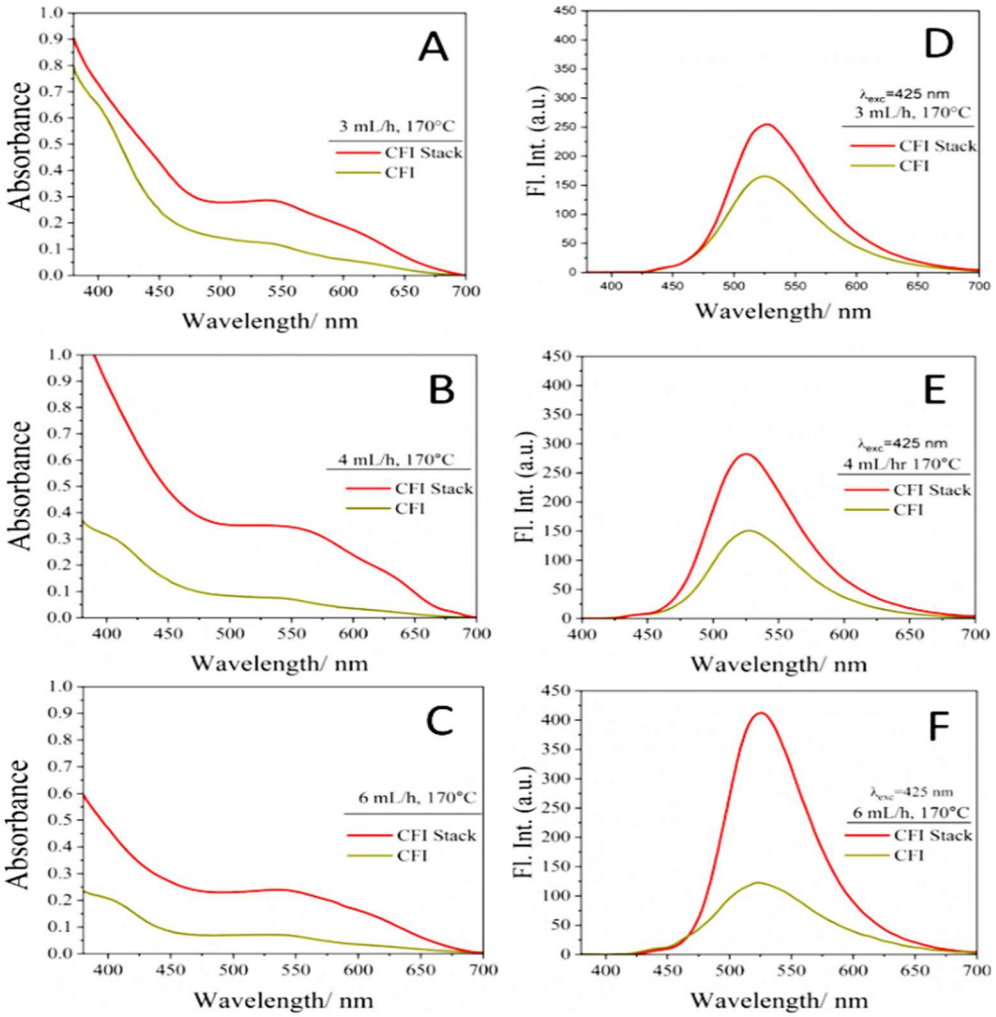


Figure 5.1: Absorption spectra of the product obtained at 170 ℃ at different flow rates– **[A]** 3 mL/h, **[B]** 4 mL/h, **[C]** 6 mL/h. Emission spectra of product at the same temperature at the respective flow rates– **[D]** 3 mL/h, **[E]** 4 mL/h, **[F]** 6 mL/h. CFI Stack (red line) and CFI (green line)

Considering the broad nature of absorption spectra, further examination on the ground state heterogeneity of products formed by flow synthesis have been performed. The dependence of emission property on excitation wavelength is often probed for identifying the product's heterogeneity. Contour plots of product's

emission spectra have thus been constructed at varied excitation wavelengths and have been depicted in Figure 5.2.

The fluorescence intensity distribution of products has been compared by using a single CFI depicted in Figure 5.2 [A]-[C] and stack CFI depicted in Figure 5.2 [D]-[F]. The intensity distribution is relatively broad for CFI suggesting an incomplete condensation reaction. However, a dominant peak is centered at 525 nm for the excitation at 425 nm and a shoulder peak at 475 nm for the excitation at 375 nm. Interestingly, the fluorescence intensity distribution is relatively sharp for products obtained from stack CFI with a peak 525 nm depicted in Figure 5.2 [D]-[F]. Notably, a significant increase in emission properties of products further emphasizes the utility of stack CFI at a high flow rate, 6mL/hr illustrated in Figure 5.1 [F].

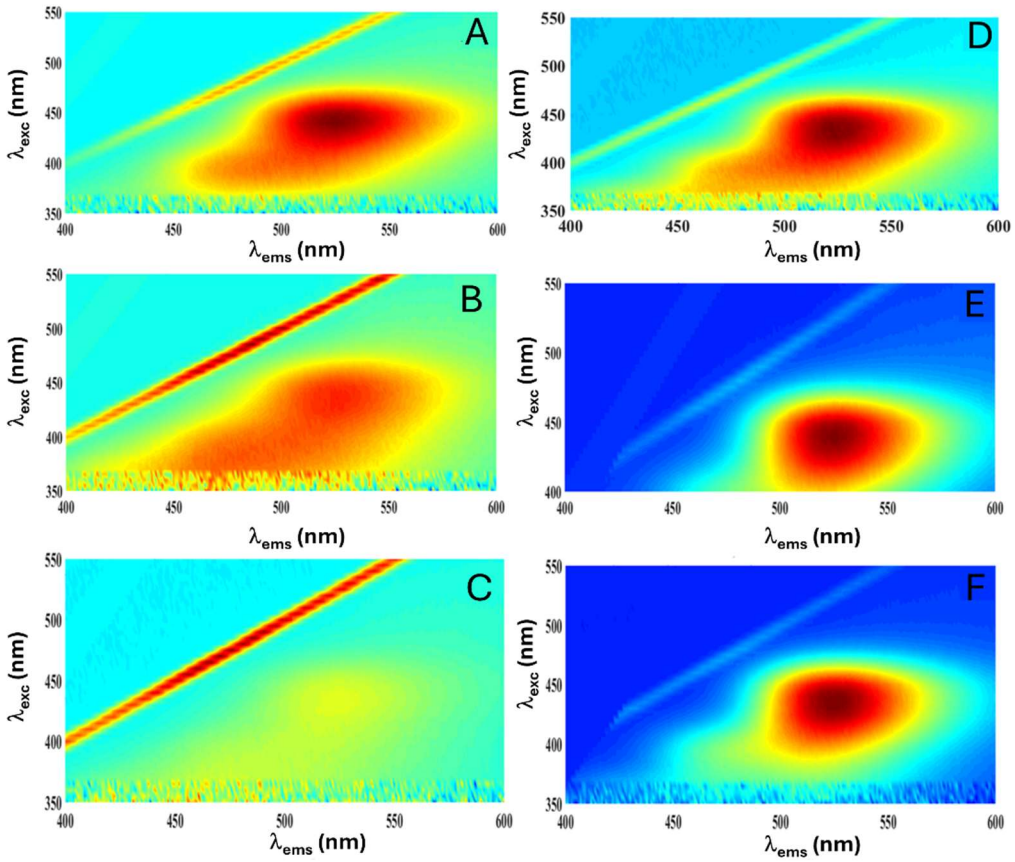


Figure 5.2: Contour plots of the emission spectra with the corresponding excitation wavelengths of product obtained at 170 ℃ by varying length of CFI and flow rate. CFI at different flow rates – **[A]** 3 mL/h, **[B]** 4 mL/h, **[C]** 6 mL/h. Stack CFI at different flow rates –[**D]** 3 mL/h, **[E]** 4 mL/h, **[F]** 6 mL/h.

The efficacy of stack CFI has been demonstrated by capturing real-time images of reactor during synthesis in ambient light and under UV-light irradiation which is illustrated in Figure 5.3. In ambient light, the colour of reactant solution in reactor gradually changes from faint yellow to dark brown colour as shown in Figure 5.3 [A]. It is also evident that liquid-vapour flow regime has been developed and vaporization of solvent, DMF (boiling point, 153°C). Thereafter, the reactor zone at which product displays its emissive properties has been resolved upon irradiation of

UV light as shown in Figure 5.3 [B]. The product flowing through the seventh coil section of stack CFI exhibits green fluorescence at high flow rate, 6mL/hr.

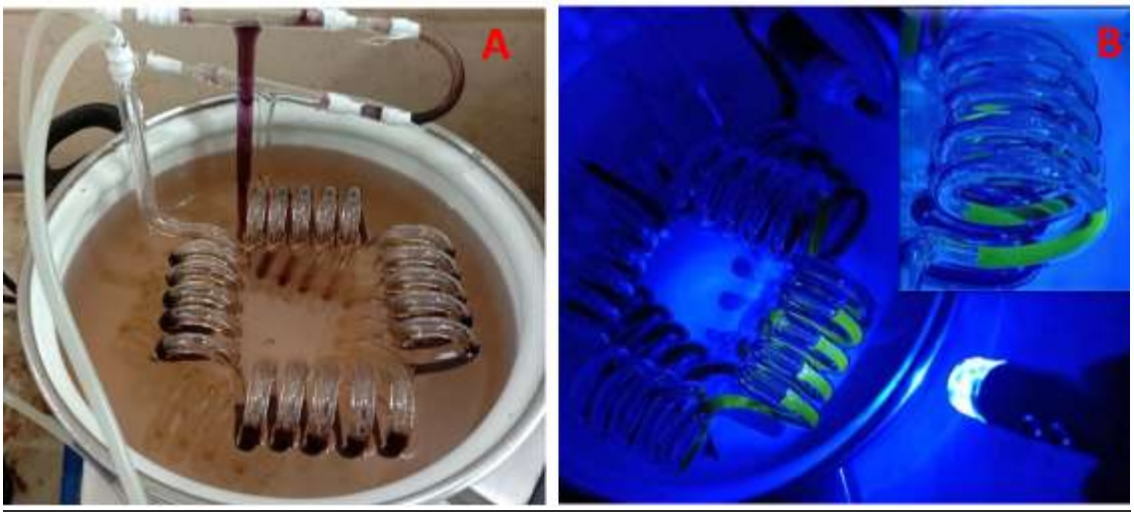


Figure 5.3: Real time images of reactor during synthesis- **[A]** in ambient light (representative), **[B]** under UV-light irradiation. Inset: Zoom-in section of stack CFI

Residence time has played a decisive role in dictating the fluorescence intensity distribution of products, thus yield of the desired organic emitter. It can be stated here the residence times for CFI at flow rate of 3 mL/hr and stack CFI at flow rate of 6 mL/hr remain nearly identical in values. That means, at the same flow rate of 6 ml/hr, the residence time of reactant solution for CFI is 5.5 hr (13.26×10^{-5} m/s flow velocity), but it gets doubled to 11 hr for stack CFI. Moroever, CFI has a high surface area to volume (area density) ratio which offers more convective heat transfer from its surface. Residence time has thus been the major factor for the formation of by-

products. The role of temperature on product yield has been discussed in the next section.

5.2.2 Effect of Temperature on Product Formation

Temperature has been a key factor in driving chemical reactions because it allows molecules to achieve activation energy for the reaction. With increase in temperature the colour of the product solution gradually changes from light brown to dark brown for a constant flow rate as shown in Figure 5.4 [A]-[B]. The product yield is monitored by the emissivity of product at 525 nm upon excitation at 425 nm. Higher fluorescence intensity at 525 nm thus signifies a higher yield of product. At a low flow rate (3 mL/h), the maximum product yield is achieved at 180 °C whereas the product yield becomes minimum at 190 °C as illustrated in Figure 5.4 [C].

Interestingly, the product yields are comparable at 180 °C and 190 °C for the flow rate of 4 mL/h as shown in Figure 5.4 [D]. Whereas, at a high flow rate (6 mL/h), maximum product yield is obtained at 190 °C, and the product yields at 160 °C and 180 °C are in the same range as shown in Figure 5.4 [E]. The dependence of operating conditions, such as reactant flow rate and temperature have been illustrated by constructing a contour plot of fluorescence intensity as shown in Figure 5.5. The optimized condition for Gallic acid condensation in DMF for yielding organic emitter at 525 nm using stack CFI is– 190 °C (±5) temperate and 5 mL /h (± 0.5) flow rate. It has been observed that with increased residence time the phenolic compounds (reactant/products) undergo oxidation and degradation at high temperatures. Whereas, at a short residence time (high flow rate) the unnecessary oxidation of phenolic compounds is minimized and that positively impacts the enhancement of

product yield. At lower temperatures the product formation is limited by activation energy.

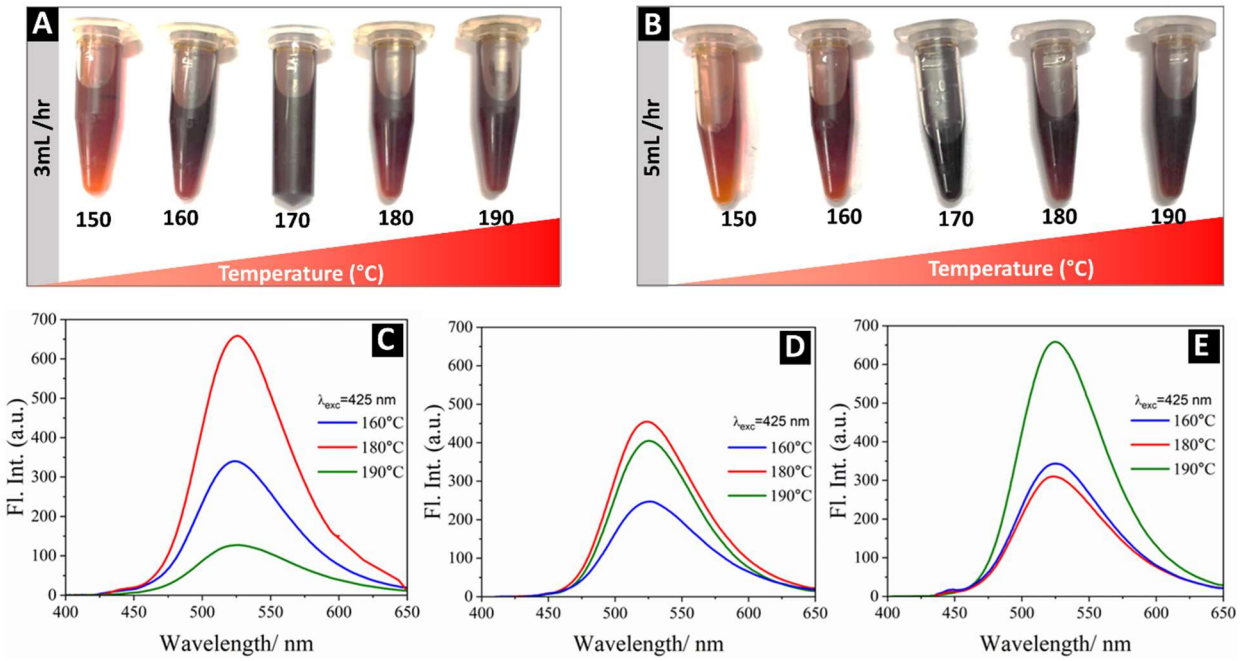


Figure 5.4: Impact of temperature on formation of fluorescent product for stack CFI. Colour of product solution obtained by varying temperature at flow rate– **[A]** 3mL/hr, **[B]** 5 mL/hr. Fluorescence spectra of product in solution at three different temperatures for flow rate- **[C]** flow 3mL/hr **[D]** 4mL/hr **[E]** 6mL/hr. 160°C (blue line), 180°C (red line), 190°C (green line), The excitation wavelength, λ_{exc} has been kept at 425 nm.

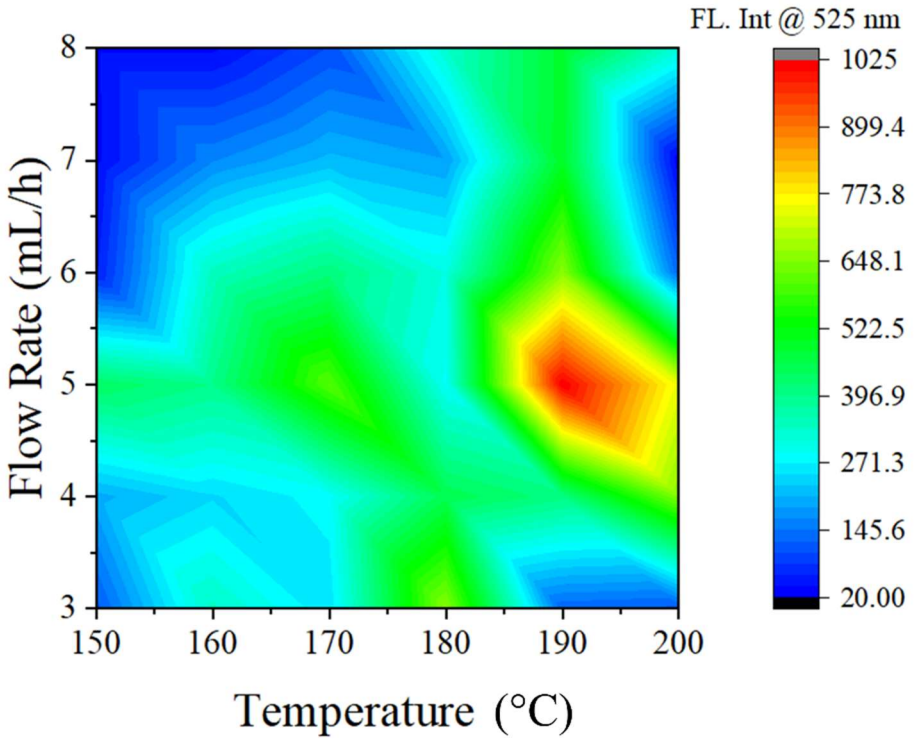


Figure 5.5: Dependence of operating conditions: flow rate and temperature on product formation for stack CFI. Contour plot of fluorescence intensity on reactant flow rate and temperature of the reaction.

5.2.3 Impact of Heat Flux on Gallic Acid Condensation

Analyzing the temperature dependence on product formation is a conventional approach but is limited to reactions carried out in a closed volume, such as continuous stirred tank reactor (CSTR). However, heat flux is rather better suited to understand the temperature effect on continuous flow synthesis. An optimum heat is required to maximize the product yield because heat higher than optimal can degrade the product and reactant both. Gallic acid precursor is completely solvated in dry DMF and homogeneous solution is formed. The fluid flows into the heating zone (180 °C-190 °C) which is well above the boiling point of the solvent 190 °C and partial in-situ vaporization causes a dynamic vapor-liquid flow regime. This phase boundary

generates strong interfacial micro-convection to promote the condensation reaction forward. These mass and heat transfer limitations afflict conventional straight tubular or standard helical coil reactors with stagnant boundary layers, broad residence time distributions and localized thermal lags which cause severe byproduct formation and phenolic oxidation. The CFI configuration circumvents these limitations. In particular, the CFI induces periodic 90° changes of the spatial direction causing cross-sectional Dean vortices and chaotic advection. The continuous disruption of the boundary layer guaranties a well-defined plug flow profile and homogeneous heat flux density 4.46 w/m2 that dynamically optimizes the tracking of the fluorescent xanthene analog while suppressing secondary degradation pathways

Here the optimum condition for heat transfer for the reaction of Gallic acid and DMF in the CFI stack have been deduced. The following presumptions have been made to quantify the heat flux associated with Gallic acid condensation−

- The velocity of reactant in the range of 10^{-5} m/s in CFI has been very low, and it is considered as free convection inside and outside of CFI.
- The specific heat is uniform during the experiment.
- Condensation reactions are exothermic in nature because of formation of new bonds. Heat of the reaction is not considered owing to low concentration of substrate.

Considering the heating power (1000 W) of oil bath, the time required to raise the temperature of reactant solution (say, 5 mL) from 30 ℃ to 200 ℃ inside the CFI is about 1 min which is negligible in comparison to residence time. Thus, there is no thermal gradient adversely impacting the product formation, temperature of solution

at the inlet is taken as 30 °C and at the exit, it is 190 °C. Heat received by the reactant solution and heat flux are calculated by using equation 1 & 2 [158] and tabulated in Table 5.2.

$$Q = m \cdot C_p(T_{out} - T_{in}) \quad W \qquad \textbf{(1)}$$

$$Q = Flow\ rate\ (kg/s) \times Cp\ \ (J/kg\ K) \times (T_{out} - T_{in})\ K$$

$$Heat\ Flux\ (W/m^2) = \frac{Heat\ received\ (W)}{Surface\ Area\ of\ reactor\ (m^2)} \qquad (\mathbf{2})$$

Here T_{out} is temperature of solution at exit of CFI stack, which is equivalent to the temperature of the surrounding i.e., the silicon oil temperature and T_{in} is temperature of solution at inlet in CFI stack, m· is mass flow rate of reactant and C_p, specific heat is taken as 2060 J/kg K [159].

Table 5.2: Quantification of heat flux for the reaction at varied flow rates.

Sl. No.	Flow rate (ml/hr)	Flow rate* (kg/s)	Velocity** (m/s)	Temperature used (°C)	Amount of Heat Received (W)	Heat flux (W/m^2)
1.	3	8.20×10^{-7}	6.63×10^{-5}	180	0.25	2.51
2.	4	10.9×10^{-7}	8.85×10^{-5}	200	0.38	3.79
3.	5	13.7×10^{-7}	11.06×10^{-5}	190	0.45	4.46
4.	6	16.4×10^{-7}	13.27×10^{-5}	190	0.54	5.35
5.	7	19.1×10^{-7}	15.48×10^{-5}	190	0.66	6.56
6.	8	21.9×10^{-7}	17.69×10^{-5}	190	0.76	7.49

*$Flow\ rate\ (kg/s) = \frac{Flow\ rate(mL/hr) \times \rho_{solution}}{3600 \times 1000}$; $where\ \rho_{solution} = 0.984\ g/mL$

**$Velocity\ (m/s) = \frac{Flow\ rate\ (mL/hr) \times 10^{-6}}{area\ of\ cross-section\ of\ reactor\ (m^2) \times 3600}$

Figure 5.6 highlights the variation of fluorescence intensity against heat flux. Heat absorbed is 0.4223 W for temperature 190 °C and flow rate, 5 mL/h. The optimized heat flux is thus $4.46\,W/m^2$ for the Gallic acid condensation to yield fluorescent product. Higher heat flux is expected to degrade both, reactant and product. The condensation of Gallic acid in DMF for yielding fluorescent product therefore demands a residence time of about 14 hours (± 1) and a heat flux of 4.46 W/m^2 (± 0.5) for using stack CFI

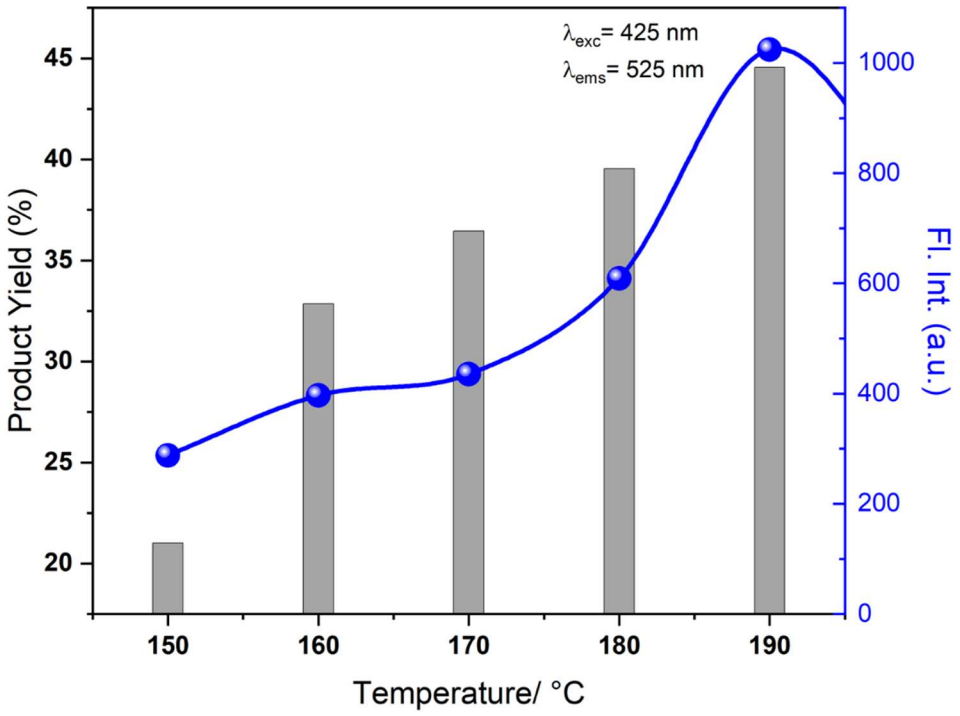


Figure 5.6: Dependence of product yield (vis-à-vis fluorescence intensity) on temperature. Product yield (%) and fluorescence intensity have been measured independently.

5.2.4 Product characterization

The organic emitter obtained from continuous flow synthesis has been characterized steady-state and time-resolved spectroscopic methods. The emission peak is centered at 525 nm irrespective of reactant flow rate suggesting strong emissivity of product and minimal by-product formation as shown in Figure 5.7 [A]. It can be mentioned here that Xanthene dyes, notably fluorescein and rhodamine derivatives, are widely investigated molecular fluorophores. Fluorescein absorbs strongly at 490 nm and emits bright green light near 515 nm, whereas rhodamine analogues (such as Rhodamine B and Rhodamine 6G exhibit absorption between 530 and 550 nm and emission spanning 560 to 580 nm. The temporal properties of product have been characterized by picosecond time-resolved measurements. The emission lifetime of the product is measured at 405 nm excitation with a fixed emission wavelength at 540 nm for the product. The decay trace is biexponential in nature with average fluorescence lifetime, 2.37 ns confirmatory of molecular rigidity as shown in Figure 5.7 [B]. To gauge the presence of functional groups, present in the product used FTIR spectroscopy as illustrated in Figure 5.7 [B] have been used. Also considering the direct role of starting material, the FTIR spectra of product and Gallic acids are overlaid as shown in Figure 5.7 [C]. A clearly visible difference can be noticed between the FTIR spectra of Gallic acid and the synthesized product. From 3700 to 3100 cm^{-1}, the stretching vibrations of O–H, and COO–H contribute to the very broad band respectively. The peaks at 2970 $cm^{-1}$and 2850 cm^{-1} are due to the stretching vibrations of aromatic (=C-H) and aliphatic C-H bonds [160]. The strong FTIR band at 1720 cm^{-1} belongs to C=O (carboxylic acid group) and relatively broad band, 1680-1510 cm^{-1} is indicative of C=O (carbonyl) and C=C vibrations

respectively. FTIR peaks at 1390 cm^{-1} and 1120 cm^{-1} are assigned to the stretching frequencies of C-N and C-O-C bonds respectively.

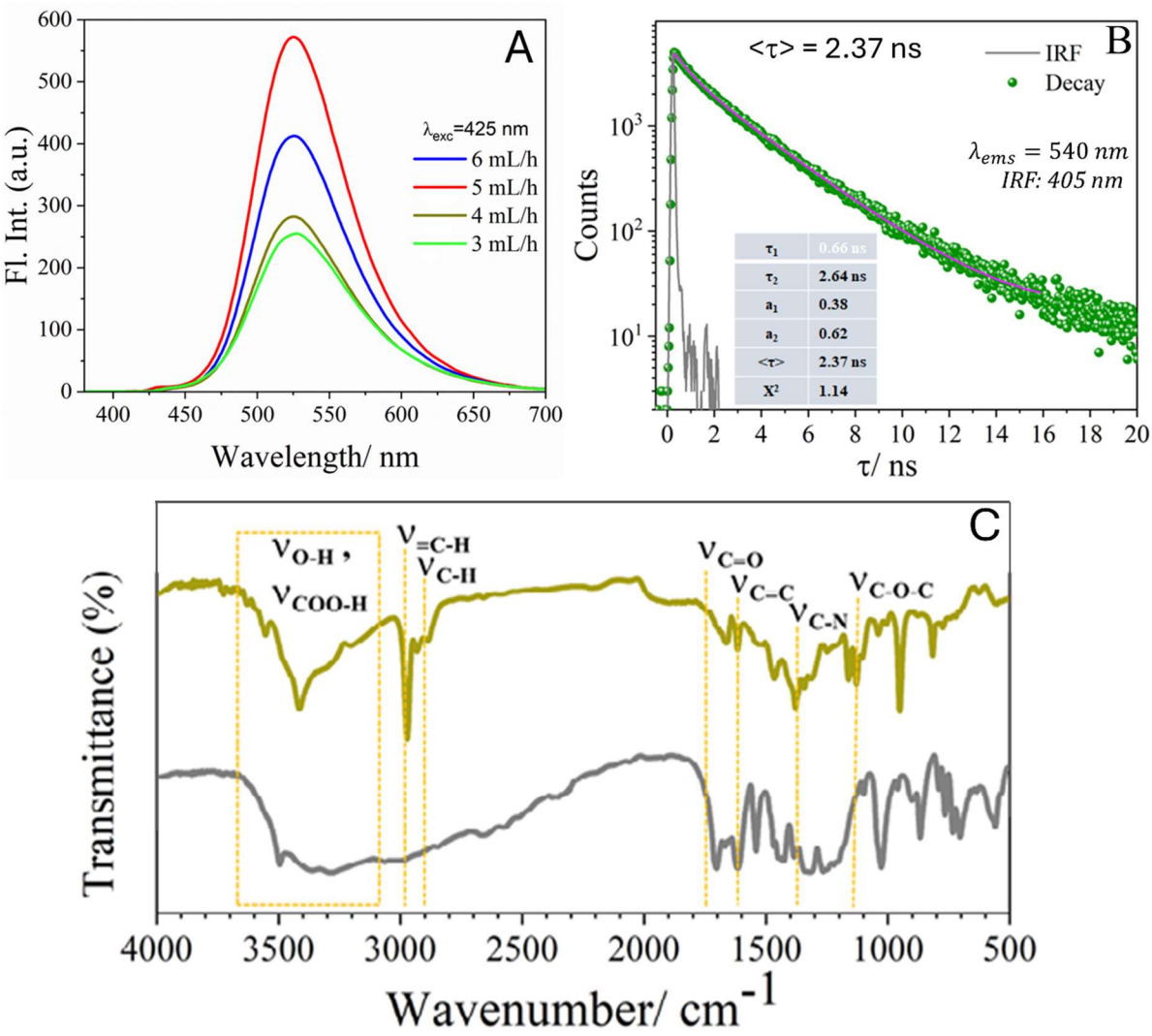


Figure 5.7: [A] Emission spectra of product obtained at 170 °C using stack CFI at different flow rates. 3 mL/hr (green line), 4 mL/hr (dark yellow line), 5 mL/hr (red line), 6 mL/hr (blue line). **[B]** Time-resolved fluorescence decay of same product. **[C]** ATR FT-IR of same product (dark yellow) and Gallic acid (grey).

Based on the above observations, the first step is proposed to involve the formation of an adduct through the condensation of two Gallic acid molecules, as depicted in Figure 5.8. Thereafter, formylation of adduct by solvent, DMF and followed by the xanthene formation. Dimethyl-formamide is serving as a formylating agent here, which is quite similar to the Vilsmeier-Haack reaction for formylation of electron-rich aromatic rings. Aromatic substitution of dimethylammonia has resulted decarboxylation at electron-deficient benzene ring of Xanthene, yielding of the fluorescent product, 1-(dimethylamino)-4,5,6-trihydroxy-3-oxo-3H-xanthene-8-carboxylic acid. ^{1}H NMR and 13CNMR spectra of product presented in Figure 5.9 & 5.10 further support the formation of above xanthene analogue.

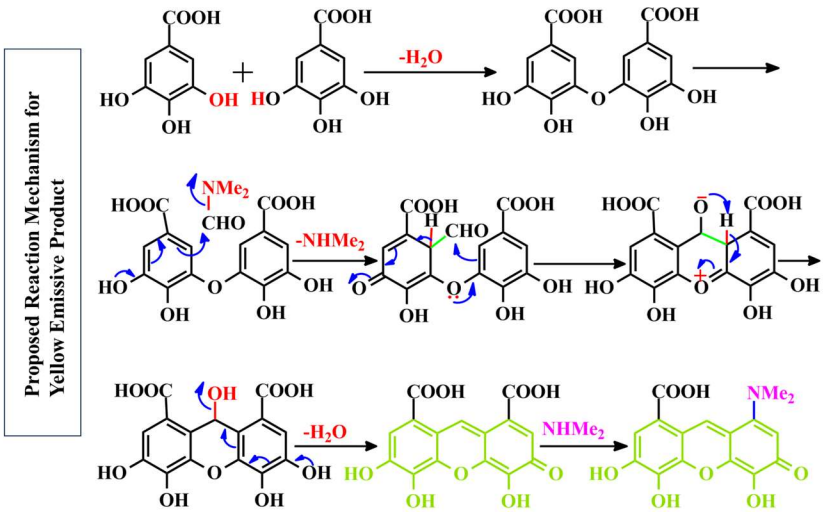


Figure 5.8: Plausible reaction mechanism for yielding Xanthene analogue by condensation of Gallic acid in DMF.

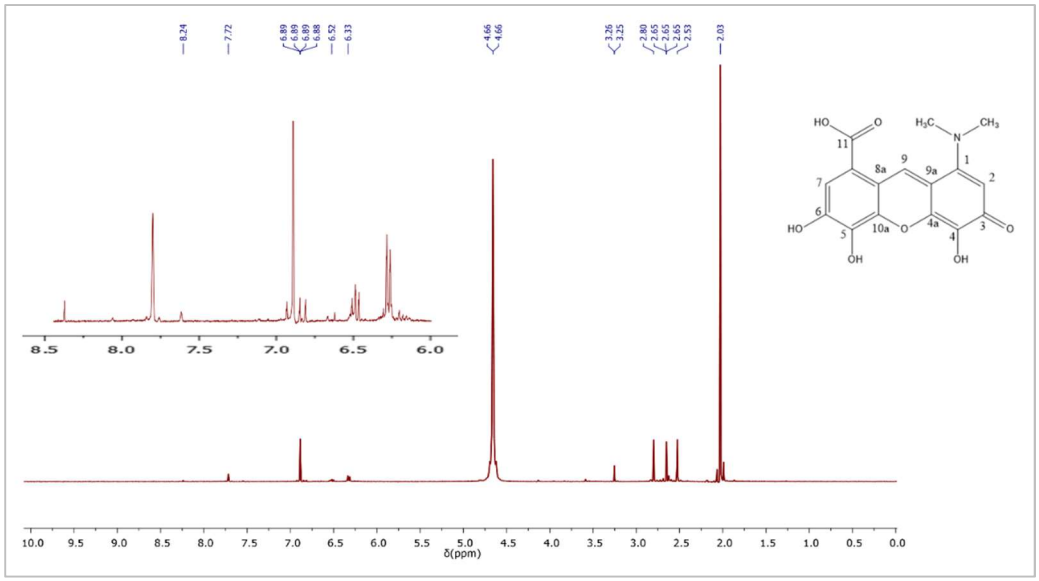


Figure 5.9: H^1-NMR (JEOL, 400MHz) spectra of the product in D_2O; δ 8.24 (s, –COOH), 7.72 (s, 1H, H–C9), 6.89 (s, 1H, H–C2, C7), 6.52 (s, –OH, C4), 6.33 (s, –OH, C5, C6), 2.03 (s, 6H, N–CH_3), δ 4.66 (solvent residual peak–because of exchangeable protons of –OH and –COOH groups, their peaks are highly diminished in the spectra). The singlet peaks at δ 2.5-2.9 are attributed to impurities, primarily due to residual DMF solvent.

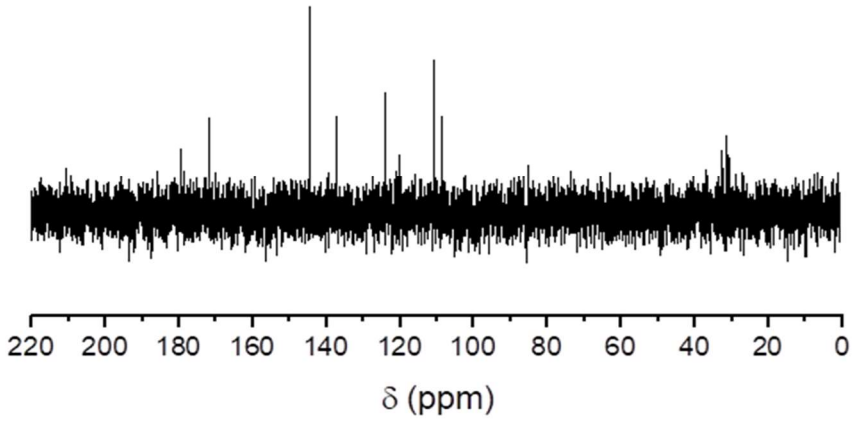


Figure 5.10: C^{13}-NMR spectra (JEOL, 400MHz) spectra of the product in D_2O; C^{13}-NMR spectra (JEOL, 400MHz): δ 179.58 (C3, C1), δ 171.77 (C11), δ 144.35 (C6, C4, C10a), δ 137.05 (C5, C4a), δ123.81 (C8), δ 120.20 (C8a), δ 110. 57 (C7, C2), δ 108.61 (C9), and δ 31.08 (C13, C12).

5.3 Conclusion

Continuous flow synthesis of fluorescent xanthene analogue from Gallic acid condensation in DMF using coiled-flow-inverter (CFI) has been demonstrated. A CFI of length 2.6 meters with an internal diameter of 4 millimeters has been used. The production yield is monitored by its fluorescence emission at 525 nm. The flow synthesis of organic emitter is optimized by regulating reactant flow rate, reactor's length, and temperature of the reaction. Real-time images of reactor captured during flow synthesis resolve the stages of desired product formation and justify the need of stack CFI connected in series. Formation of liquid-vapour phase boundary enhances the interfacial area that perhaps contributes to drive the product formation even at low vapor pressure. The reaction condition have been optimized for Xanthene analogue emitting at 525 nm using stack CFI, which is 190 °C (± 5) temperature and 5 mL /h (±0.5) flow rate. The condensation of Gallic acid in DMF requires a residence time of about 14 hours (± 1) and a heat flux of 4.46 W/m^2 (± 0.5) for stack CFI.

Chapter 6: Conclusions and Future Work

6.1 Conclusions

The present work represents various applications of process intensification for CO_2 capture and reaction kinetics study. The work particularly focusses on enhancement of gas-liquid CO_2 absorption and chemical synthesis with millimeter-sized reactors, particularly with the Coiled Flow Inverter (CFI) and Helical Coil Reactor (HCR). The present work investigates CO_2 absorption in aqueous alkanolamine solutions using a Coiled Flow Inverter (CFI) and a Helically Coiled Reactor (HCR), with a focus on hydrodynamic intensification of gas–liquid mass transfer. A comparative study employing millimeter-scale CFI and HCR of identical dimensions demonstrated that the CFI consistently achieved higher CO_2 absorption efficiency than the HCR, highlighting its superior mixing and mass transfer characteristics. The periodic inversion of Dean vortices in the CFI improves radial mixing, renews the gas–liquid interface and extends the slug-flow regime, thereby increasing interfacial area and mass-transfer rates. The reactor geometry is employed as a process intensification tool to achieve CO_2 absorption efficiency of up to 98% through the optimization of gas and liquid flow rates with blended amine systems. The absorption of CO_2 through bio derived lignin and amine functionalized lignin via CFI which is second part of the work which aims in development of cost effective bio-solvents for CO_2 capture. Sustainable CO_2 absorbents based on amine-functionalized bio-derived lignin and human urine plus lignin solutions have been developed. The integration of these renewable absorbents with the intensified hydrodynamics of the CFI enabled highly efficient continuous CO_2 capture, achieving absorption efficiencies of 95–

96%, while significantly reducing the reliance on conventional alkanolamine-based solvents. The developed absorbents also exhibited good recyclability, indicating that solvent intensification coupled with reactor intensification offers a sustainable, circular-economy-based approach for carbon capture. The work also focusses on the organic synthesis via milli meter scale CFI (continuous-flow synthesis of a fluorescent xanthene analogue from gallic acid and DMF). The transparent glass-made CFI enabled direct visualization of the reaction progress and at the same time improved heat transfer and mixing. Further CFI stacks have been used in the study which significantly increased the residence time, and the conversion due to increase in the total reactor length. The optimum reaction conditions for maximizing the product formation in continuous-flow operation are established by the optimization of flow rate, temperature, residence time and heat flux.

In summary, this thesis demonstrates that process intensification can be achieved through the combined application of hydrodynamic intensification, solvent intensification, reactor geometry modification, and operating-condition optimization. Together, these complementary strategies significantly enhance mass transfer, reaction kinetics, CO_2 absorption efficiency, and overall process performance. The results demonstrate the versatility of the glass-made Coiled Flow Inverter as a successful reactor for chemical synthesis and enhanced carbon capture applications.

6.2 Future Work

This work provides fundamental insight into hydrodynamics and reaction kinetics in millimeter-sized reactors, with particular focus on the glass Coiled Flow Inverter (CFI), for applications such as gas-liquid CO_2 capture and continuous-flow chemical

synthesis. The present study demonstrated that the process intensification by reactor geometry, solvent modifications and optimization of operating conditions can substantially enhance the CO_2 absorption efficiency and product yield. Although this thesis presents extensive experimental investigations, further research may be done to address the remaining challenges and expand the scope of the work. The following future works are therefore recommended

- Development of chemically modified bio-derived Nano cellulose (NC) with higher density of active functional groups for improved CO_2 absorption capacity and gas-liquid mass transfer.
- Scale-up of the glass-made Coiled Flow Inverter (CFI) to pilot scale operation for continuous industrial CO_2 scrubbing.
- Integration of carbon capture with CO_2 utilization through the catalytic conversion of CO_2-loaded absorbents into fuels and value-added chemicals.
- CFD modeling of gas-liquid flow in CFI reactors.
- Design and development of photo-flow reactors for efficient regeneration (desorption) of CO_2-loaded absorbents using solar or visible-light-driven processes, thereby reducing regeneration energy demands.

References

[1] T. Grützner, D. Ziegenbalg, R. Güttel, Process Intensification – An Unbroken Trend in Chemical Engineering, Chemie Ing. Tech. 90 (2018) 1823–1831. https://doi.org/10.1002/cite.201800032.

[2] V. Russo, S. Haase, P. Tolvanen, Process Intensification in Chemical Reaction Engineering, Processes 10 (2022) 1294. https://doi.org/10.3390/pr10071294.

[3] F.. Dautzenberg, M. Mukherjee, Process intensification using multifunctional reactors, Chem. Eng. Sci. 56 (2001) 251–267. https://doi.org/10.1016/S0009-2509(00)00228-1.

[4] Andrzej I. Stankiewicz,Jacob A. Moulijn, Process Intensification: Transforming Chemical Engineering, Chem. Eng. Prog. (2000) 22–34. https://www.aiche.org/sites/default/files/docs/news/010022_cep_stankiewicz.pdf.

[5] W.R. Dean, LXXII. The stream-line motion of fluid in a curved pipe (Second paper) , London, Edinburgh, Dublin Philos. Mag. J. Sci. 5 (1928) 673–695. https://doi.org/10.1080/14786440408564513.

[6] M. Mridha, K.D.P. Nigam, Coiled flow inverter as an inline mixer, Chem. Eng. Sci. 63 (2008) 1724–1732. https://doi.org/10.1016/j.ces.2007.10.028.

[7] E. López-Guajardo, E. Ortiz-Nadal, A. Montesinos-Castellanos, K.D.P. Nigam, Coiled flow inverter as a novel alternative for the intensification of a liquid-liquid reaction, Chem. Eng. Sci. 169 (2017) 179–185. https://doi.org/10.1016/j.ces.2017.01.016.

[8] Y. Zhang, C. Du, Z. Zhang, J. Du, Y. Tu, Z. Ren, Process Intensification of Gas–Liquid Separations Using Packed Beds: A Review, Separations 11 (2024) 284. https://doi.org/10.3390/separations11100284.

[9] M. Bouaifi, G. Hebrard, D. Bastoul, M. Roustan, A comparative study of gas hold-up, bubble size, interfacial area and mass transfer coefficients in stirred gas–liquid

reactors and bubble columns, Chem. Eng. Process. Process Intensif. 40 (2001) 97–111. https://doi.org/10.1016/S0255-2701(00)00129-X.

[10] G. Chen, J. Yue, Q. Yuan, Gas-Liquid Microreaction Technology: Recent Developments and Future Challenges, Chinese J. Chem. Eng. 16 (2008) 663–669. https://doi.org/10.1016/S1004-9541(08)60138-X.

[11] M.-Y. Pan, Z. Qian, L. Shao, M. Arowo, J.-F. Chen, J.-X. Wang, Absorption of carbon dioxide into N-methyldiethanolamine in a high-throughput microchannel reactor, Sep. Purif. Technol. 125 (2014) 52–58. https://doi.org/10.1016/j.seppur.2014.01.033.

[12] W.R. Dean, 14786440708564324, Philos. Mag. J. Sci. LXXXV (1911) 208–223.

[13] L.A.M. Janssen, Axial dispersion in laminar flow through coiled tubes, Chem. Eng. Sci. 31 (1976) 215–218. https://doi.org/10.1016/0009-2509(76)85059-2.

[14] D. Hobbs, F. Muzzio, Reynolds number effects on laminar mixing in the Kenics static mixer, Chem. Eng. J. 70 (1998) 93–104. https://doi.org/10.1016/s1385-8947(98)00065-5.

[15] A.K. Saxena, K.D.P. Nigam, Coiled configuration for flow inversion and its effect on residence time distribution, AIChE J. 30 (1984) 363–368. https://doi.org/10.1002/aic.690300303.

[16] S.P. Vanka, G. Luo, C.M. Winkler, Numerical study of scalar mixing in curved channels at low Reynolds numbers, AIChE J. 50 (2004) 2359–2368. https://doi.org/10.1002/aic.10196.

[17] S.K. Kurt, F. Warnebold, K.D.P. Nigam, N. Kockmann, Gas-liquid reaction and mass transfer in microstructured coiled flow inverter, Chem. Eng. Sci. 169 (2017) 164–178. https://doi.org/10.1016/j.ces.2017.01.017.

[18] M.M. Mandal, K.D.P. Nigam, Experimental study on pressure drop and heat transfer of turbulent flow in tube in tube helical heat exchanger, Ind. Eng. Chem. Res. 48 (2009) 9318–9324. https://doi.org/10.1021/ie9002393.

[19] V.K. Jha, L. Sharma, S. Roy, K.D.P. Nigam, S.K. Bhaumik, Comparative

assessment of mixing in compact coiled flow inverters under diffusion free laminar flow condition, Chem. Eng. Res. Des. 159 (2020) 455–467. https://doi.org/10.1016/j.cherd.2020.04.028.

[20] M.M. Mandal, C. Serra, Y. Hoarau, K.D.P. Nigam, Numerical modeling of polystyrene synthesis in coiled flow inverter, Microfluid. Nanofluidics 10 (2011) 415–423. https://doi.org/10.1007/s10404-010-0679-z.

[21] M.M. Mandal, P. Aggarwal, K.D.P. Nigam, Liquid–Liquid Mixing in Coiled Flow Inverter, Ind. Eng. Chem. Res. 50 (2011) 13230–13235. https://doi.org/10.1021/ie2002473.

[22] V. Verma, A. Topalović, G. Monechi, A. Alsudani, K.D.P. Nigam, J.T. Padding, Mixing of Viscoelastic Fluid Flows in a Coiled Flow Inverter, Ind. Eng. Chem. Res. 59 (2020) 3854–3864. https://doi.org/10.1021/acs.iecr.9b05142.

[23] P. Khot, M. Mansour, D. Thévenin, K.D.P. Nigam, K. Zähringer, Improving the mixing characteristics of coiled configurations by early flow inversion, Chem. Eng. Res. Des. 146 (2019) 324–335. https://doi.org/10.1016/j.cherd.2019.04.016.

[24] A. Mirzazadeh Ghanadi, A. Heydari Nasab, D. Bastani, A.A. Seife Kordi, The Effect of Nanoparticles on the Mass Transfer in Liquid–Liquid Extraction, Chem. Eng. Commun. 202 (2015) 600–605. https://doi.org/10.1080/00986445.2013.858037.

[25] S.K. Kurt, M.G. Gelhausen, N. Kockmann, Axial Dispersion and Heat Transfer in a Milli/Microstructured Coiled Flow Inverter for Narrow Residence Time Distribution at Laminar Flow, Chem. Eng. Technol. 38 (2015) 1122–1130. https://doi.org/10.1002/ceat.201400515.

[26] M.R. Gaddem, S. Ookawara, K.D.P. Nigam, S. Yoshikawa, H. Matsumoto, Numerical modeling of segmented flow in coiled flow inverter: Hydrodynamics and mass transfer studies, Chem. Eng. Sci. 234 (2021) 116400. https://doi.org/10.1016/j.ces.2020.116400.

[27] A.A.H. Laporte, T.M. Masson, S.D.A. Zondag, T. Noël, Multiphasic Continuous-Flow Reactors for Handling Gaseous Reagents in Organic Synthesis: Enhancing

Efficiency and Safety in Chemical Processes, Angew. Chemie - Int. Ed. 63 (2024). https://doi.org/10.1002/anie.202316108.

[28] J. Bobers, J. Grühn, S. Höving, T. Pyka, N. Kockmann, Two-Phase Flow in a Coiled Flow Inverter: Process Development from Batch to Continuous Flow, Org. Process Res. Dev. 24 (2020) 2094–2104. https://doi.org/10.1021/acs.oprd.0c00152.

[29] P.N. Singh, A. Tripathi, A. Kashyap, S. Patel, D. Panda, K.G. Biswas, Nanofluid-directed mass transfer intensification in a coiled flow inverter: hydrodynamic–interfacial synergy in a liquid–liquid system, Chem. Pap. (2026). https://doi.org/10.1007/s11696-026-05092-x.

[30] S. Soni, L. Sharma, P. Meena, S. Roy, K.D.P. Nigam, Compact coiled flow inverter for process intensification, Chem. Eng. Sci. 193 (2019) 312–324. https://doi.org/10.1016/j.ces.2018.09.008.

[31] L. Yang, K. Loubière, N. Dietrich, C. Le Men, C. Gourdon, G. Hébrard, Local investigations on the gas-liquid mass transfer around Taylor bubbles flowing in a meandering millimetric square channel, Chem. Eng. Sci. 165 (2017) 192–203. https://doi.org/10.1016/j.ces.2017.03.007.

[32] M.Y. Khan, S.S. Joshi, V. V. Ranade, Continuous Hydrogenation of Cinnamaldehyde: Gas–Liquid–Liquid–Solid Helical Coil Reactor, Ind. Eng. Chem. Res. (2023). https://doi.org/10.1021/acs.iecr.3c00841.

[33] H. Wibowo, H. Susanto, N. Grisdanurak, D. Hantoko, K. Yoshikawa, H. Qun, M. Yan, Recent developments of deep eutectic solvent as absorbent for CO_2 removal from syngas produced from gasification: Current status, challenges, and further research, J. Environ. Chem. Eng. 9 (2021) 105439. https://doi.org/10.1016/j.jece.2021.105439.

[34] G. Lin, S. Jiang, C. Zhu, T. Fu, Y. Ma, Mass-Transfer Characteristics of CO_2 Absorption into Aqueous Solutions of N -Methyldiethanolamine + Diethanolamine in a T-Junction Microchannel, ACS Sustain. Chem. Eng. 7 (2019) 4368–4375. https://doi.org/10.1021/acssuschemeng.8b06231.

[35] X.Y.D. Soo, J.J.C. Lee, W.Y. Wu, L. Tao, C. Wang, Q. Zhu, J. Bu, Advancements

in CO_2 capture by absorption and adsorption: A comprehensive review, J. CO2 Util. 81 (2024) 102727. https://doi.org/10.1016/j.jcou.2024.102727.

[36] A. Durgadevi, S. Pushpavanam, An experimental and theoretical investigation of pure carbon dioxide absorption in aqueous sodium hydroxide in glass millichannels, J. CO2 Util. 26 (2018) 133–142. https://doi.org/10.1016/j.jcou.2018.05.002.

[37] V. Hessel, P. Angeli, A. Gavriilidis, H. Löwe, Gas−Liquid and Gas−Liquid−Solid Microstructured Reactors: Contacting Principles and Applications, Ind. Eng. Chem. Res. 44 (2005) 9750–9769. https://doi.org/10.1021/ie0503139.

[38] J. Yue, G. Chen, Q. Yuan, L. Luo, Y. Gonthier, Hydrodynamics and mass transfer characteristics in gas–liquid flow through a rectangular microchannel, Chem. Eng. Sci. 62 (2007) 2096–2108. https://doi.org/10.1016/j.ces.2006.12.057.

[39] C.O. Vandu, H. Liu, R. Krishna, Mass transfer from Taylor bubbles rising in single capillaries, Chem. Eng. Sci. 60 (2005) 6430–6437. https://doi.org/10.1016/j.ces.2005.01.037.

[40] D. Mikaelian, B. Haut, B. Scheid, Bubbly flow and gas–liquid mass transfer in square and circular microchannels for stress-free and rigid interfaces: dissolution model, Microfluid. Nanofluidics 19 (2015) 899–911. https://doi.org/10.1007/s10404-015-1619-8.

[41] D. Mikaelian, B. Haut, B. Scheid, Bubbly flow and gas–liquid mass transfer in square and circular microchannels for stress-free and rigid interfaces: CFD analysis, Microfluid. Nanofluidics 19 (2015) 523–545. https://doi.org/10.1007/s10404-015-1578-0.

[42] C.P. Tiwari, F. Delgado-Licona, M. Valencia-Llompart, S. Nuñez-Correa, K.D.P. Nigam, A. Montesinos-Castellanos, E.A. López-Guajardo, A. Aguirre-Soto, Shining Light on the Coiled-Flow Inverter - Continuous-Flow Photochemistry in a Static Mixer, Ind. Eng. Chem. Res. 59 (2020) 3865–3872. https://doi.org/10.1021/acs.iecr.9b05008.

[43] J. Grühn, A.S. Behr, T.H. Eroglu, V. Trögel, K. Rosenthal, N. Kockmann, From Coiled Flow Inverter to Stirred Tank Reactor – Bioprocess Development and

Ontology Design, Chemie-Ingenieur-Technik 94 (2022) 852–863. https://doi.org/10.1002/cite.202100177.

[44] S.S. Tomar, N. Verma, K.D.P. Nigam, Process Intensification for Enhanced Photocatalytic Degradation of Aqueous Paracetamol Using a Coiled Flow Inverter, Ind. Eng. Chem. Res. 64 (2025) 2036–2048. https://doi.org/10.1021/acs.iecr.4c03547.

[45] Y. Ning, C. Si, B. Wang, Y. Xiang, T. Yan, Study on Gas–Liquid Two-Phase Flow and Mass Transfer Characteristics in Microchannel Reactors, Processes 14 (2026) 1–15. https://doi.org/10.3390/pr14040619.

[46] O. Mierka, R. Münster, J. Surkamp, S. Turek, N. Kockmann, Direct numerical simulation of dispersion and mixing in gas–liquid Dean-Taylor flow with influence of a 90° bend, Chem. Eng. Sci. 301 (2025) 120691. https://doi.org/10.1016/j.ces.2024.120691.

[47] M. Wang, A. Lawal, P. Stephenson, J. Sidders, C. Ramshaw, Post-combustion CO_2 capture with chemical absorption: A state-of-the-art review, Chem. Eng. Res. Des. 89 (2011) 1609–1624. https://doi.org/10.1016/j.cherd.2010.11.005.

[48] P. Markewitz, W. Kuckshinrichs, W. Leitner, J. Linssen, P. Zapp, R. Bongartz, A. Schreiber, T.E. Müller, Worldwide innovations in the development of carbon capture technologies and the utilization of CO_2, Energy Environ. Sci. 5 (2012) 7281. https://doi.org/10.1039/c2ee03403d.

[49] E.L. Smith, A.P. Abbott, K.S. Ryder, Deep Eutectic Solvents (DESs) and Their Applications, Chem. Rev. 114 (2014) 11060–11082. https://doi.org/10.1021/cr300162p.

[50] G.T. Rochelle, Amine Scrubbing for CO 2 Capture, Science (80-.). 325 (2009) 1652–1654. https://doi.org/10.1126/science.1176731.

[51] Z. Zoundi, CO2 emissions, renewable energy and the Environmental Kuznets Curve, a panel cointegration approach, Renew. Sustain. Energy Rev. 72 (2017) 1067–1075. https://doi.org/10.1016/j.rser.2016.10.018.

[52] K.A. Triplett, S.M. Ghiaasiaan, S.I. Abdel-Khalik, A. LeMouel, B.N. McCord, Gas–liquid two-phase flow in microchannels, Int. J. Multiph. Flow 25 (1999) 395–410. https://doi.org/10.1016/S0301-9322(98)00055-X.

[53] S. Bangerth, H. Ganapathy, M. Ohadi, T.S. Khan, M. Alshehhi, Study of CO_2 Absorption Into Aqueous Diethanolamine (DEA) Using Microchannel Reactors, in: Vol. 6A Energy, American Society of Mechanical Engineers, 2014. https://doi.org/10.1115/IMECE2014-36348.

[54] H. Ganapathy, A. Shooshtari, S. Dessiatoun, M. Alshehhi, M.M. Ohadi, Experimental Investigation of Enhanced Absorption of Carbon Dioxide in Diethanolamine in a Microreactor, in: ASME 2013 11th Int. Conf. Nanochannels, Microchannels, Minichannels, American Society of Mechanical Engineers, 2013. https://doi.org/10.1115/ICNMM2013-73162.

[55] H. Ganapathy, A. Shooshtari, S. Dessiatoun, M. Alshehhi, M.M. Ohadi, Experimental Investigation of Advanced Microscale Reactors for Enhanced Carbon Capture and Natural Gas Sweetening Applications, in: ASME 2013 7th Int. Conf. Energy Sustain., American Society of Mechanical Engineers, 2013. https://doi.org/10.1115/ES2013-18394.

[56] C. Zhu, H. Guo, C. Chu, T. Fu, Y. Ma, Gas-liquid distribution and mass transfer of CO2 absorption into sodium glycinate aqueous solution in parallel multi-channel microreactor, Int. J. Heat Mass Transf. 157 (2020) 119943. https://doi.org/10.1016/j.ijheatmasstransfer.2020.119943.

[57] Z. Pan, X. Zhang, Y. Xie, W. Cai, Instantaneous Mass Transfer under Gas-Liquid Taylor Flow in Circular Capillaries, Chem. Eng. Technol. 37 (2014) 495–504. https://doi.org/10.1002/ceat.201300354.

[58] N. Shao, A. Gavriilidis, P. Angeli, Mass transfer during Taylor flow in microchannels with and without chemical reaction, Chem. Eng. J. 160 (2010) 873–881. https://doi.org/10.1016/j.cej.2010.02.049.

[59] L. Wang, M.G. Olsen, R. Dennis Vigil, Reappearance of azimuthal waves in turbulent Taylor–Couette flow at large aspect ratio, Chem. Eng. Sci. 60 (2005)

5555–5568. https://doi.org/10.1016/j.ces.2005.05.024.

[60] F.J. dos Santos, L. Goldstein, Experimental aspects of biomass fuels in a bubbling fluidized bed combustor, Chem. Eng. Process. Process Intensif. 47 (2008) 1541–1549. https://doi.org/10.1016/j.cep.2007.07.004.

[61] V. Hessel, H. Löwe, F. Schönfeld, Micromixers—a review on passive and active mixing principles, Chem. Eng. Sci. 60 (2005) 2479–2501. https://doi.org/10.1016/j.ces.2004.11.033.

[62] Y. Liu, G. Chen, J. Yue, Manipulation of gas-liquid-liquid systems in continuous flow microreactors for efficient reaction processes, J. Flow Chem. 10 (2020) 103–121. https://doi.org/10.1007/s41981-019-00062-9.

[63] H. Niu, L. Pan, H. Su, S. Wang, Effects of Design and Operating Parameters on CO_2 Absorption in Microchannel Contactors, Ind. Eng. Chem. Res. 48 (2009) 8629–8634. https://doi.org/10.1021/ie8018966.

[64] P. Chasanis, A. Lautenschleger, E.Y. Kenig, Numerical investigation of carbon dioxide absorption in a falling-film micro-contactor, Chem. Eng. Sci. 65 (2010) 1125–1133. https://doi.org/10.1016/j.ces.2009.09.067.

[65] T. Cubaud, M. Sauzade, R. Sun, CO_2 dissolution in water using long serpentine microchannels, Biomicrofluidics 6 (2012). https://doi.org/10.1063/1.3693591.

[66] C. Yao, Z. Dong, Y. Zhao, G. Chen, Gas-liquid flow and mass transfer in a microchannel under elevated pressures, Chem. Eng. Sci. 123 (2015) 137–145. https://doi.org/10.1016/j.ces.2014.11.005.

[67] F. Vega, A. Sanna, B. Navarrete, M.M. Maroto-Valer, V.J. Cortés, Degradation of amine-based solvents in CO_2 capture process by chemical absorption, Greenh. Gases Sci. Technol. 4 (2014) 707–733. https://doi.org/10.1002/ghg.1446.

[68] Z.L. Ooi, P.Y. Tan, L.S. Tan, S.P. Yeap, Amine-based solvent for CO_2 absorption and its impact on carbon steel corrosion: A perspective review, Chinese J. Chem. Eng. 28 (2020) 1357–1367. https://doi.org/10.1016/j.cjche.2020.02.029.

[69] L. Dumée, C. Scholes, G. Stevens, S. Kentish, Purification of aqueous amine

solvents used in post combustion CO_2 capture: A review, Int. J. Greenh. Gas Control 10 (2012) 443–455. https://doi.org/10.1016/j.ijggc.2012.07.005.

[70] T. Supap, C. Saiwan, R. Idem, P.P. Tontiwachwuthikul, Part 2: Solvent management: solvent stability and amine degradation in CO_2 capture processes, Carbon Manag. 2 (2011) 551–566. https://doi.org/10.4155/cmt.11.55.

[71] J. Orozco-Agamez, D. Tirado, L. Umaña, A. Alviz-Meza, S. Garcia, D. Peña, Effects of Composition, Structure of Amine, Pressure and Temperature on CO_2 Capture Efficiency and Corrosion of Carbon Steels using Amine-Based Solvents: a Review, Chem. Eng. Trans. 96 (2022) 505–510. https://doi.org/10.3303/CET2296085.

[72] C. Mao, J. Byun, H.W. MacLeod, C.T. Maravelias, G.A. Ozin, Green urea production for sustainable agriculture, Joule 8 (2024) 1224–1238. https://doi.org/10.1016/j.joule.2024.02.021.

[73] J. Meessen, Urea synthesis, Chemie Ing. Tech. 86 (2014) 2180–2189. https://doi.org/10.1002/cite.201400064.

[74] M. Appl, Ammonia, Wiley, 1999. https://doi.org/10.1002/9783527613885.

[75] I. Santos Mesquita, P. Albuquerque Melo, A. Resende Secchi, Novel pathways for urea synthesis decarbonization: An analytical review from Bosch–Meiser to electroreduction processes, Appl. Energy 400 (2025) 126527. https://doi.org/10.1016/j.apenergy.2025.126527.

[76] A. Patel, A.A. Mungray, A.K. Mungray, Technologies for the recovery of nutrients, water and energy from human urine: A review, Chemosphere 259 (2020) 127372. https://doi.org/10.1016/j.chemosphere.2020.127372.

[77] M. Maurer, W. Pronk, T.A. Larsen, Treatment processes for source-separated urine, Water Res. 40 (2006) 3151–3166. https://doi.org/10.1016/j.watres.2006.07.012.

[78] H. Kirchmann, S. Pettersson, Human urine - Chemical composition and fertilizer use efficiency, Fertil. Res. 40 (1995) 149–154. https://doi.org/10.1007/BF00750100.

[79] A.R. Ferrão, P. Pestana, L. Borges, R. Palmeira-de-Oliveira, A. Palmeira-de-

Oliveira, J. Martinez-de-Oliveira, Quantification of Ions in Human Urine—A Review for Clinical Laboratories, Biomedicines 12 (2024) 1848. https://doi.org/10.3390/biomedicines12081848.

[80] H. Ray, D. Saetta, T.H. Boyer, Characterization of urea hydrolysis in fresh human urine and inhibition by chemical addition, Environ. Sci. Water Res. Technol. 4 (2018) 87–98. https://doi.org/10.1039/C7EW00271H.

[81] M. Afkhamipour, M. Mofarahi, Review on the mass transfer performance of CO_2 absorption by amine-based solvents in low- and high-pressure absorption packed columns, RSC Adv. 7 (2017) 17857–17872. https://doi.org/10.1039/C7RA01352C.

[82] X. Zhang, D. Bao, Y. Huang, H. Dong, X. Zhang, S. Zhang, Gas–liquid mass-transfer properties in CO_2 absorption system with ionic liquids, AIChE J. 60 (2014) 2929–2939. https://doi.org/10.1002/aic.14507.

[83] R. Ramezani, I.M. Bernhardsen, R. Di Felice, H.K. Knuutila, Physical properties and reaction kinetics of CO_2 absorption into unloaded and CO_2 loaded viscous monoethanolamine (MEA) solution, J. Mol. Liq. 329 (2021) 115569. https://doi.org/10.1016/j.molliq.2021.115569.

[84] W.L. Bourcier, T.J. Wolery, T. Wolfe, C. Haussmann, T.A. Buscheck, R.D. Aines, A preliminary cost and engineering estimate for desalinating produced formation water associated with carbon dioxide capture and storage, Int. J. Greenh. Gas Control 5 (2011) 1319–1328. https://doi.org/10.1016/j.ijggc.2011.06.001.

[85] E. Akiyama, Y. Nabata, Y. Yago, Thickening Mechanisms and Emulsion Stabilizing Properties of Polymer Thickeners, Nihon Reoroji Gakkaishi 49 (2021) 261–265. https://doi.org/10.1678/rheology.49.261.

[86] M.P. Amaya-Gómez, L.M. Sanabria-Rivas, A.M. Díaz-Lasprilla, C. Ardila-Suárez, R.H. Castro-García, H.I. Quintero-Pérez, G.E. Ramírez-Caballero, Copolymer Based on Polyglycerol-Acrylate-Lactate as Potential Water Viscosifier and Surfactant for Enhanced Oil Recovery, Int. J. Polym. Sci. 2020 (2020) 1–9. https://doi.org/10.1155/2020/3464670.

[87] X. Li, Z. Xu, H. Yin, Y. Feng, H. Quan, Comparative Studies on Enhanced Oil

Recovery: Thermoviscosifying Polymer Versus Polyacrylamide, Energy & Fuels 31 (2017) 2479–2487. https://doi.org/10.1021/acs.energyfuels.6b02653.

[88] R. Wu, C. Liu, Y. Zhang, J. Xu, A. Pranovich, J. Hemming, T. Tirri, X. Wang, C. Xu, In situ amino–lignin production via biomass fractionation for high-efficacy CO_2 capture, Green Chem. 27 (2025) 6764–6775. https://doi.org/10.1039/D5GC00429B.

[89] S. Sani, X. Liu, L. Stevens, H. Wang, C. Sun, Amine functionalized lignin-based mesoporous cellular carbons for CO_2 capture, Fuel 351 (2023) 128886. https://doi.org/10.1016/j.fuel.2023.128886.

[90] E. Atta-Obeng, B. Dawson-Andoh, E. Felton, G. Dahle, Carbon Dioxide Capture Using Amine Functionalized Hydrothermal Carbons from Technical Lignin, Waste and Biomass Valorization 10 (2019) 2725–2731. https://doi.org/10.1007/s12649-018-0281-2.

[91] C. Wang, Z. Liang, C. Bai, J. Sun, S. Qadir, Y. Liao, C. Zhang, M. Sajjad, H. Yang, S. Bai, In Situ Amination of Lignin Waste for CO_2 Capture, ChemistrySelect 10 (2025). https://doi.org/10.1002/slct.202504276.

[92] Q. Zheng, G. Nong, N. Li, Preparation and Structural Analysis of a Water-Soluble Aminated Lignin, Polymers (Basel). 16 (2024) 1237. https://doi.org/10.3390/polym16091237.

[93] A. Ghorai, H. Chung, Ionic Lignin Polymers for Controlled CO_2 Capture, Release, and Conversion into High-Value Chemicals, Adv. Mater. 36 (2024). https://doi.org/10.1002/adma.202406610.

[94] K. Cheng, S. Jiao, M. Xu, S. Luo, R. Wang, C. Ma, B. Tian, W. Li, S. Liu, Aminated lignin derived sub-nanometer porous N-doped carbon via a low-corrosion grafting-activation strategy for CO_2 capture and energy storage, Ind. Crops Prod. 244 (2026) 123098. https://doi.org/10.1016/j.indcrop.2026.123098.

[95] K.L. Kadam, L.H. Forrest, W.A. Jacobson, Rice straw as a lignocellulosic resource: collection, processing, transportation, and environmental aspects, Biomass and Bioenergy 18 (2000) 369–389. https://doi.org/10.1016/S0961-9534(00)00005-2.

[96] A. Satlewal, R. Agrawal, S. Bhagia, P. Das, A.J. Ragauskas, Rice straw as a feedstock for biofuels: Availability, recalcitrance, and chemical properties, Biofuels, Bioprod. Biorefining 12 (2018) 83–107. https://doi.org/10.1002/bbb.1818.

[97] Y. Singh, S. Sharma, U. Kumar, P. Sihag, P. Balyan, K.P. Singh, O.P. Dhankher, Strategies for economic utilization of rice straw residues into value-added by-products and prevention of environmental pollution, Sci. Total Environ. 906 (2024) 167714. https://doi.org/10.1016/j.scitotenv.2023.167714.

[98] R. Prasad, Y.S. shivay, Management options to alleviate the menace of rice (Oryza sativa) straw burning - An overview, Indian J. Agric. Sci. 88 (2018) 1651–1660. https://doi.org/10.56093/ijas.v88i11.84879.

[99] D. Klemm, F. Kramer, S. Moritz, T. Lindström, M. Ankerfors, D. Gray, A. Dorris, Nanocelluloses: A New Family of Nature-Based Materials, Angew. Chemie Int. Ed. 50 (2011) 5438–5466. https://doi.org/10.1002/anie.201001273.

[100] R.J. Moon, A. Martini, J. Nairn, J. Simonsen, J. Youngblood, Cellulose nanomaterials review: structure, properties and nanocomposites, Chem. Soc. Rev. 40 (2011) 3941. https://doi.org/10.1039/c0cs00108b.

[101] A. Dufresne, Nanocellulose: a new ageless bionanomaterial, Mater. Today 16 (2013) 220–227. https://doi.org/10.1016/j.mattod.2013.06.004.

[102] S.J. Eichhorn, A. Dufresne, M. Aranguren, N.E. Marcovich, J.R. Capadona, S.J. Rowan, C. Weder, W. Thielemans, M. Roman, S. Renneckar, W. Gindl, S. Veigel, J. Keckes, H. Yano, K. Abe, M. Nogi, A.N. Nakagaito, A. Mangalam, J. Simonsen, A.S. Benight, A. Bismarck, L.A. Berglund, T. Peijs, Review: current international research into cellulose nanofibres and nanocomposites, J. Mater. Sci. 45 (2010) 1–33. https://doi.org/10.1007/s10853-009-3874-0.

[103] W. Li, J. Guan, H. Fang, Y. Jiang, Y. Zhong, S. Shi, F. Cheng, Continuously enhanced versatile nanocellulose films enabled by sustaining CO_2 capture and in-situ calcification, Carbohydr. Polym. 342 (2024) 122362. https://doi.org/10.1016/j.carbpol.2024.122362.

[104] H. Ibrahim, N. Sazali, W.N.W. Salleh, M.N. Zainal Abidin, A short review on

recent utilization of nanocellulose for wastewater remediation and gas separation, Mater. Today Proc. 42 (2019) 45–49. https://doi.org/10.1016/j.matpr.2020.09.245.

[105] C. Quan, Y. Zhou, J. Wang, C. Wu, N. Gao, Biomass-based carbon materials for CO_2 capture: A review, J. CO_2 Util. 68 (2023) 102373. https://doi.org/10.1016/j.jcou.2022.102373.

[106] J. Liu, X. Wang, Z. Fan, Z. Liu, P. Xu, T.R. Sawant, G. Huang, X. Deng, J. Guo, J. Wang, M. Zhou, Valorization of agricultural residues: Challenges and opportunities in the production of bio-based materials, BioResources 20 (2025). https://doi.org/10.15376/biores.20.2.Liu.

[107] M. Mergbi, M.G. Galloni, D. Aboagye, E. Elimian, P. Su, B.M. Ikram, W. Nabgan, J. Bedia, H. Ben Amor, S. Contreras, F. Medina, R. Djellabi, Valorization of lignocellulosic biomass into sustainable materials for adsorption and photocatalytic applications in water and air remediation, Environ. Sci. Pollut. Res. 30 (2023) 74544–74574. https://doi.org/10.1007/s11356-023-27484-2.

[108] M. Umar, B.O. Yusuf, M. Aliyu, I. Hussain, A.M. Alhassan, M.M. Awad, O.A. Taialla, B. Ali, K.R. Alhooshani, S.A. Ganiyu, Advancing frontiers in CO_2 capture: The renaissance of biomass-derived carbon materials, Coord. Chem. Rev. 526 (2025) 216380. https://doi.org/10.1016/j.ccr.2024.216380.

[109] G. Rochelle, E. Chen, S. Freeman, D. Van Wagener, Q. Xu, A. Voice, Aqueous piperazine as the new standard for CO_2 capture technology, Chem. Eng. J. 171 (2011) 725–733. https://doi.org/10.1016/j.cej.2011.02.011.

[110] R. Apaiyakul, B. Chalermsinsuwan, S. Ngamprasertsith, P. Tontiwachwuthikul, H. Gao, Z. Liang, T. Sema, Comprehensive investigation on carbon dioxide absorption capacity, cyclic capacity, and regeneration heat duty of blended 2–amino–2–methyl–1–propanol (AMP) and N–methyl–4–piperidinol (MPDL) solvent, Int. J. Greenh. Gas Control 131 (2024) 104019. https://doi.org/10.1016/j.ijggc.2023.104019.

[111] M.E. Hamzehie, H. Najibi, Carbon dioxide absorption in aqueous solution of potassium glycinate + 2-amino-2-methyl-1-propanol as new absorbents, RSC Adv. 6 (2016) 62612–62623. https://doi.org/10.1039/C6RA09600J.

[112] X. Xu, M.B. Myers, F.G. Versteeg, E. Adam, C. White, E. Crooke, C.D. Wood, Next generation amino acid technology for CO_2 capture, J. Mater. Chem. A 9 (2021) 1692–1704. https://doi.org/10.1039/D0TA10583J.

[113] B.E. Gurkan, J.C. de la Fuente, E.M. Mindrup, L.E. Ficke, B.F. Goodrich, E.A. Price, W.F. Schneider, J.F. Brennecke, Equimolar CO_2 Absorption by Anion-Functionalized Ionic Liquids, J. Am. Chem. Soc. 132 (2010) 2116–2117. https://doi.org/10.1021/ja909305t.

[114] A.J. Al Abdulghani, F. Weisshar, J. Hack, A.T.N. Fajar, G. Lambard, N. Maeda, Toward Low-Temperature Regeneration of CO_2 Capture Adsorbents: Functionalization of Polyethylenimine, ACS Sustain. Chem. Eng. 13 (2025) 6325–6332. https://doi.org/10.1021/acssuschemeng.5c01250.

[115] F. Liu, M. Fang, N. Yi, T. Wang, Q. Wang, Biphasic behaviors and regeneration energy of a 2-(diethylamino)-ethanol and 2-((2-aminoethyl)amino) ethanol blend for CO_2 capture, Sustain. Energy Fuels 3 (2019) 3594–3602. https://doi.org/10.1039/C9SE00821G.

[116] R. Wang, Y. Yang, M. Wang, J. Lin, S. Zhang, S. An, L. Wang, Energy efficient diethylenetriamine–1-propanol biphasic solvent for CO_2 capture: Experimental and theoretical study, Appl. Energy 290 (2021) 116768. https://doi.org/10.1016/j.apenergy.2021.116768.

[117] W. Choi, K. Min, C. Kim, Y.S. Ko, J.W. Jeon, H. Seo, Y.-K. Park, M. Choi, Epoxide-functionalization of polyethyleneimine for synthesis of stable carbon dioxide adsorbent in temperature swing adsorption, Nat. Commun. 7 (2016) 12640. https://doi.org/10.1038/ncomms12640.

[118] D. Spinu, K.R. Rout, D. Chen, Unveiling the Desorption Performance and Thermal Stability of Unmodified Polyamine-Containing CO_2 Adsorbents, Energy & Fuels 38 (2024) 13176–13185. https://doi.org/10.1021/acs.energyfuels.4c02091.

[119] S. Nakrak, P. Tontiwachwuthikul, H. Gao, Z. Liang, T. Sema, Comprehensive mass transfer analysis of CO_2 absorption in high potential ternary AMP-PZ-MEA solvent using three-level factorial design, Environ. Sci. Pollut. Res. 30 (2022) 10001–10023.

https://doi.org/10.1007/s11356-022-22819-x.

[120] L.D. Lavis, R.T. Raines, Bright Ideas for Chemical Biology, ACS Chem. Biol. 3 (2008) 142–155. https://doi.org/10.1021/cb700248m.

[121] B. Valeur, Design principles of fluorescent molecular sensors for cation recognition, Coord. Chem. Rev. 205 (2000) 3–40. https://doi.org/10.1016/S0010-8545(00)00246-0.

[122] R.H. Friend, R.W. Gymer, A.B. Holmes, J.H. Burroughes, R.N. Marks, C. Taliani, D.D.C. Bradley, D.A. Dos Santos, J.L. Brédas, M. Lögdlund, W.R. Salaneck, Electroluminescence in conjugated polymers, Nature 397 (1999) 121–128. https://doi.org/10.1038/16393.

[123] M.B. Plutschack, B. Pieber, K. Gilmore, P.H. Seeberger, The Hitchhiker's Guide to Flow Chemistry, Chem. Rev. 117 (2017) 11796–11893. https://doi.org/10.1021/acs.chemrev.7b00183.

[124] D. Webb, T.F. Jamison, Continuous flow multi-step organic synthesis, Chem. Sci. 1 (2010) 675. https://doi.org/10.1039/c0sc00381f.

[125] J.C. Pastre, D.L. Browne, S. V. Ley, Flow chemistry syntheses of natural products, Chem. Soc. Rev. 42 (2013) 8849. https://doi.org/10.1039/c3cs60246j.

[126] P.V. Danckwerts, Continuous flow systems, Chem. Eng. Sci. 2 (1953) 1–13. https://doi.org/10.1016/0009-2509(53)80001-1.

[127] R.L. Hartman, J.P. McMullen, K.F. Jensen, Deciding Whether To Go with the Flow: Evaluating the Merits of Flow Reactors for Synthesis, Angew. Chemie Int. Ed. 50 (2011) 7502–7519. https://doi.org/10.1002/anie.201004637.

[128] K.F. Jensen, Microreaction engineering — is small better?, Chem. Eng. Sci. 56 (2001) 293–303. https://doi.org/10.1016/S0009-2509(00)00230-X.

[129] G.A. Tafete, N.G. Habtu, Reactor configuration, operations and structural catalyst design in process intensification of catalytic reactors: A review, Chem. Eng. Process. - Process Intensif. 184 (2023) 109290. https://doi.org/10.1016/j.cep.2023.109290.

[130] D. Alique, Reactors for Process Intensification: Recent Advances and Key Applications, Membranes (Basel). 11 (2021) 745. https://doi.org/10.3390/membranes11100745.

[131] F.J. Keil, Process intensification, Rev. Chem. Eng. 34 (2018) 135–200. https://doi.org/10.1515/revce-2017-0085.

[132] A. Górak, A. Stankiewicz, Intensified Reaction and Separation Systems, Annu. Rev. Chem. Biomol. Eng. 2 (2011) 431–451. https://doi.org/10.1146/annurev-chembioeng-061010-114159.

[133] C. Liu, Y. Bai, J. Chen, G. Bi, M. Zhang, D. Wang, M. Deng, Heat transfer performance of CuCrZr/AlSi7Mg multi-material heat sinks with triply periodic minimal surface manufactured by laser powder bed fusion, Virtual Phys. Prototyp. 20 (2025) 119824. https://doi.org/10.1080/17452759.2025.2523642.

[134] T. Razzaq, C.O. Kappe, Continuous Flow Organic Synthesis under High-Temperature/Pressure Conditions, Chem. – An Asian J. 5 (2010) 1274–1289. https://doi.org/10.1002/asia.201000010.

[135] C. Wiles, P. Watts, Continuous flow reactors: a perspective, Green Chem. 14 (2012) 38–54. https://doi.org/10.1039/C1GC16022B.

[136] M.S. Naughton, V. Kumar, Y. Bonita, K. Deshpande, P.J.A. Kenis, High temperature continuous flow synthesis of CdSe/CdS/ZnS, CdS/ZnS, and CdSeS/ZnS nanocrystals, Nanoscale 7 (2015) 15895–15903. https://doi.org/10.1039/C5NR04510J.

[137] S.K. Pal, V. Jha, A. Mandal, E.S.S. Iyer, D. Panda, Continuous Making, Stretch Breaking, and Exciton Dynamics of a Red-Emissive Organic Submicrometer-Sized Triangular Pyramid, J. Phys. Chem. C 127 (2023) 10174–10184. https://doi.org/10.1021/acs.jpcc.3c01076.

[138] N.G. Patil, F. Benaskar, E. V. Rebrov, J. Meuldijk, L.A. Hulshof, V. Hessel, J.C. Schouten, Continuous Multitubular Millireactor with a Cu Thin Film for Microwave-Assisted Fine-Chemical Synthesis, Ind. Eng. Chem. Res. 51 (2012) 14344–14354. https://doi.org/10.1021/ie300754z.

[139] U. Mishra, M.A. Ansari, A. Chaurasiya, A.K. Singh, D. Panda, Transparent, Fluorophore-Doped Cellulose Nanocrystal Films Prepared from Crop Residue: Superior Radiative Cooler and Organic Photodetector, ACS Sustain. Chem. Eng. 13 (2025) 2086–2096. https://doi.org/10.1021/acssuschemeng.4c08984.

[140] S.K. Crossno, L.H. Kalbus, G.E. Kalbus, Determinations of carbon dioxide by titration: New experiments for general, physical, and quantitative analysis courses, J. Chem. Educ. 73 (1996) 175–176. https://doi.org/10.1021/ed073p175.

[141] L. Dubois, D. Thomas, Carbon dioxide absorption into aqueous amine based solvents: Modeling and absorption tests, Energy Procedia 4 (2011) 1353–1360. https://doi.org/10.1016/j.egypro.2011.01.194.

[142] S. Komati, A.K. Suresh, CO_2 absorption into amine solutions: a novel strategy for intensification based on the addition of ferrofluids, J. Chem. Technol. Biotechnol. 83 (2008) 1094–1100. https://doi.org/10.1002/jctb.1871.

[143] H. Hikita, S. Asai, T. Takatsuka, Absorption of carbon dioxide into aqueous sodium hydroxide and sodium carbonate-bicarbonate solutions, Chem. Eng. J. 11 (1976) 131–141. https://doi.org/10.1016/S0300-9467(76)80035-4.

[144] A.M. Kozlowski, M. Hasani, Cellulose interactions with CO_2 in NaOH(aq): The (un)expected coagulation creates potential in cellulose technology, Carbohydr. Polym. 294 (2022) 119771. https://doi.org/10.1016/j.carbpol.2022.119771.

[145] G. Reyes, R. Ajdary, E. Kankuri, J.J. Kaschuk, H. Kosonen, O.J. Rojas, Cellulose gelation in NaOH(aq) by CO_2 absorption: Effects of holding time and concentration on biomaterial development, Carbohydr. Polym. 302 (2023) 120355. https://doi.org/10.1016/j.carbpol.2022.120355.

[146] E.A. López-Guajardo, G.M. Garza-Cantú, A. Marques-Camarena, E. Ortiz-Nadal, K.D.P. Nigam, A. Montesinos-Castellanos, Liquid–Liquid Flow Pattern Visualization and Mapping in a Millimetric Size Coiled Tube, Ind. Eng. Chem. Res. 58 (2019) 1075–1086. https://doi.org/10.1021/acs.iecr.8b05315.

[147] P. Jaiswal, R. Shukla, D. Panda, K.D.P. Nigam, K.G. Biswas, Non-Newtonian nanofluids mediated 15-fold enhancement of mass transfer for two-phase flow

systems in microchannel, Chem. Eng. Process. - Process Intensif. 186 (2023) 109342. https://doi.org/10.1016/j.cep.2023.109342.

[148] U. Kumar, D. Panda, K.G. Biswas, Augmented mass transfer in liquid-liquid flow through microchannels of different geometries, Chem. Eng. Process. - Process Intensif. 137 (2019) 72–79. https://doi.org/10.1016/j.cep.2019.02.005.

[149] P. Jaiswal, Y. Kumar, R. Shukla, K.D.P. Nigam, D. Panda, K. Guha Biswas, Covalently Immobilized Nickel Nanoparticles Reinforce Augmentation of Mass Transfer in Millichannels for Two-Phase Flow Systems, Ind. Eng. Chem. Res. 61 (2022) 3672–3684. https://doi.org/10.1021/acs.iecr.1c04419.

[150] K.G. Biswas, G. Das, S. Ray, J.K. Basu, Mass transfer characteristics of liquid–liquid flow in small diameter conduits, Chem. Eng. Sci. 122 (2015) 652–661. https://doi.org/10.1016/j.ces.2014.07.029.

[151] S. Voltolina, P. Marín, F. V. Díez, S. Ordóñez, Open-cell foams as beds in multiphase reactors: Residence time distribution and mass transfer, Chem. Eng. J. 316 (2017) 323–331. https://doi.org/10.1016/j.cej.2017.01.113.

[152] M.I. Jaramillo-Gutiérrez, M.I. Carreño-Lizcano, J.O. Ruiz–Lizarazo, J.A. Pedraza–Avella, E.P. Rivero, M.R. Cruz-Díaz, Design, mathematical modelling, and numerical simulation of a novel tubular photoelectrochemical reactor and experimental validation by residence time distribution and mass transfer coefficients, Chem. Eng. J. 386 (2020) 123895. https://doi.org/10.1016/j.cej.2019.123895.

[153] Y. Gu, D. Wang, Y. Gao, Y. Yue, W. Yang, C. Mei, X. Xu, Y. Xu, H. Xiao, J. Han, Solar-Powered High-Performance Lignin-Wood Evaporator for Solar Steam Generation, Adv. Funct. Mater. 33 (2023). https://doi.org/10.1002/adfm.202306947.

[154] Z. Sun, B. Fridrich, A. de Santi, S. Elangovan, K. Barta, Bright Side of Lignin Depolymerization: Toward New Platform Chemicals, Chem. Rev. 118 (2018) 614–678. https://doi.org/10.1021/acs.chemrev.7b00588.

[155] C. Wang, J. Huang, H. Ji, B. Wang, Z. Huang, Liquid Slug Length Measurement for Slug Flow in Small Channels Based on a Contactless Impedance Detection Sensor,

IEEE Sens. J. 26 (2026) 4435–4452. https://doi.org/10.1109/JSEN.2025.3643459.

[156] Z. Pang, C. Zhu, Y. Ma, T. Fu, CO 2 Absorption by Liquid Films under Taylor Flow in Serpentine Minichannels, Ind. Eng. Chem. Res. 59 (2020) 12250–12261. https://doi.org/10.1021/acs.iecr.0c02217.

[157] J. Singh, V. Verma, K.D.P. Nigam, Flow Characteristics of Power-Law Fluids in Coiled Flow Inverter, Ind. Eng. Chem. Res. 52 (2013) 207–221. https://doi.org/10.1021/ie300516w.

[158] P. Polak, Liquid and Vapour Properties, in: Theory Pract. Eng. Thermodyn., Macmillan Education UK, London, 1983: pp. 16–18. https://doi.org/10.1007/978-1-349-17235-1_3.

[159] C. De Visser, G. Perron, J.E. Desnoyers, W.J.M. Heuvelsland, G. Somsen, Volumes and heat capacities of mixtures of N,N-dimethylformamide and water at 298.15K, J. Chem. Eng. Data 22 (1977) 74–79. https://doi.org/10.1021/je60072a016.

[160] S. Anantharaj, U. Nithiyanantham, S.R. Ede, E. Ayyappan, S. Kundu, π-stacking intercalation and reductant assisted stabilization of osmium organosol for catalysis and SERS applications, RSC Adv. 5 (2015) 11850–11860. https://doi.org/10.1039/C4RA15521A.

Appendix A

A.1 Calculation of amount of heat received by oil bath and Heat flux

$$Q = m \cdot C_p(T_{out} - T_{in}) \quad watt - (A1)$$

$$Mass\ flow\ rate\ (m^{\cdot}) = Volume\ flow\ rate\left({}^{mL}/_{hr}\right) \times \rho_{Solution} \quad \frac{Kg}{hr} - - (A2)$$

$$Heat\ Flux\ (q') = \frac{Heat\ Transfer}{Surface\ \ area\ of\ reactor} \quad \frac{W}{m^2} - - - - - - - - - - (A3)$$

A.2 Calculation of Velocity of reactant in reactor

$$Velocity\ (U) = \frac{Mass\ Flow\ rate\ in \frac{kg}{hr}}{Area\ of\ cross\ section\ of\ reactor} \quad \frac{m}{sec} - - - - - - - (A4)$$

A.3 Calculation of Residence Time

$$\tau = \frac{Effevtive\ Length\ of\ reactor(m)}{Velocity\ of\ reactant\ in\ reactor(m/sec)} \quad sec - - - - - - - - (A5)$$

A.4 Calculation of percentage of CO_2 absorption by Acid –Base Titration (Chemical Method)

In the present study for Acid-base titration 1M HCL and 1M NaOH is used as neutralizer and for end point phenolphthalein is used as indicator. Volume of 1M HCL consumed (when pink colour disappears in CO_2 loaded liquid when Amine used as CO_2 absorbing medium) = Volume of CO_2 leave from CO_2 loaded liquid

This Volume of CO_2 is actual absorbing volume of liquid in amines. The supplied CO_2 volume is calculated as:

Volume of CO_2 suppled in reactor (mL) = Reaction time (min) × CO_2 gas flow rate (mL/min)

The Ratio of Absorbed volume of CO_2 to the Volume of supplied CO_2 in reactor is percentage of absorption of CO_2 in amines.

The same calculation is also verified with analytical method and percentage of absorption of CO_2 gas in absorbing medium is in limiting error range of $\pm 5\%$

A.4 Calculation of Reynolds Number (Re) of Gas-Liquid mixture

The following equations have been used to determine the Reynold number for the respective rates [161]

$$Re = \frac{\rho_{mix} U_{mix} d}{\mu_{mix}} \text{-----------------------------} (A6)$$

Where: $$\rho_{mix} = \beta\rho_G + (1-\beta)\rho_L \text{---------------------------} (A7)$$

$$\mu_{mix} = \beta\mu_G + (1-\beta)\mu_L \text{------------------------------} (A8)$$

$$\beta = \frac{Q_G}{Q_G + Q_L}; \quad Q_G = Gas\ flow\ rate\ (mL/\text{min})\ and\ Q_L = Liquid\ flow\ rate\ (mL/\text{min})$$

$$U_{mix} = \frac{Q_G + Q_L}{A_{CS}}$$

$$A_{CS} = \frac{\pi d^2}{4}$$

List of Publications

International Journals

1. **A**. **Tripathi,** K. Sarkar, S. Patel, U. Mishra, K. D. P. Nigam, D. Panda, K. G. Biswas, *Elucidating flow-directed 98% CO_2 absorption using millimeter-sized coiled flow inverters: Nano cellulose-aided sustainable scope.*

   Chemical Engineering and Processing - Process Intensification, 2024, 205, 110022

2. **A. Tripathi,** S.K.Pal**,** S. Patel, P. Singh, K. D. P. Nigam, K. G. Biswas, D. Panda

   Fluorescence on the Flow: Continuous Xanthene Dye Synthesis from Gallic Acid in a Coiled Flow Inverter

   Chem Plus Chem 2025, e202500313

3. **A. Tripathi,** S. Kumar**,** S. Patel, A. Singh, D. Panda, K. G. Biswas

   Turing Urine into Carbon Sink: Continuous 96% CO_2 Capture using Urea-Lignin Solution in a Coiled Flow Inverter (**2026)** (Revision submitted in Energy & Fuels, ACS)

4. A. Kumar, A. Anand, **A**. **Tripathi,** P. N. Singh, U. Mishra, D. Panda, K. G. Biswas

   A Sustainable Route of Mass Transfer for Liquid-Liquid Flow in Millimeter-Sized Conduit: Unearthing the Potential of Agro waste-Derived Nanomaterials.

   Waste and Biomass Valorization 2025, 17, 295–306

5. P. N. Singh, **A. Tripathi**, A. Kashyap, S. Patel, D. Panda, K. G. Biswas

   Nano fluid-directed Mass Transfer Intensification in a Coiled Flow Inverter: Hydrodynamic–Interfacial Synergy in a Liquid–Liquid System

   Chemical Papers (2026)

Conferences

1. **A. Tripathi,** S. Kumar, S. Patel, A. Singh, D. Panda, K. G. Biswas, Synthesis of toluene and Gallic acid with N, N Dimethylformamide (DMF) through CFI in heating environment. Chemcon 2022.

2. P. N. Singh, **A. Tripathi**, D. Panda, K. G. Biswas, Nanoparticle aided hydrodynamics of liquid - liquid flow in milli channels. Chemcon 2022.